AD-A179 039 MODELLING OF TIME-VARIANT FLOWS USING VORTEX DYNAMICS (U) ADVISORY GROUP FOR AEROSPACE RESEARCH AND DEVELOPMENT NEUILLY-SUR-SEINE (FRANCE) FEB 87 1/2

UNCLASSIFIED AGARD-AR-239 F/G 20/4 NL

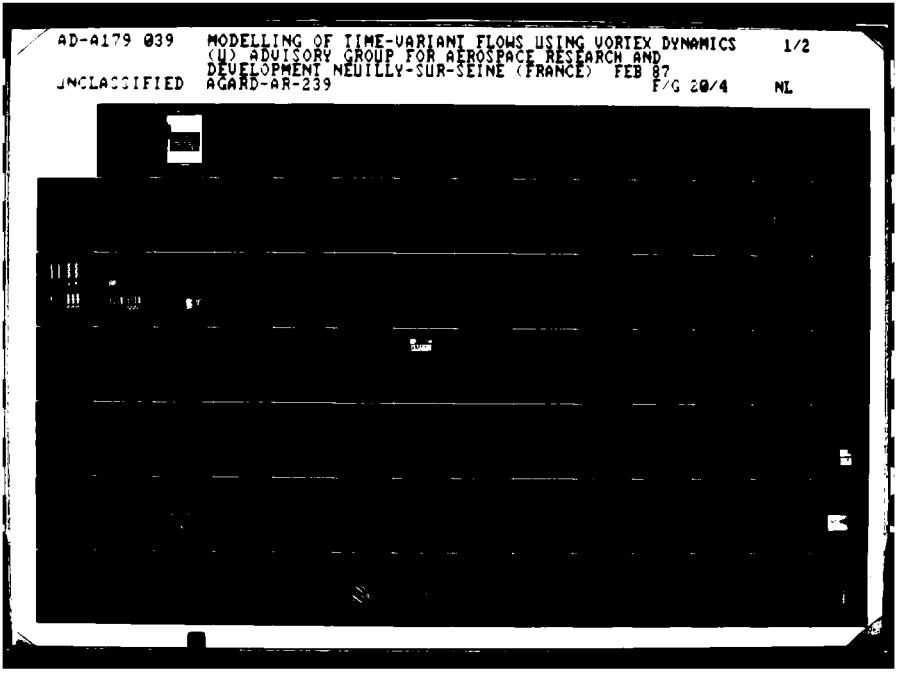

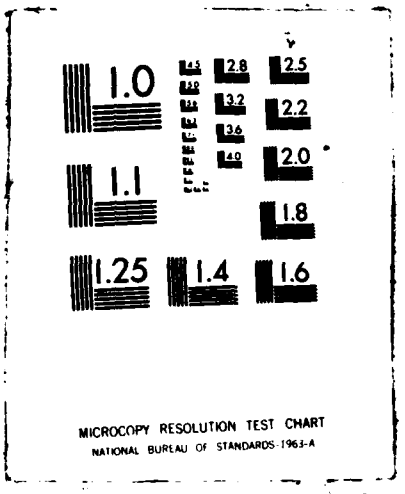
1.0
1.1
1.25
1.4
1.6
2.8
3.2
3.6
4.0
2.5
2.2
2.0
1.8
MICROCOPY RESOLUTION TEST CHART
NATIONAL BUREAU OF STANDARDS-1963-A

AGARD ADVISORY REPORT No.239

Round Table Discussion
on
Modelling of Time-Variant Flows using Vortex Dynamics

NORTH ATLANTIC TREATY ORGANIZATION

ADVISORY GROUP FOR AEROSPACE RESEARCH AND DEVELOPMENT

(ORGANISATION DU TRAITE DE L'ATLANTIQUE NORD)

AGARD Advisory Report No.239

ROUND TABLE DISCUSSION ON MODELLING OF TIME-VARIANT FLOWS USING VORTEX DYNAMICS

The information in this report was presented at an AGARD Fluid Dynamics Panel Round-Table Discussion on Modelling of Time-Variant Flows using Vortex Dynamics held at the Palais des Congrès, Aix-en-Provence, France, on 10 April 1986.

THE MISSION OF AGARD

The mission of AGARD is to bring together the leading personalities of the NATO nations in the fields of science and technology relating to aerospace for the following purposes:

- Exchanging of scientific and technical information;
- Continuously stimulating advances in the aerospace sciences relevant to strengthening the common defence posture;
- Improving the co-operation among member nations in aerospace research and development;
- Providing scientific and technical advice and assistance to the Military Committee in the field of aerospace research and development (with particular regard to its military application);
- Rendering scientific and technical assistance, as requested, to other NATO bodies and to member nations in connection with research and development problems in the aerospace field;
- Providing assistance to member nations for the purpose of increasing their scientific and technical potential;
- Recommending effective ways for the member nations to use their research and development capabilities for the common benefit of the NATO community.

The highest authority within AGARD is the National Delegates Board consisting of officially appointed senior representatives from each member nation. The mission of AGARD is carried out through the Panels which are composed of experts appointed by the National Delegates, the Consultant and Exchange Programme and the Aerospace Applications Studies Programme. The results of AGARD work are reported to the member nations and the NATO Authorities through the AGARD series of publications of which this is one.

Participation in AGARD activities is by invitation only and is normally limited to citizens of the NATO nations.

Published February 1987

ISBN 92-835-0405-4

Printed by Specialised Printing Services Limited
40 Chigwell Lane, Loughton, Essex IG10 3TZ

AGARD FLUID DYNAMICS PANEL

PROGRAMME COMMITTEE MEMBERS

PANEL EXECUTIVE

R.H.Rollins II

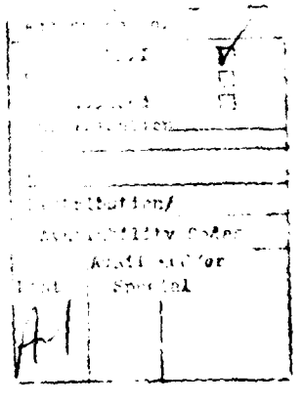

INTRODUCTORY REMARKS

by

A.D.Young
Dept. of Aero. Engineering
Queen Mary College
Mile End Rd
London E1 4NS
UK

In recent years there have been growing interest and activity in a number of countries in the application of methods involving vortex dynamics to appropriate problems in fluid mechanics. In such methods the flow is modelled by vortex elements ranging from simple singularities with fields determined by the Biot-Savart law to more complex, if more realistic, vortical forms involving finite cores, feeding vortex sheets and sometimes with viscosity effects modelled by diffusion simulated by a random walk method.

These methods are particularly suited to time-varying problems involving salient edges with separated flows and well defined vortical structures. They generally use a Lagrangian approach and their applications include the flow past bluff bodies, manoeuvring wings, wing-body arrangements, missiles, strakes, helicopter rotors, aero-acoustics, shear layers, jets and wakes. Non-aeronautical applications of interest are the rolling of boats, marine propellers, the dynamics of off-shore rigs and pollution concentrations in vortical flows.

The Fluid Dynamics Panel of AGARD decided that it was timely to hold a Round Table Discussion (RTD) to survey these developments. The main object was to provide the Panel with the information needed to decide whether the subject might be suitable for a Symposium or a Specialists' Meeting in the near future. It was thought opportune to hold the Round Table Discussion on 10 April 1986 at Aix-en-Provence, France, immediately following a FDP Symposium there on 'Applications of Computational Fluid Dynamics in Aeronautics'. Attendees at the Symposium were encouraged to participate in the Round Table Discussion and many of them did so.

This Report presents extended versions of the invited talks given at the RTD. Each speaker was asked to review the relevant activities in the field of vortex dynamics in his country. Presentations were made by:

Y.Morchoisne (France)
H.Oertel (Germany)
A.G.Panaras (Greece)
M.Germano (Italy)
H.W.Hoeymakers (Netherlands)
D.J.Maull (UK)
A.Leonard (USA)

It was felt that these presentations were of sufficient general interest to justify their collation and publication in this Report. The reader will find in them useful if condensed discussions of the basic theoretical concepts, illuminating assessments of the pros and cons of the models used, some interesting current applications, problem areas requiring further work and promising future developments.

Like Euler methods, these methods are based on inviscid flow but they can be used in viscous-inviscid coupling schemes in combination with boundary layer calculations, or as noted above the effects of viscosity can be simulated by a random marching process. The validity of the latter process, particularly for turbulent flows is a matter for future work. The methods have the additional limitation of being confined to incompressible flow, but hope is offered that ways for allowing for compressibility will be developed.

The models used of the vortex core and of vortex sheets as well as of the merging of vortex filaments are not yet fully satisfactory and further work is needed.

However, it will be evident from these presentations that for many important problems involving large scale vortical flows the use of vortex dynamics offers special advantages, not least in the conceptual simplicity and graphic help that it gives in our understanding of the structure and physics of such flows.

CONTENTS

CALCUL D'ECOULEMENTS INSTATIONNAIRES PAR LA METHODE DES TOURBILLONS PONCTUELS

par

Y.Morchoisne
ONERA
B.P. 72
92322 Châtillon
France

1 - INTRODUCTION

Le calcul d'un écoulement instationnaire de fluide non-visqueux et incompressible autour de configurations de type aile, rotor ou fuselage peut être effectué grâce à diverses méthodes de singularités.

Trois critères de choix peuvent être avancés, ils concernent :

- la qualité et la simplicité dans la prise en compte des conditions de glissement sur les corps considérés par l'emploi de singularités surfaciques (sources, tourbillons, doublets....),

- la facilité de traitement de la condition d'émission (généralisation d'une condition de Kutta-Joukowski) au voisinage des bords de fuite,

- la possibilité de calculer des évolutions complexes des zones rotationnelles ou nappes issues des bords de fuite à l'aide d'une équation de transport du vecteur tourbillon et d'une régularisation des champs de vitesse et de déformation discrétisés.

En proposant dès 1977 (réf. [7]) une discrétisation des nappes à l'aide de tourbillons ponctuels C.REHBACH a permis le développement et la mise en oeuvre à l'ONERA de méthodes répondant aux 3 critères ci-dessus. Les caractéristiques de ces méthodes sont les suivantes (fig.1) :

- les singularités surfaciques principales sont de type "doublet",

- l'émission tourbillonnaire est obtenue à l'aide d'une discrétisation de l'équation de convection des intensités des doublets,

- la représentation par tourbillons ponctuels des nappes permet la prise en compte des divers déchirements et interactions fortes (non-visqueuses) et l'approche Lagrangienne évite en grande partie la diffusion purement numérique qui résulterait de l'emploi d'un schéma Eulérien.

L'objet du présent article est de décrire brièvement ces méthodes doublet-tourbillon ponctuel et de présenter quelques unes des applications déjà effectuées..

2 - EQUATIONS DU PROBLEME

Le calcul de l'écoulement est ramené, à chaque instant, à la détermination de f solution de (voir fig.2) :

$$\Delta f(\underline{x}) = 0 \qquad \forall \underline{x} \in \Omega_0 - \overline{\Omega}_a - \Gamma_b = \Omega = \Omega_e \cup \Omega_b$$

avec $\partial \Omega_b = \Gamma_b$

$\Omega_0, \Omega_e, \Omega_b$ ouverts de $\mathbb{R}^3$

$$\begin{matrix} \Omega_a \\ \Omega_b \end{matrix} \subset \Omega_0$$

La fonction f est le potentiel d'un champ de vitesse totale ou de perturbation $\underline{V}$ défini quelque soit $\underline{x} \in \Omega$:

$$\forall \underline{x} \in \Omega : \underline{\nabla} f = \underline{V} \qquad (\underline{\nabla} \wedge \underline{V} = 0)$$

f est C^m en tout point de Ω

mais f et $\underline{\nabla}$ f peuvent être discontinus le long de Γ_D .

L'ouvert Ω_R est la zone rotationnelle. La frontière Γ_∞ de l'ouvert Ω_∞ représente la frontière externe du domaine de calcul. Γ_D surface de discontinuité correspond aux corps et aux nappes présents dans l'écoulement et est la frontière de l'ouvert Ω_D .

Le potentiel f est donc prolongé dans les zones "internes" comprises dans Ω_D.

En utilisant les identités de Green, il est facile de démontrer que (les intégrales étant prises au sens de Lebesgue) :

$$\forall\ \underline{x} \in \Omega = \Omega_E \cup \Omega_D \ :$$

$$4\pi f(\underline{x}) = \int_{\Gamma_D} \left\{ \left[\partial f / \partial n_y \right] \frac{1}{r} - [f] \frac{\partial}{\partial n_y}\left(\frac{1}{r}\right) \right\} dA_y - \int_{\Gamma_\infty \cup \Gamma_R} \left\{ \frac{\partial f}{\partial n_y} \frac{1}{r} - f \frac{\partial}{\partial n_y}\left(\frac{1}{r}\right) \right\} dA_y \qquad (1)$$

avec :

$$\underline{r} = \underline{x} - \underline{y} \qquad \underline{y} \in \Gamma_D \text{ ou } \Gamma_\infty \cup \Gamma_R$$
$$r = |\underline{r}|$$

et :

$$[f]_{(\underline{y})} = f^-(\underline{y}) - f^+(\underline{y}) \qquad \underline{y} \in \Gamma_D$$

où
$$\begin{cases} f^-(\underline{y}) = \lim\limits_{\substack{\underline{z} \to \underline{y} \in \Gamma_D \\ \underline{z} \in \Omega_D}} f(\underline{z}) \\ f^+(\underline{y}) = \lim\limits_{\substack{\underline{z} \to \underline{y} \in \Gamma_D \\ \underline{z} \in \Omega_E}} f(\underline{z}) \end{cases}$$

La dérivée normale sur la frontière Γ d'un ouvert Ω est notée :

$$\partial f / \partial n \big|_{\underline{y} \in \Gamma} = \underline{n} \cdot \underline{\nabla} f(\underline{y} \in \Gamma)$$

pour une fonction C^1 sur Γ, où $\underline{n}$ est la normale unitaire extérieure à Ω.

Pour une fonction C^* ($\underline{y} \in \Gamma_D$) le saut de la dérivée normale est fourni par (f C^1 pour $\underline{y} \notin \Gamma_D$):

$$\left[\partial f / \partial n_y \right] = \underline{n}_y \cdot \left((\underline{\nabla} f)^- - (\underline{\nabla} f)^+ \right)$$

Lorsque $\underline{x} \in \Gamma_D$ la formule (1) devient :

$$2\pi \left(f^+(\underline{x}) + f^-(\underline{x}) \right) = \int_{\Gamma_D} \{\ \}\, dA_y - \int_{\Gamma_\infty \cup \Gamma_R} \{\ \}\, dA_y \qquad (2)$$

Lorsque la frontière Γ_∞ tend vers l'infini, l'intégrale $\int_{\Gamma_\infty}$ tend vers $-4\pi f_\infty(\underline{x})$ où f_∞ est une fonction harmonique représentant le comportement à l'infini de f .

Pour $\underline{x} \notin \Gamma_D$ ($\underline{x} \in \Omega_P \cup \Omega_E$) (1) devient :

$$4\pi\left(f(\underline{x})-f_\infty(\underline{x})\right) = \int_{\Gamma_D}\{\ \}\,ds_y - \int_{\Gamma_R}\{\ \}\,ds_y \qquad (3)$$

L'intégrale $\int_{\Gamma_D}$ représente l'influence des discontinuités de f et de sa dérivée normale le long de Γ_D . L'intégrale $\int_{\Gamma_R}$ représente l'influence de la zone rotationnelle.

Deux discrétisations sont a priori possibles.

Si la zone rotationnelle est considérée comme une simple surface de discontinuité pour f l'ouvert Ω_R est alors un ensemble vide et la surface de discontinuité est formée de l'union des surfaces des obstacles et des nappes :

$$\Gamma_D = \underset{\text{Corps}}{\Gamma_{D_1}} \cup \underset{\text{Nappes}}{\Gamma_{D_2}}$$

Sur les obstacles $[f]$ et $[\partial f/\partial n]$ peuvent être non nuls, sur les nappes seul $[f]$ est différent de zéro (discontinuité de la composante tangentielle de la vitesse uniquement).

La relation (3) devient donc :

$$4\pi\left(f(\underline{x})-f_\infty(\underline{x})\right) = \int_{\Gamma_{D_1}}\left\{\left[\frac{\partial f}{\partial n_y}\right]\frac{1}{r} - [f]\frac{\partial}{\partial n_y}\left(\frac{1}{r}\right)\right\}ds_y - \int_{\Gamma_{D_2}}[f]\frac{\partial}{\partial n_y}\left(\frac{1}{r}\right)ds_y \qquad (4)$$

Dans le cas d'une zone rotationnelle considérée comme porteuse d'un tourbillon volumique, le potentiel f est défini dans le complémentaire de $\Omega_R \cup \Gamma_{D_1}$ (fig.3).

L'intégrale surfacique $\int_{\partial\Omega_R=\Gamma_R}$ peut-être transformée en une intégrale volumique (voir réf. 8) :

$$\forall \underline{x} \notin \Omega_R \qquad -\int_{\Gamma_R}\left\{\left[\frac{\partial f}{\partial n}\right]\frac{1}{r} - [f]\frac{\partial}{\partial n}\left(\frac{1}{r}\right)\right\}ds_y = \int_{\Omega_R}\underline{A}\cdot\underline{\omega}\,dv_y$$

avec
$$\begin{cases} \underline{\nabla} f = \underline{V} & \text{vitesse totale ou de perturbation} \\ \underline{\omega} = \underline{\nabla}\wedge\underline{V} \\ \underline{A} = (\underline{e}\wedge\underline{r})/\{r\,(r+\underline{r}\cdot\underline{e})\} \end{cases}$$

$\underline{e}$ vecteur unitaire quelconque

La relation (3) devient alors :

$$\forall \underline{x} \in \Omega_R \cup \Gamma_{D_1}$$

$$4\pi\left(f-f_\infty\right)(\underline{x}) = \int_{\Gamma_{D_1}}\{[\ ]-[\ ]\} + \int_{\Omega_R}\underline{A}\cdot\underline{\omega}\,dv_y \qquad (5)$$

Divers potentiels (et donc champs de vitesse associés) peuvent être considérés.

Le potentiel total ϕ est en effet la somme :

- d'un potentiel ϕ_∞ (comportement à l'infini),
- d'un potentiel ϕ_T (lié à la zone rotationnelle "épaisse" Ω_R ou à la nappe "mince" Γ_{D_2}),
- d'un potentiel dit de perturbation φ (dû aux discontinuités sur les surfaces des corps Γ_{D_1}).

$$\forall\, \underline{x} \in \Omega_\varepsilon \;:\quad \phi(\underline{x}) = \phi_\infty(\underline{x}) + \phi_T(\underline{x}) + \varphi(\underline{x})$$

Une première formulation consiste à choisir :

$$\text{et} \begin{cases} f(\underline{x}) = \phi(\underline{x}) & \forall\, \underline{x} \in \Omega_\varepsilon \\ f(\underline{x}) = 0 & \forall\, \underline{x} \in \Omega_D \end{cases}$$

Dans le cas d'un obstacle <u>immobile</u> (cas seul considéré dans le paragraphe 2) ϕ vérifie sur Γ_{D_1} :

$$\text{et} \begin{cases} [\partial\phi/\partial n] = 0 \\ [\phi] \neq 0 \end{cases}$$

<u>Remarque</u> :

Dans le cas d'un obstacle en mouvement la condition de glissement fournirait :

$$[\partial\phi/\partial n] = (\partial\phi/\partial n)^- - (\partial\phi/\partial n)^+ = -\underline{V}_P \cdot \underline{n}$$

où $\underline{V}_P$ représente la vitesse de l'obstacle au point considéré.

Pour une nappe mince (4) fournit :

$$\forall\, \underline{x} \in \Gamma_D \;:\; 4\pi(\phi - \phi_\infty)_{(\underline{x})} = -\int_{\Gamma_{D_1} \cup \Gamma_{D_2}} [\phi]\, \frac{\partial}{\partial n_y}\left(\frac{1}{r}\right) d\Delta_y \qquad (6)$$

Pour une zone à tourbillon volumique (5) nous donne ($\forall\, \underline{x} \notin \Gamma_{D_1} \cup \Omega_R$) :

$$4\pi\left(\phi - \phi_\infty\right)_{(\underline{x})} = -\int_{\Gamma_{D_1}} [\phi]\frac{\partial}{\partial n_y}\left(\frac{1}{r}\right) d\Delta_y + \int_{\Omega_R} \underline{A} \cdot \underline{\omega}_y \, d\nu_y \qquad (7)$$

corps — zone rotationnelle

Une seconde formulation consiste à choisir :

$$\begin{cases} f(\underline{x}) = \varphi(\underline{x}) & \forall\, \underline{x} \in \Omega_\varepsilon \\ f(\underline{x}) = 0 & \forall\, \underline{x} \in \Omega_D \end{cases}$$

Dans le cas d'un obstacle immobile la condition de glissement s'écrit sur les corps :

$$[\partial\varphi/\partial n] = (\partial\varphi/\partial n)^- - (\partial\varphi/\partial n)^+ = -\frac{\partial\varphi^+}{\partial n} = \underline{n}\cdot(\underline{U}_\infty + \underline{U}_T)$$

avec $\begin{cases} \underline{U}_\infty = \underline{\nabla}\,\phi_\infty \\ \underline{U}_T = \underline{\nabla}\,\phi_T \end{cases}$

Comme $\lim_{\underline{x}\to\infty} \varphi(\underline{x}) = 0$ nous avons donc $\varphi_\infty(\underline{x}) = 0$.

Dans le cas d'une zone rotationnelle (volumique) ou d'une nappe (mince) φ est donné par $(\forall \underline{x} \in \Omega)$:

$$4\pi\varphi(\underline{x}) = \int_{\Gamma_{D_1}} \left\{ [\partial\varphi/\partial n_y]\,\frac{1}{r} - [\varphi]\,\frac{\partial}{\partial n_y}(1/r) \right\} d\sigma_y \qquad (8)$$

où $[\partial\varphi/\partial n]_{(\underline{y})} = \underline{n}_y \cdot (\underline{U}_\infty + \underline{U}_T)(\underline{y}) \quad (\forall \underline{y} \in \Gamma_{D_1})$

représente une intensité donnée de sources surfaciques sur Γ_{D_1} (surface des corps).

• Pour une nappe :

$$\forall \underline{x} \notin \Gamma_{D_2} \;:\; \underline{U}_T(\underline{x}) = -\frac{1}{4\pi}\,\underline{\nabla}_{\underline{x}} \int_{\Gamma_{D_2}} [\phi]\,\frac{\partial}{\partial n_y}(1/r)\,d\sigma_y \qquad (9)$$

où $[\phi]$ est sur Γ_{D_2} l'intensité des doublets surfaciques.

• Pour une zone rotationnelle :

$$\forall \underline{x} \notin \Omega_R \;:\; \underline{U}_T(\underline{x}) = \frac{1}{4\pi} \int_{\Omega_R} \left(\frac{\underline{\omega} \wedge \underline{r}}{r^3} \right)_{(\underline{y})} d\nu_y \qquad (10)$$

où $\underline{\omega} = \underline{\nabla} \wedge \underline{U}$ est le rotationnel de la vitesse totale $\underline{U}$.

La formulation retenue est celle où la zone rotationnelle est considérée comme épaisse et, principalement pour des questions de précision, le prolongement utilisé sera celui consistant à prolonger le potentiel de perturbation par zéro à l'intérieur des obstacles.

D'où, $\forall \underline{x} \notin \Gamma_{D_1}$:

$$4\pi\varphi(\underline{x}) = \int_{\Gamma_{D_1}} \left\{ [\partial\varphi/\partial n_y]\,\frac{1}{r} - [\varphi]\,\frac{\partial}{\partial n_y}\left(\frac{1}{r}\right) \right\} d\sigma_y \qquad (11)$$

avec $[\partial\varphi/\partial n_y] = \underline{n}_y \cdot (\underline{U}_\infty + \underline{U}_T) \qquad \forall \underline{y} \in \Gamma_{D_1}$

$$\underline{U}_\infty = \underline{\nabla}\,\phi_\infty$$

et

$$\underline{U}_T = \frac{1}{4\pi}\int_{\Omega_R} \frac{\underline{\omega}\wedge\underline{r}}{r^3}\, d\nu_y$$

$$\begin{cases} \underline{\omega}(\underline{y}) = \underline{\nabla}\wedge\underline{U}(\underline{y}) & \forall\, \underline{y}\in\Omega_R \\ \underline{\omega}(\underline{y}) = 0 & \forall\, \underline{y}\notin\Omega_R \end{cases}$$

Pour $\underline{X}\in\Gamma_{D_1}$, un passage à la limite fournit :

$$-2\pi[\varphi]_{(\underline{x})} = \int_{\Gamma_{D_1}}\left\{\left[\frac{\partial\varphi}{\partial n_y}\right]\frac{1}{r} - [\varphi]\frac{\partial}{\partial n_y}\left(\frac{1}{r}\right)\right\} d\sigma_y \qquad (12)$$

$[\partial\varphi/\partial n]$ représente l'intensité des sources σ et $[\varphi]$ l'intensité des doublets à axe normal μ répartis sur Γ_{D_1} surface des corps.

Remarque : *Cas particulier des corps minces* (réf. 2 , 3)

La formulation-potentiel est alors remplacée par une formulation-vitesse obtenue en calculant le gradient en $\underline{X}$ de la relation (7) :

$$4\pi\left(\underline{U}-\underline{U}_\infty\right)_{(\underline{x})} = -\underline{\nabla}_{\underline{x}}\int_{\Gamma_{D_1}}[\phi]\frac{\partial}{\partial n_y}\left(\frac{1}{r}\right)d\sigma_y + \underline{\nabla}_{\underline{x}}\int_{\Omega_R}\underline{\underline{A}}\cdot\underline{\omega}_y\, d\nu_y$$

$$\forall\, \underline{X}\notin\Omega_R\cup\Gamma_{D_1}$$

Soit, après multiplication scalaire par $\underline{n}_x$ et passage à la limite lorsque $\underline{X}$ tend vers Γ_{D_1} :

$$-4\pi\,\underline{n}_x\cdot\underline{U}_\infty(\underline{x}) = -\underline{n}_x\cdot\underline{\nabla}_{\underline{x}}\int_{\Gamma_{D_1}}[\phi]\frac{\partial}{\partial n_y}\left(\frac{1}{r}\right)d\sigma_y + \int_{\Omega_R}\frac{\underline{\omega}\wedge\underline{r}}{r^3}\, d\nu_y \qquad (13)$$

L'intégrale $\int_{\Gamma_{D_1}}$ correspond aux doublets surfaciques répartis sur Γ_{D_1} et l'intégrale $\int_{\Omega_R}$ aux tourbillons volumiques répartis dans Ω_R .

2.1 - Condition de Kutta-Joukowski

Pour un fluide incompressible non-visqueux et dans le cas d'écoulements irrotationnels sauf sur des nappes ouvertes, le deuxième théorème de Bernoulli s'écrit :

$$\partial\phi/\partial t + U^2/2 + P/\rho = C \qquad (14)$$

avec P = pression

ρ = masse volumique

U = module de la vitesse = $|\underline{U}|$

C = constante indépendante de $\underline{X}$

La relation (14) appliquée au voisinage d'un bord de fuite fournit :

$$\partial[\phi]/\partial t + [U^2]/2 + [P]/\rho = 0$$

où (∇g) $[g] = g_i - g_e$ représente le saut de g à travers la nappe

(g_i valeur intrados, g_e valeur extrados, figure 4).

L'équilibre des pressions au bord de fuite ($P_e = P_i$) est traduit par la relation :

$$\partial [\phi]/\partial t + (U_i^2 - U_e^2)/2 = 0$$

soit, en posant $[\phi] = \mu$ (densité surfacique de doublets) :

$$\partial \mu/\partial t + (U_i^2 - U_e^2)/2 = 0 \qquad (15)$$

soit, sous une forme équivalente :

$$\partial \mu/\partial t + \underline{U}_m \cdot \underline{\nabla} \mu = 0 \qquad (16)$$

avec :

$$\begin{cases} \underline{U}_m = (\underline{U}_i + \underline{U}_e)/2 \\ \underline{\nabla} \mu = [\underline{U}] = \underline{U}_i - \underline{U}_e \end{cases}$$

Le membre de gauche de la relation (16) est, en fait, la dérivée particulaire de μ : $\underline{U}_m$ est en effet la vitesse moyenne le long de la nappe.

Une troisième forme approchée peut être déduite du non contournement du bord de fuite par le champ des vitesses : cette condition impose à la nappe d'être issue du bord de fuite et d'avoir une normale de direction donnée ($\underline{n}$) .

La condition de Kutta-Joukowski peut donc être traduites par les trois relations suivantes :

$$\text{ou} \quad \begin{cases} \partial \mu/\partial t + (U_i^2 - U_e^2)/2 = 0 & (17) \\ \text{ou} \quad D\mu/Dt = 0 & (18) \\ \text{ou} \quad \underline{U}_m \cdot \underline{n} = 0 & (19) \end{cases}$$

Dans les méthodes de tourbillons ponctuels instationnaires développées à l'ONERA la relation (18) dont la discrétisation semble la plus aisée est généralement utilisée, la relation (19) ne servant que pour des calculs d'écoulements en stationnaire ou pseudo-instationnaire.

2.2 - Transport du tourbillon

Les équations d'Euler fournissent, pour cet écoulement de fluide incompressible et non-visqueux, une équation de transport du vecteur tourbillon :

$$\partial \underline{\omega}/\partial t + \underline{\nabla} \wedge (\underline{\omega} \wedge \underline{U}) = 0 \qquad (20.a)$$

Cette équation admet deux formes équivalentes obtenues en utilisant les relations :

$$\text{et} \quad \begin{cases} \underline{\nabla} \wedge (\underline{\omega} \wedge \underline{U}) = (\underline{U} \cdot \underline{\nabla})\, \underline{\omega} - (\underline{\omega} \cdot \underline{\nabla})\, \underline{U} \\ \underline{\omega} = \underline{\nabla} \wedge \underline{U} \end{cases}$$

(20.a) devient :

$$\partial \underline{\omega}/\partial t + (\underline{U} \cdot \underline{\nabla})\, \underline{\omega} = (\underline{\omega} \cdot \underline{\nabla})\, \underline{U}$$

D'où la relation (20.b) :

$$D\underline{\omega}/Dt = (\underline{\omega}\cdot\underline{\nabla})\underline{U} \qquad (20.b)$$

où $D\underline{\omega}/Dt$ représente la dérivée particulaire de $\underline{\omega}$:

Posons :

$$S_{ij} = (\partial U_i/\partial x_j + \partial U_j/\partial x_i)/2$$

Le report dans (20.b) nous donne :

$$D\omega_i/Dt = \omega_j \partial U_i/\partial x_j = \omega_j S_{ij} + \omega_j \left(\frac{\partial U_i}{\partial x_j} - \frac{\partial U_j}{\partial x_i}\right)/2$$

Le dernier terme du membre de droite est nul :

$$\omega_j \left(\frac{\partial U_i}{\partial x_j} - \frac{\partial U_j}{\partial x_i}\right) = (\underline{\omega}\wedge\underline{\omega})_i = 0$$

La relation (20.c) s'écrit alors :

$$D\omega_i/Dt = \omega_j S_{ij} \qquad (20.c)$$

Cette dernière forme sera utilisée lors des discrétisations de préférence à (20.a) et (20.b).

3 - DISCRETISATION ET APPLICATIONS

3.1 - Singularités de surface

Dans le cas d'un corps épais l'utilisation de la relation (12) conduit à traiter un problème de Dirichlet interne c'est-à-dire à imposer :

$$\varphi^-(\underline{X}) = 0 \qquad \text{pour} \quad \underline{X} \in \Gamma_D$$

Dans le cas d'un corps mince la relation (14) est la traduction d'un problème de Neumann sur la surface des obstacles.

Les conditions aux limites sur les surfaces des corps sont prises en compte à l'aide d'une discrétisation par facettes quadrangulaires porteuses de densités constantes (doublets et/ou sources).

Dans le cas d'une facette de doublets l'influence sur le potentiel (en $\underline{X}$)est fournie par l'angle solide sous lequel est vue la facette (fig.5.a), l'influence sur la vitesse est fournie en remplaçant la facette par l'anneau tourbillonnaire équivalent (fig.5.b).

Pour une facette de sources (utilisation de la formule (12)) l'influence sur le potentiel est fournie par les formules de "Hess et Smith" (réf. [4]).

3.2 - Condition de Kutta-Joukowski : Emission

La relation (18) $(D\mu/Dt) = 0$

est à chaque pas de temps vérifiée en assurant la continuité de la densité μ à travers la ligne de bord de fuite :

$$\mu_s + \mu_i - \mu_e = 0 \qquad (21)$$

avec (fig.6) :

μ_s = densité de doublet sur la nappe
μ_i = " " l'intrados
μ_e = " " l'extrados

La relation (18) peut être prise en compte par l'étirement des anneaux tourbillonnaires (équivalents

aux panneaux de doublets à densité constante) au voisinage des divers bords de fuite.

Pour un corps mince la figure 7 indique les cinq étapes de l'émission discrétisée.

3.3 - Transport du $\underline{\omega}$

L'équation de transport de la densité tourbillonnaire volumique $\underline{\omega}$ (20) est transformée en une équation relative à $(\underline{\omega}\,\delta v)$ tourbillon ponctuel où δv est l'élément de volume support du vecteur densité volumique $\underline{\omega}$.

Par suite de l'incompressibilité du fluide $(\delta v = C^{te})$ l'équation est :

$$D(\underline{\omega}\,\delta v)/Dt = ((\underline{\omega}\,\delta v)\cdot\underline{\nabla})\,\underline{U} \qquad (22)$$

La relation (22) est discrétisée à l'aide d'un schéma en temps du second ordre de type Adams Bashforth et fournit l'évolution du tourbillon.

Le principal problème est celui de la régularité des champs de vitesse et de déformation : après discrétisation par tourbillons ponctuels le champ continu est remplacé par un champ singulier qu'il s'agit de régulariser pour approcher la solution exacte.

Pour un tourbillon ponctuel $(\delta v\,\underline{\omega})$ le champ de vitesse associé est :

$$\underline{U}(\underline{X}) = \frac{(\delta v\,\underline{\omega})\wedge\underline{r}}{r^3} \qquad \text{avec} \quad \underline{r} = \underline{X} - \underline{Y}$$

$$\text{et} \quad r = |\underline{r}|$$

Ce champ doit être remplacé au voisinage du point $\underline{Y}$ par un champ régulier aussi bien pour la vitesse que pour le tenseur gradient associé (fig.8).

Diverses études théoriques et numériques permettent de déterminer à la fois l'étendue et la nature de la régularisation nécessaire (réf. [1]).

4 - APPLICATIONS

4.1 - Aile plane double-delta (fig.9)

Le calcul de l'écoulement autour de cette aile mince mise en incidence a été effectué avec une émission tourbillonnaire le long du bord de fuite et du bord d'attaque.

L'évolution en temps du coefficient de portance après une mise en mouvement subite ainsi que les nappes de l'écoulement établi (visualisées grâce aux lignes d'émission issues du contour) sont présentées.

Le fort taux d'enroulement est un signe de faible viscosité numérique du schéma.

On voit apparaître un déchirement de la nappe dont la partie issue du bord d'attaque à flèche élevée est fortement enroulée alors que la partie issue du bord d'attaque à flèche modérée est sans enroulement.

4.2 _ Rotor en vol d'avancement (fig.10, réf. [2] [3])

Ce rotor bipale est également traité en tant que surface mince. Chaque vecteur correspond à un tourbillon ponctuel ($\underline{\omega}\,\delta v$) émis du bord de l'une des deux pales.

On voit apparaître pour le sillage lointain une légère désorganisation liée sans doute à l'utilisation d'une régularisation trop faible.

4.3 - Hélice avec moyeux (fig. 11, réf. [2], [3])

Sur cette figure sont représentées les lignes d'émission issues des bords de fuites des pales. L'influence du moyeux semble correctement prise en compte au niveau de la condition de glissement.

4.4 - Culot droit (réf.[5])

Le calcul de l'écoulement autour de cet obstacle avec culot droit a été effectué soit sans émission tourbillonnaire soit avec émission le long de l'arête.

Pour ces deux calculs le maillage est d'environ 600 facettes. Les résultats visualisés sont les vitesses pariétales et les coefficients de pression :

- les vecteurs représentent les vitesses,

- la couleur correspond à la pression.

Pour l'écoulement sans émission, un fort contournement apparaît au niveau de l'arête. Des gradients de pression importants sont observables sur le culot.

Pour l'écoulement avec émission, le coefficient de pression de culot est compris entre - 0,2 et - 0,3 en bon accord avec les résultats expérimentaux. Ce niveau est essentiellement fourni par le terme $\frac{\partial \Phi}{\partial t} - C$ (équation 14) la vitesse étant pratiquement nulle pour toute cette zone.

4.5 - Fuselage d'hélicoptère (réf.[5])

Un calcul de couche limite préliminaire a fourni la position des points d'émission utilisés dans le calcul de fluide parfait.

Sur la figure (13.a) sont montrées les lignes d'émission issues du raccord entre la "niche à chien" et le fuselage proprement dit.

Sur la figure (13.b) l'écoulement pariétal a été représenté en utilisant les mêmes principes de visualisation que pour le culot droit.

Avec 800 facettes et 200 tourbillons ponctuels les temps de calcul obtenus sont de l'ordre de 20 mn sur CRAY 1S.

4.6 - Hélicoptère en vol d'avancement (fig.12)

Pour démontrer la grande généralité de la méthode utilisée, l'écoulement autour d'une configuration fuselage + rotor a été numériquement simulé. Les premiers résultats obtenus semblent très encourageants pour de futurs calculs.

5 - CONCLUSION

Divers travaux sont en cours pour l'amélioration des méthodes de singularités développées à l'ONERA, ils portent sur :

- la prise en compte des conditions aux limites par des méthodes de type collocation (réf. 6) ou variationnelles,

- l'amélioration de la condition d'émission par une résolution locale des équations de Navier-Stokes,

- la mise en oeuvre de techniques de régularisation plus efficaces pour le transport des vecteurs tourbillons,

- l'utilisation de méthodes de résolution mieux adaptées aux ordinateurs vectoriels et aux techniques de singularités.

Dès à présent ces méthodes sont caractérisées par les points forts suivants :

- un traitement des conditions aux limites à l'aide d'une singularité de base simple (panneau de doublet à densité constante) associée à une condition de Dirichlet sur le potentiel interne de perturbation pour un corps épais et à une condition de Neumann pour un corps mince.

- une condition d'émission déduite de la condition de Kutta-Joukowski et pouvant être appliquée sur toute ligne donnée sur les obstacles,

- un traitement des nappes sous forme de zones rotationnelles à l'aide d'une discrétisation en tourbillons ponctuels et d'un schéma Lagrangien qui rendent possible le calcul d'interactions fortes (canard-voilure, hélice-fuselage, voilure-empennage....) avec nappes enroulées et déchirées.

REFERENCES

[1] J.T. BEALE, A. MAJDA
"High order accurate vortex methods with explicit velocity kernel". PAM-178, Center for Pure and Applied Mathematics, University of California at Berkeley, 1983.

[2] B. CANTALOUBE
"A new approach using vortex point method for prediction of rotor performance in hever and forward flight".
9th Helicopter Forum, Stresa, 13-15 sept.1983.

[3] B. CANTALOUBE, S. HUBERSON
"Calcul d'écoulements de fluide incompressible non-visqueux autour de voilures tournantes par une méthode particulaire".
La Recherche Aérospatiale, 1984-6.

[4] J.L. HESS, A.M.O SMITH
"Calculation of non-lifting potential flow around arbitrary three dimensional bodies".
Journal of Ship Research, vol. 8 n°2, p. 22-44, 1964.

[5] T.H. LE, C.REHBACH
"Simulation numérique d'écoulements décollés autour de corps aérodynamiques tronqués".
10e Congrès Canadien de Mécanique Appliquée.
June 2-7, London, Ontario, Canada.

[6] T.H. LE, Y. MORCHOISNE, J. RYAN
"Techniques numériques nouvelles dans les méthodes de singularités pour l'application à des configurations tridimensionnelles complexes".
58th Meeting of the Fluid Dynamics panel symposium on applications of computational fluid dynamics en aeronautics.
7-10 Avril 86, Aix-en-Provence, France.

[7] C. REHBACH
"Calcul numérique d'écoulements tridimensionnels instationnaires avec nappes tourbillonnaires".
La Recherche Aérospatiale, 1977-5.

[8] J.P. GUIRAUD
"Potentiel des vitesses crées par une distribution localisée de tourbillons".
La Recherche Aérospatiale, 1978-6.

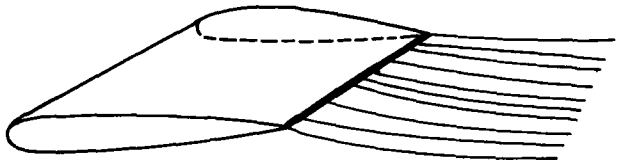

Corps :	Bord de fuite :	Nappe :
Condition de glissement	Condition de Kutta-Joukowski :	Equation de transport du tourbillon
Singularités surfaciques : Doublets	Continuité des doublets	Tourbillons ponctuels

Figure 1

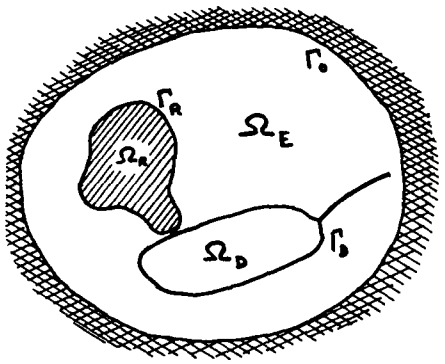

Figure 2

Surface des Corps Zone rotationnelle

Figure 3

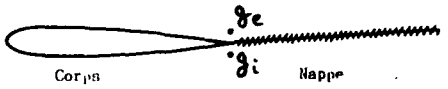

Figure 4

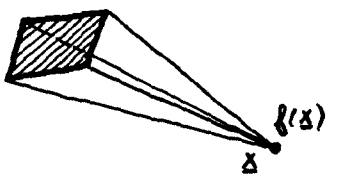

Figure 5.a

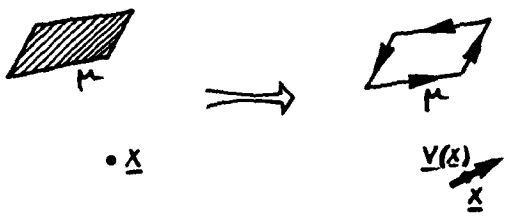

Figure 5.b

Figure 6

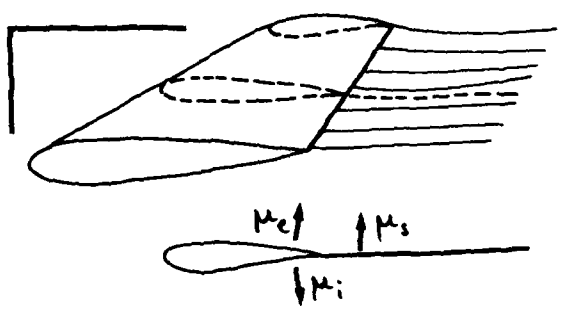

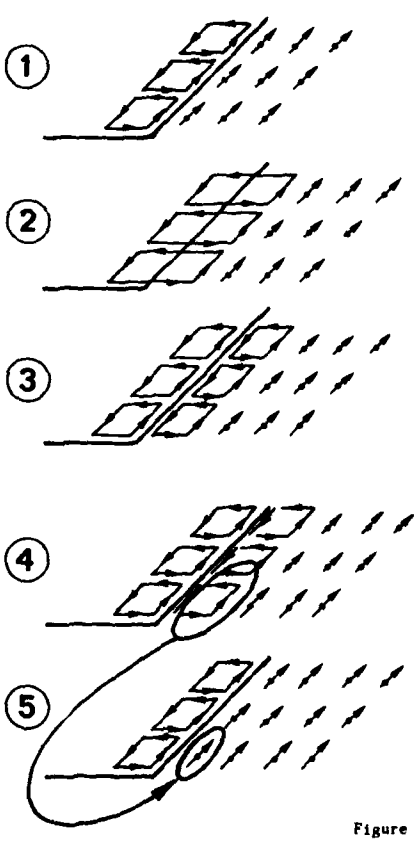

instant n.5t :

panneau doublet

anneau tourbillon

instant (n + 1).5t :

étirement des anneaux

et déplacement des tourbillons

scission

cassure des anneaux libres

Remplacement des filaments

par des tourbillons ponctuels

Figure 7

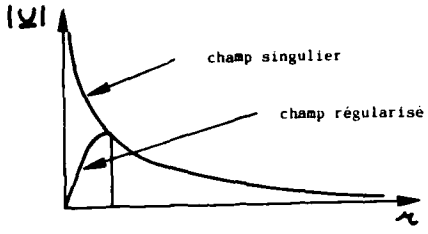

Figure 8

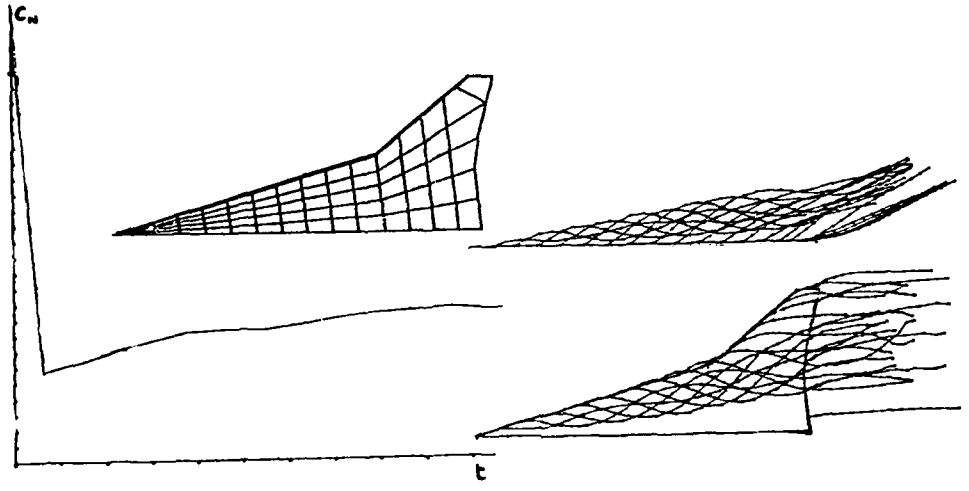

Figure 9 : Aile double delta, incidence 25°

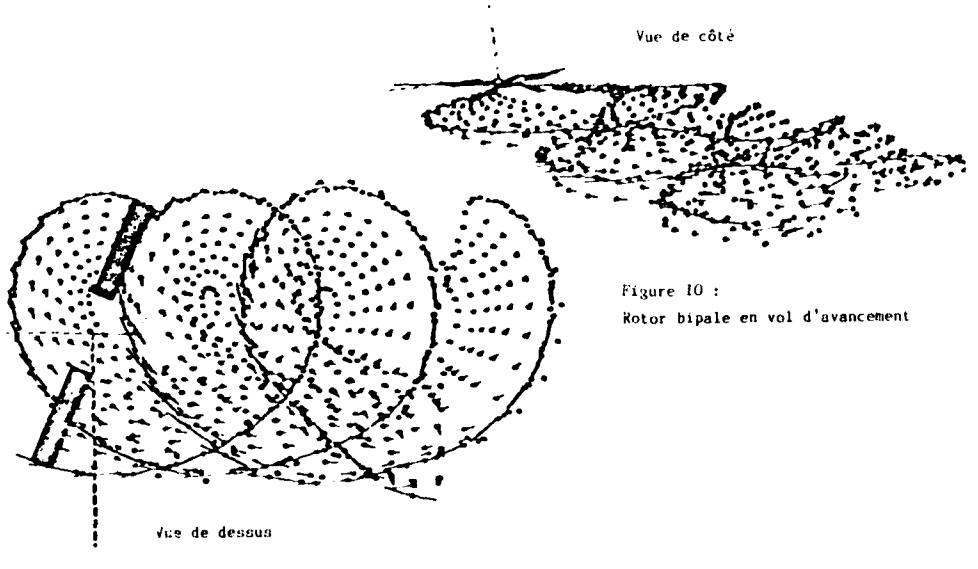

Figure IO :
Rotor bipale en vol d'avancement

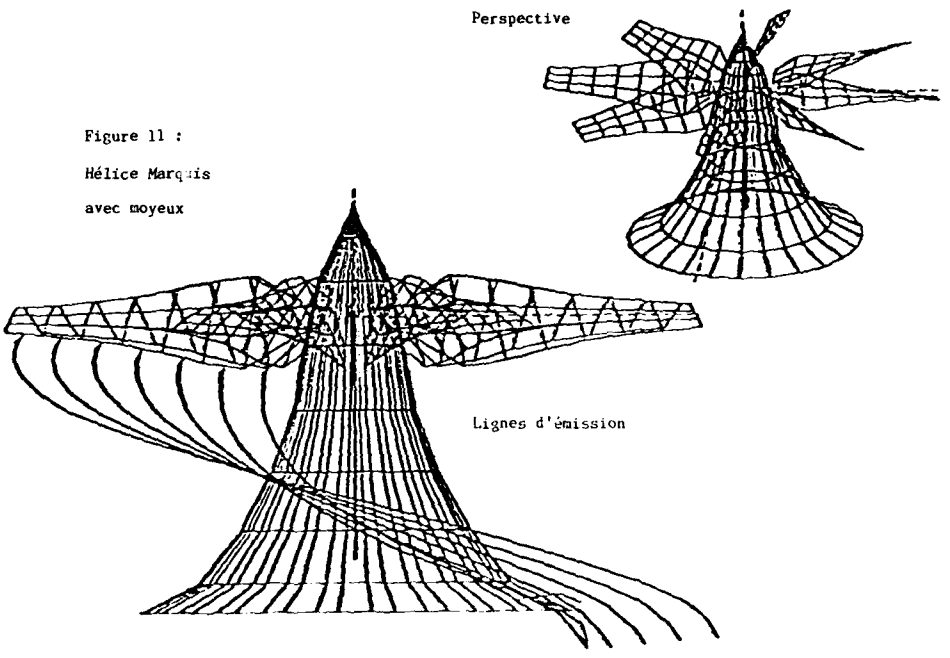

Figure 11 :
Hélice Marquis
avec moyeux

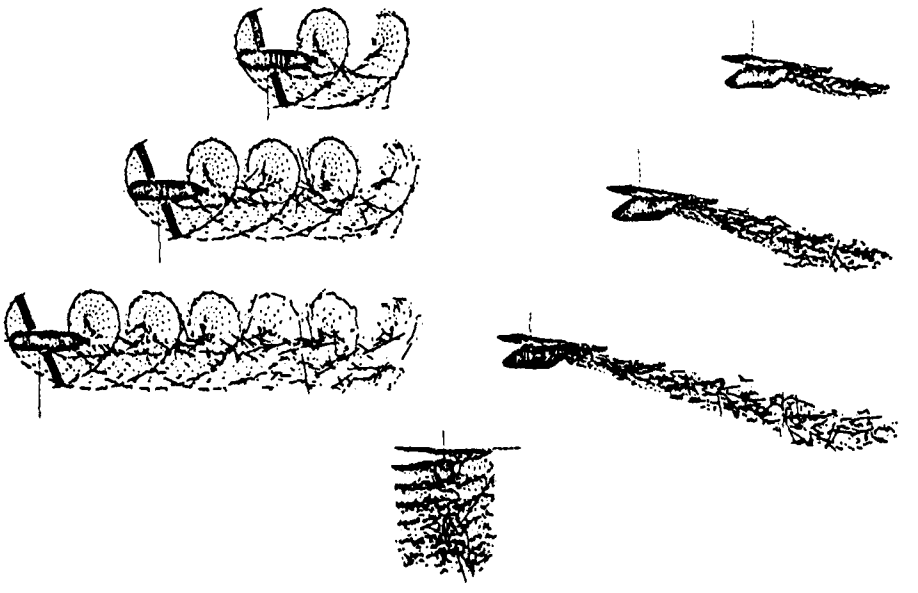

Figure 12 : Hélicoptère en vol d'avancement

VORTEX DYNAMICS

A Report on Work in Germany

H. Oertel

DFVLR - AVA Göttingen
Institute for Theoretical Fluid Mechanics

SUMMARY

This article reviews the numerical work relevant to the vortex dynamics method carried out in Germany supplemented by results from the Franco-German Research Institute Saint Louis, ISL. The introduction includes the development of two- and three-dimensional simultation methods and is followed by a discussion of the results in shear layers, trailing far wakes, aerodynamical profile flow simulation with spoiler and the simulation of three-dimensional structures in wakes.

1. Basis of Vortex Dynamics

The Vortex dynamics method allows the numerical simulation of nonlinear dynamics of incompressible flows. Starting point is the vorticity transport equation with the vorticity vector $\vec{\omega} = \nabla \times \vec{v}$

$$\frac{\partial \vec{\omega}}{\partial t} + \vec{v} \cdot \nabla \vec{\omega} - \vec{\omega} \cdot \nabla \vec{v} = \frac{1}{Re} \nabla^2 \vec{\omega}$$

We treat flows for the limit case Re >>1 in which the vorticity only fills one part of the flow field. The connection between vorticity and velocity field is described by the Biot-Savart Law, which in turn is derived from the non-divergence of the velocity field and the definition of vorticity.

$$\vec{v}\,(\vec{x},t) = -\frac{1}{4\pi} \int \frac{(\vec{x}-\vec{x}') \times \vec{\omega}(\vec{x},t)}{|\vec{x}-\vec{x}'|^3}\, dV\,(\vec{x}') + \nabla\phi$$

The integration is carried out over all parts of the flow field having vorticity. The whole velocity field is thus composed of a vorticity part and a potential flow component $\nabla\phi$ where $\nabla\phi$ is computed as solution of the Poisson equation

$$\nabla^2 \vec{v} = -\nabla \times \vec{\omega}$$

The dynamics of the vorticity field of threedimensional vortex filaments is determined by Kelvin's circulation theorem, which states that for inviscid, incompressible fluids, vortex tubes with uniform core structure move with constant circulation Γ_i with the flow field. Γ_i is defined by a surface integral over the vortex filament i.

$$\Gamma_i = \int_S \vec{\omega} \cdot d\vec{s}$$

By applying the vortex dynamics method, the vorticity of the flow field is divided into Lagrangian vortex filaments. The velocities result from the integration of the Biot-Savart Law. The two-dimensional velocity field calculated in such a manner satisfies approximately the inviscid vortex transport equation. The review articles of LEONARD [1,2] provide both a review and the state of the art of the application of the vortex dynamics method.

2. Numerical Methods

2.1 Point Vortex and Vortex Blob Method

The first simulation of a flow by the vortex method was performed by ROSENHEAD [3] who approximated a two-dimensional vortex sheet by a system of point vortices. The vorticity is given at N discrete locations $\vec{x}_i$ with their respective circulations Γ_i

$$\vec{\omega}\,(\vec{x},t) = \sum_{i=1}^{N} \Gamma_i\, \delta(\vec{x}-\vec{x}_i(t))$$

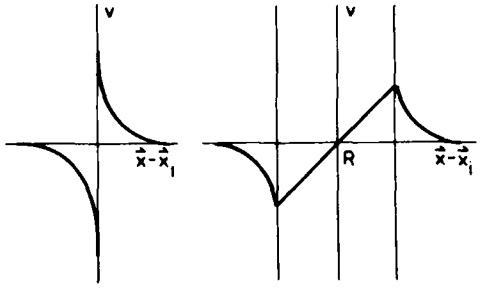

Point Vortex Vortex Blob

Fig. 1: Vortex models

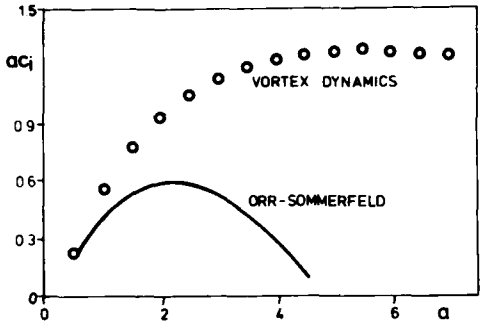

Fig. 2: Temporal amplification rates in two-dimensional wakes

The vortices move with the velocity which the flow has at their respective point.

$$\frac{d\vec{x}_i}{dt} = \vec{v}\ (x_i, t)$$

The disadvantage of the point vortex method lies in the singularity of the vorticity distribution shown in figure 1 which, in general terms, does not lead to a stable solution. Assistance is provided by the selection of vortex blobs with finite core diameter R and an algebraic or exponential vorticity distribution over the core. The vorticity field of these vortex blobs introduced by CHORIN [4] is represented by

$$\vec{\omega}(\vec{x},t) = \sum_{i=1}^{N} \Gamma_i\ \gamma_i(\vec{x}-\vec{x}_i(t))$$

where γ_i is the vorticity distribution within the vortex.

The limits of the application of the vortex blob method to wave instabilities in shear layers and wakes were shown in particular at the DFVLR in Göttingen. MEIBURG [5] compares the linear amplification rates of two-dimensional wave perturbations in parallel wake profiles with the solution of the Orr-Sommerfeld stability analysis. Fig. 2 shows that, with the given resolution, the vortex blob method can only reproduce the temporally amplified wave perturbations in the long wave length regime. The reason lies in the neglect of the modification of the vortex filaments core form, which occurs under the influence of the local distortion. An improvement could be reached by a dense collection of several filaments sheets. Considering the three-dimensional simulation of shear layers and wakes, there seems to be little change of doing this, since the numerical effort involved exceeds the present possibilities.

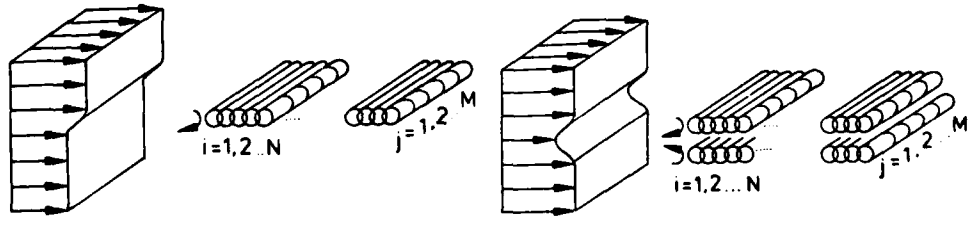

Shear layer Wake

Fig. 3a, 3b: Spatial discretisation with vortex filaments

2.2 Vortex Filaments

The three-dimensional extension of the vortex blob method leads to the discretisation of the vorticity tubes by vortex filaments. In analogy with the two-dimensional method the vorticity field is now approximated by

$$\vec{\omega}(\vec{x},t) = \sum_{i=1}^{N} \Gamma_i \int_{\gamma_i} (\vec{x}-\vec{x}_i(\xi,t)) \frac{\partial \vec{x}}{\partial \xi} i \, d\xi$$

for the space curve $\vec{x}_i(\xi,t)$ and the parameter ξ, which describes the surface contour of the filaments i. Each vortex filament is divided into M segments, whereby each segment continues to move at the corresponding local velocity permitting the simulation of the filaments' three-dimensional deformation. The segments are redistributed at each time step and approximated by cubic splines. The integration of the velocity field is now carried out over all the segments of the filaments.

Based on the work of ASHURST [6,7], MEIBURG [5] of the DFVLR in Göttingen has simulated three-dimensional structure development of shear layers and wakes. The discretisation in vortex filaments is sketched in fig. 3. The method is tested by a self-induced velocity distribution U_R of a vortex ring with vorticity Γ, radius R and core radius T. In the limit case $T/R^R << 1$ there corresponds a Gauss distribution over the core. This analytical result was achieved with only a few calculation points on the contour of the vortex ring using the filament method as shown in fig. 4.

For $T/R = 10^{-2}$ 40 points are sufficient to calculate the ring velocity to within 5%
For $T/R = 10^{-1}$ the analytical velocity was approximated already by 4 points

2.3 Random-Vortex Method

The diffusion of vorticity due to viscous effects can be approximated in two ways. Similarly to the decay of a potential vortex, it is possible to simulate the vorticity diffusion by the growth of the core radius R (t). An alternative way was shown by CHORIN [4] in analogy to the Brownian movement. He simulated the viscosity through the random motion of the vortex elements. This random-vortex method was further developed by PETERS and THIES [8,9] at the RWTH Aachen, showing that the probability density of the vortices fulfills a Fokker-Planck equation, which corresponds to the vorticity transport equation.

The two-dimensional motion of the i-th vortex is given by

$$\Delta x_i = u_i \Delta t + (\Delta x_i')_{random}$$

$$\Delta y_i = v_i \Delta t + (\Delta y_i')_{random}$$

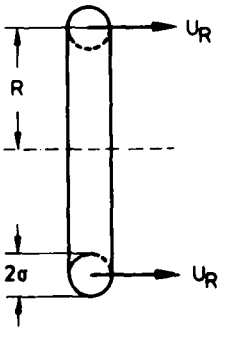

Principle sketch

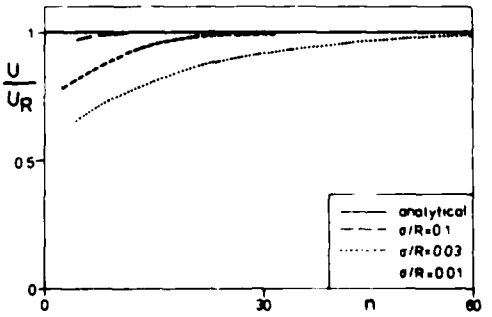

Comparison of analytical and numerical results

Fig. 4a, 4b: Self-induced velocity of a vortex ring

where Δt is the time step of the numerical simulation. The velocities u_i and v_i are in turn calculated by means of the Biot-Savart Law. The random part is calculated by

$$(\Delta x_i)_{random} = (-4\nu\Delta t \ln s_i)^{1/2} \cos(2\pi q_i)$$

$$(\Delta y_i)_{random} = (-4\nu\Delta t \ln s_i)^{1/2} \sin(2\pi q_i)$$

where s_i and q_i are random numbers between 0 and 1. ν denotes the diffusion coefficient and must be interpreted as turbulent viscosity. Through the formulation for Δx_i and Δy_i, a turbulent length-scale distribution is introduced a priori, being largely dependent on the choice of the time step Δt. PETERS and THIES [8] have shown that the analogy between diffusion and random motion remains valid even in the presence of convective flow.

3. Results

3.1 Point Vortex Simulation of Two-Dimensional Wakes

In connection with the classical profile theory for the calculation of inviscid potential flows, the point-vortex method was implemented at the Franco-German Research Institute Saint Louis to calculate the flow around a profile with spoiler. Fig. 5 shows a momentary plot of the simulation calculation compared with the measured temporally averaged velocity field and the integrated momentary streamlines. The initial circulation distribution required for the simulation was taken from the measured boundary-layer profiles at the separation points. The time step that influences the solution was numerically optimized. The calculated lift coefficient shows, as a function of the dimensionsless time, the starting process with the periodical vortex separation at the spoiler and the transition to a lower shedding frequency of the fully developed flow. The mean value of the calculated lift coefficient lies by - 0.25, while with a 40^0 spoiler a value of - 0.2 was measured.

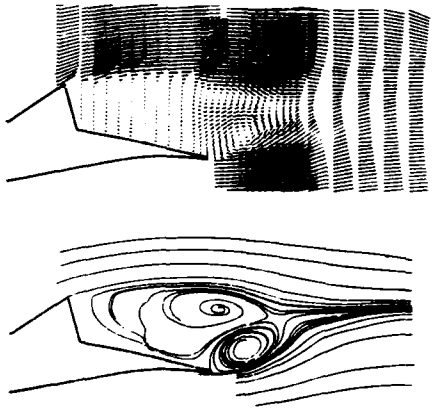

Mean velocity field and streamlines:
Re = $4 \cdot 10^5$, spoiler 40°
Experiment of Meyer et al. [12]

Point vortex simulation
CZICHOWSKY et al. [11]

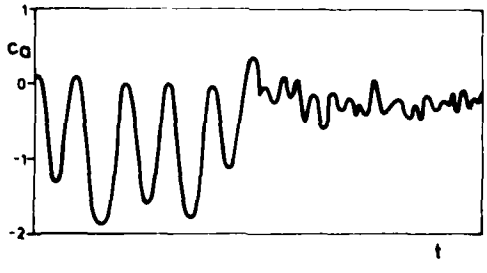

Unsteady lift coefficient

Fig. 5a, 5b, 5c: Wake of a profile with spoiler

3.2 Trailing Edge Far Wake

The random-vortex method development at the RWTH Aachen served to simulate a vortex system behind a model airfoil with finite wing span. The simulation calculation was started with 100 single vortices. The coalescence of the single vortices to a trailing-edge vortex in the far wake was then followed in the course of the calculation. Fig. 6 shows the principle sketch of the rolling up wakes starting with a parabolic circulation distribution. The results are presented as path-time lines of the single vortices on one-half of the airfoil. The coalescence of the single vortices shows that the trailing vorticity becomes concentrated into one vortex core. The presented interaction time is 1 second and the total circulation $\Gamma = 1\ m^2/s$. Varied were the viscosity ν and the initial fluctuation quantities with which a modification of the airfoil can be associated. The path lines of fig. 6 make clear that an increase in the viscosity as well as an increase in the degree of turbulence lead to a faster coalescence of the vortices. If the simulation is carried out with an elliptical initial circulation distribution the single vortices coalesce faster, but the trailing edge vortices appear further downstream.

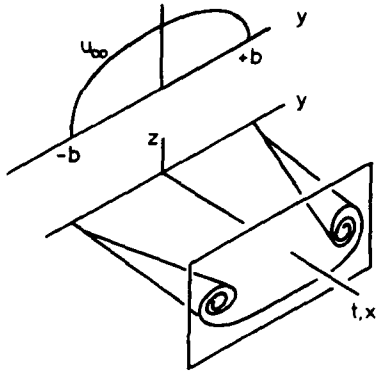

Principle sketch

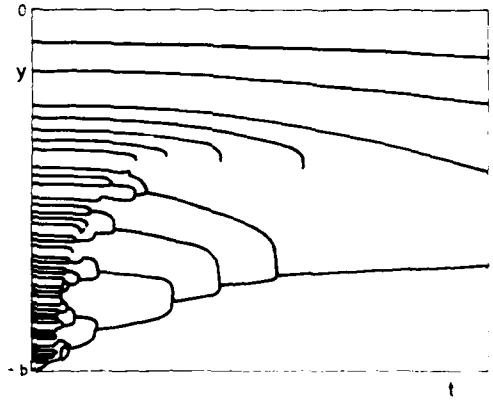

Path lines: $\overline{\Gamma^2}_{x_i} = \overline{\Gamma^2}_{y_i} = 0$, $\nu = 10^{-6}$

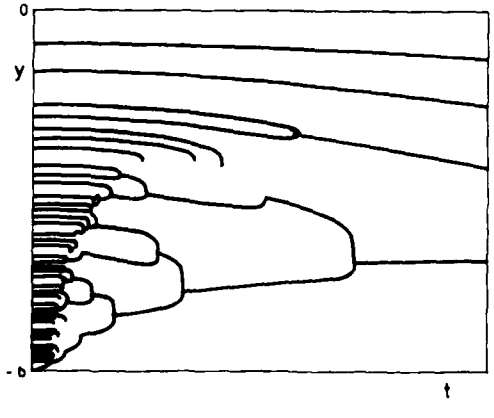

$\overline{\Gamma^2}_{x_i} = \overline{\Gamma^2}_{y_i} = 10^{-8}$, $\nu = 10^{-6}$

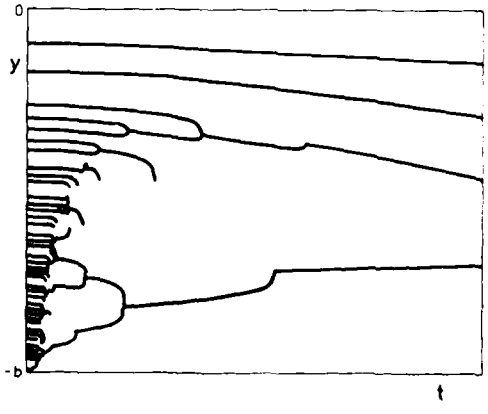

$\overline{\Gamma^2}_{x_i} = \overline{\Gamma^2}_{y_i} = 0$, $\nu = 10^{-4}$

Fig. 6a, 6b, 6c, 6d: Trailing edge vortices (PETERS and STÜTTGEN [10])

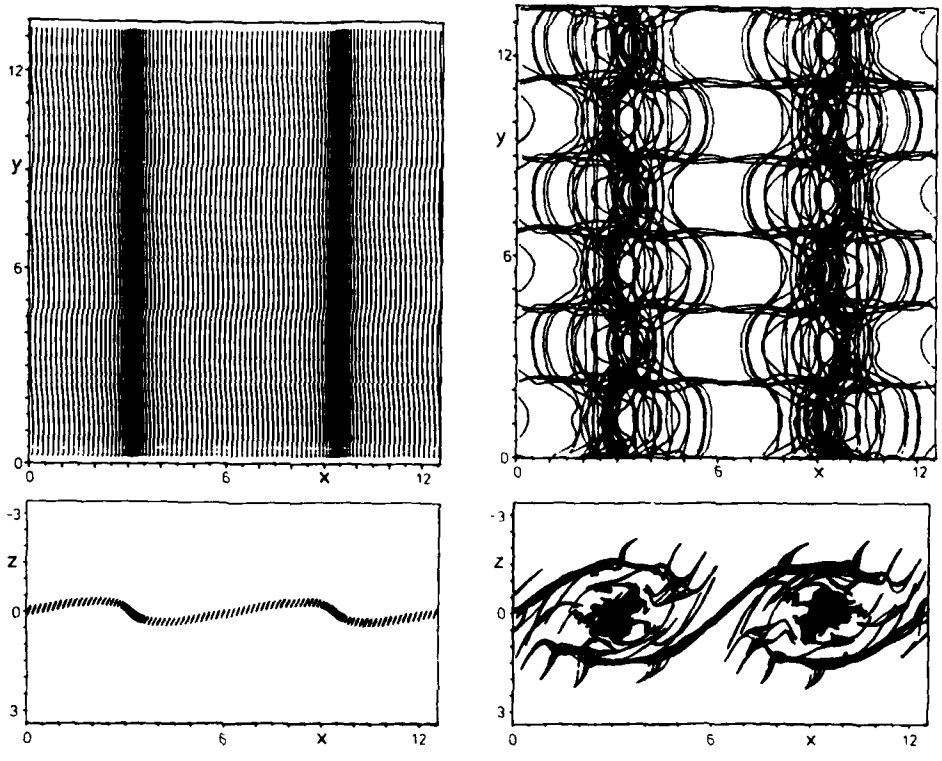

side and top view t = 117 t = 245

Fig. 7: Three-dimensional simulation of the instabilities in a shear layer (MEIBURG [5])

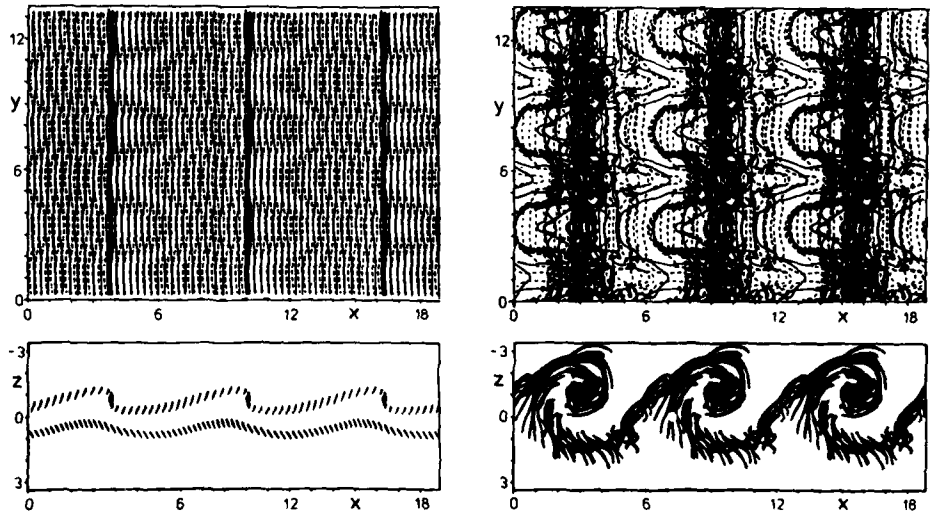

t = 129 t = 223

Fig. 8: Simulation with two opposite layers of filaments (MEIBURG and ASHURST [5,7])

3.3 Shear Layers

The three-dimensional calculations with the vortex filament method carried out at the DFVLR in Göttingen consider a shear layer as sketched in fig. 3. We assume a spatially periodic flow in x and y-direction and neglect the spreading of the shear layer downstream. The temporal development of the primary Kelvin-Helmholtz instability and the three-dimensional structure development due to secondary instabilities are simulated based on the work of ASHURST [6]. The horizontal boundary layers are represented by two layers of vorticity with opposite circulation and different intensity which make the shear profile.

In the first calculation the shear layer is discretised into 99 overlapping vortex filaments with circular cross-sections and 13 initial spanwise segments. As initial disturbance we assume a wave moving in flow direction with length 2π and amplitude 10^{-3} and a spanwise wave of amplitude 10^{-2}. Following experimental observations, the value 2/3 was chosen for the spanwise and flow direction wave length relationship. The selected integration volume comprises two wavelengths in flow direction and three wavelengths in spanwise direction. The first picture of fig. 7 shows, at a dimensionless time of 117, the roll up of the filaments and the concentration in vortices. Additional small scale three-dimensional motion occurs by formation of streamwise vorticity. After a simulation time of 245, it becomes clear that a dominant vorticity component ensues in flow direction as a result of the strong vortex stretching. During the flowfield evolution the filament arc length increases due to relative velocities along the filament. As the filament stretches, the core area is reduced and so the vorticity volume is conserved.

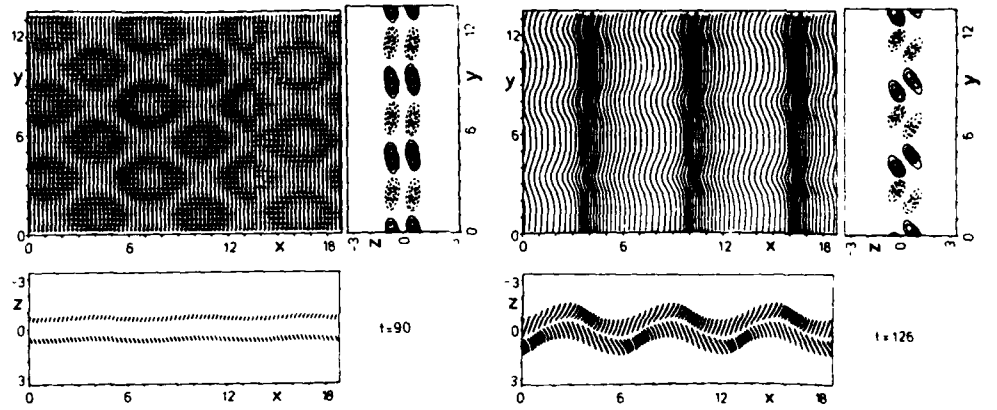

t = 90 t = 126
top and side views of the filaments

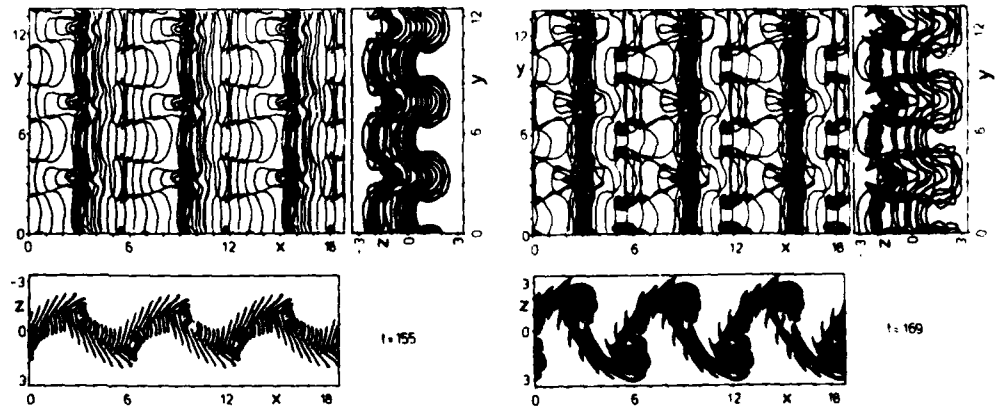

t = 155 t = 169
Fig. 9: Simulation of three-dimensional wake flows (MEIBURG [5])

The computational result with two superimposed layers of filaments in the original two-dimensional shear layer are shown in fig. 8. In the top view the upper layer of filaments is shown by full lines and the lower by dotted lines. The upper and lower shear layers are discretised into 75 filaments with 27 spanwise segments each. The control volume and the initial distribution are the same as in the simulation with one layer of filaments.

After a dimensionless time of 129 we observe that the upper part of the shear layer developes similarly to fig. 7. The Kelvin-Helmboltz instability provides for the rolling up of the stronger shear layer into large-scale vortices. The layer of filaments with the smaller vorticity, does not form large-scale vortices, but experiences a rather steady stretching, whereby part of the vorticity passes to the upper layer. The interaction of the two layers of filaments makes the longitudinal vortices incline against flow direction. This is similar to the λ-structures, as known from the Poiseuille and boundary-layer flows.

3.4 Three-Dimensional Wakes

We apply the numerical model of chapter 3.3 to the far field of wake flows. According to the sketch of fig. 3 the two shear layers of the wake profile are discretised into two rows of filaments with opposite vorticity. At the beginning of the simulation, vorticity components develop in flow direction in both shear layers, a process made clear by the y-z side view. The longitudinal vortex component causes the interaction of both wake shear layers determining the three-dimensional structure development.

In those areas where the lower layer becomes slower, the upper one becomes faster. This causes superimposed longitudinal vortices to have the same rotating direction and to move pairwise towards one another. Superposed on this process is the development of the von Karman vortex street. The x-z side view shows, at a dimensionless time of 169, two face to face shifted rows of large-scale vortices in span direction. The superposition of the two processes leads, in turn, to the development of λ-structures. Caution is required when interpreting the results, for our simulation does not correctly reproduce the short-wave deflections of the filaments. The arc length has doubled by the time the simulation is finished. The number of segments has increased fourfold to permit a constant resolution in spite of growing curvature effects.

With a suitably modified initial distribution it is also possible to simulate the subharmonic structure development in the wake. The initial disturbance now consists of a two-dimensional basic wave with amplitude 0.1 as well as of two diagonally moving waves of equal amplitude. Fig. 10 shows the integrated streak lines. The top view shows that at first the shape of the streak lines develops a few wavelengths fully undisturbed. Later, periodical domains will develop, in which particles gather together. The subharmonic structure is clearly recognizable, being in agreement with the experiments. The areas with higher particle concentration are staggered in successive rows. The side views arranged in equal intervals over a spanwise wavelength likewise show the periodical accumulation of particles downstream. The vortex pairing process in the upper shear layer of the wake stands out clearly towards the end of the range of integration.

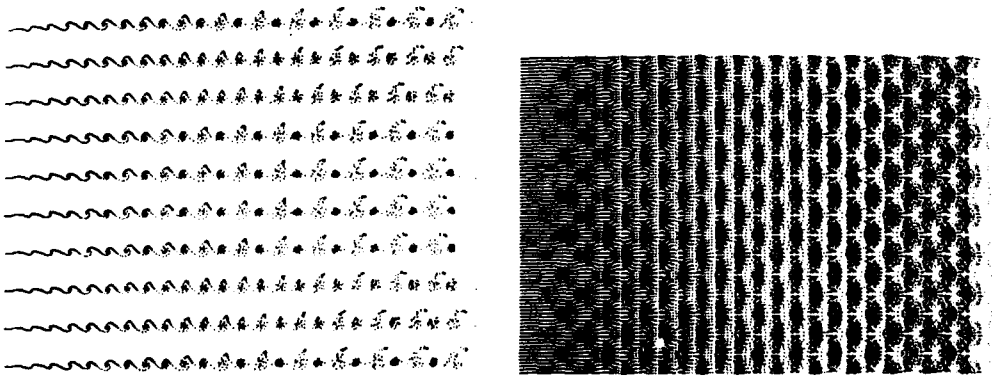

t = 59
spanwise side views top view

Fig. 10: Streak line of the subharmonic transition in a wake (MEIBURG [5])

4. CONCLUSION

The vortex dynamics method permits the numerical simulation of incompressible, inviscid fluids at high Reynolds numbers. The simulation of the viscous diffusion can be approximately done by the random vortex method. For the physical interpretation of the results it is important that the Fokker-Planck equation, which describes the statistics of the diffusive fluctuation quantities, can be transferred to the vortex-transport equation.

The advantage of the vortex dynamics method is the fact that vortex elements are required only where the vorticity is nonzero. In the case of a three-dimensional simulation with vortex filaments, the vortex stretching requires an increasing total length of vortex elements with time. The increasing growth rate of the filaments' arc length is connected with the transfer of energy to small scales. Here does the filament method find is limits, for it can only correctly reproduce the temporal development of small wave number disturbances. We have a method which conserves linear and angular momentum but does not conserve the energy in the short wavelength limit. Another disadvantage of the currently applied filament method is the fact that although the vortex filaments modify their diameter with increasing time, the spatial modification of the vortex core is not allowed. This violates local strain effects.

The limitation to periodical boundaries of the integration domain and the parallel flow assumption constitute a fundamental restriction to the calculation of three-dimensional structure development in shear layers and wakes. This numerical model is only applicable as approximation when the temporal and spatial amplification of the disturbance is small.

With the computers available nowadays, the vortex dynamics method permits the modelling of time-variant incompressible flows. Its application to unsteady aerodynamics requires, however, the combination with classical boundary-layer or Navier-Stokes methods. The development of combination strategies between viscous solutions and vortex dynamics simulation is in progress.

5. REFERENCES

[1] LEONHARD, A.
Vortex Method for Flow Simulation
J. of Comp. Phys. 37,289-335 (1980)

[2] LEONHARD, A.
Computing Three-Dimensional Incompressible Flows with Vortex Elements
Ann. Rev. Fluid Mech. 17, 523-559 (1985)

[3] ROSENHEAD, L.
The Formation of Vortices from a Surface of Discontinuity
Proc. Roy. Soc. London A 134, 170-192 (1931)

[4] CHORIN, A. J.
Numerical Study of Slightly Viscous Flow
J. Fluid Mech. 57, 785-796 (1973)

[5] MEIBURG, E.
Numerische Simulation der zwei- und dreidimensionalen Strukturbildung in Scherschichten und Nachläufen
DFVLR FB 86-10 (1986)

[6] ASHURST, W. T.
Numerical Simulation of Turbulent Mixing Layers via Vortex Dynamics
Turbulent Shear Flows I, 402-413
Springer (1979)

[7] ASHURST, W. T., MEIBURG, E.
Three-Dimensional Shear Layers via Vortex Dynamics
Sandia Report SAND 85-8777 (1985)

[8] PETERS, N., THIES, H. J.
Random Walk and Diffusion in Two-Dimensional Lagrangian Systems
Recent Contributions to Fluid Mechanics, ed. W. Haase, Springer (1982)

[9] THIES, H. J.
Kohärente Strukturen in einer turbulenten Zweikomponenten-Scherschicht
Ph. D. Thesis RWTH Aachen (1982)

[10] PETERS, N. STÜTTGEN, W.
Das Zusammenwachsen und der Zerfall von Längswirbeln an Tragflächen
DFG-Bericht (1985)

[11] CZICHOWSKY, W., JAEGGY, B. C., KOERBER, G., MEYER, P.
Theoretische und experimentelle Untersuchung der Wirbelströmung hinter einem Tragflügel mit Spoiler
ISL-Bericht CO 243/84 (1984)

[12] MEYER, P., KAUFFMANN, R., KOERBER, G.
Theoretische Untersuchung der Karman'schen Wirbelstraße. Anwendung auf die experimentelle Unersuchung der Umströmung eines dicken Objektes.
ISL-Bericht R 105/85 (1985)

GROUPS CONTACTED IN GERMANY AND FRANCE

University of Aachen (RWTH)	(Prof. Peters)
German Aerospace and Research Establishment (DFVLR)	(Dr. Meiburg, Prof. Oertel)
German French Institute (ISL)	(Dr. Jaeggy, Dr. Vogel)

INSTITUTION	METHOD	PROBLEM
RWTH Aachen [8,9,10]	Random Vortex	Shear Layer Trailing Far Wake
DFVLR [5,7]	Filaments	Vortex Ring Shear Layer Wake
ISL [11,12]	Point Vortex	Cylinder Wake Profile with Spoiler

SIMULATION OF IMPINGING SHEAR LAYERS USING VORTEX DYNAMICS

Argyris G. Panaras
Defense Industries Directorate (YPOVI)
Holargos, Athens, Greece

SUMMARY

Organized vortices have been observed within the oscillating shear layers that impinge on a surface. It is believed that the feedback force necessary for the generation of these vortices is produced by their interaction with the reattachment surface. In the present work models for studying the interaction of line or of finite-area vortices with edges that simulate cavity-type of flows or edge-tones are examined. According to the analysis, the interaction of vortices with an edge induces periodic pressure fluctuations similar to those measured in oscillating flows. Also, when the geometry of an edge is such that no oscillation has been observed, the amplitude of the induced pressure pulses is insignificant. Thus, the hypothesis about the role of the vortex/edge interaction is supported.

1. INTRODUCTION

The self-sustained oscillations of an impinging shear layer is a well known phenomenon that appears to a variaty of applications, such as about slots betwee the moving parts of control surfaces of aeroplanes, hydraulic gates and spiked cones of re-entry vehicles. Experimentally it has been found that in such a flow, the shear layer that impinges on a surface may oscillate periodically. This oscillation leads to emission of strong acoustic radiation, to an increase of the drag and heat transfer (in case of high speeds) and, possibly, to vibrations of the local structure.

Rayleigh (1) has been the first to describe the feedback cycle leading to the establishment of self-sustained oscillations of impinging shear flows. He mentions that when an instability wave leaving an upstream plate reaches a downstream plate, it is unable to pass with freedom and a pressure fluctuation is thrown back to the upstream plate, where it gives rise to further instability waves. Under appropriate circumstances, this cyclic process is self-sustained and resonance occurs. Furthermore, the classical pictures of Brown (2) revealed that in an edge-tone system vortices are shed periodically near the separation point and travel downstream towards the edge. Periodic vortices were also detected in a cavity flow by Rossiter (3), who speculated that they are shed at the upstream corner in sympathy with the pressure oscillation produced by interaction of the vortices with the downstream corner.

The contemporary views are well summarized by Rockwell (4):"for most of these oscillations to be self-sustained, a chain of events must occur: impingement of organized vorticity fluctuations upon the edge/surface; resultant upstream influence (interpreted as Biot-Savart induction or upstream pressure waves); conversion of disturbances incident upon the region of the shear layer in the vicinity of the separation edge to velocity fluctuations within the shear layer; and amplification of these fluctuations in the streamwise direction". Visualization pictures taken from the papers of Ziada & Rockwell (5) and of Rockwell & Knisely (6) are shown in figure 1 for an edge-tone and for a cavity flow.

Concerning the theoretical investigation of the conversion of the pressure perturbations at the shear-layer separation to vorticity fluctuations within the shear layer, to our knowledge, little has been done. Rockwell & Naudascher (7) mention that according to an experimental analysis of Morkovin, the back and forth motion of the flow detachment point allows the transformation from irrotational pressure to rotational vorticity pertur-

bations. In many theoretical studies, this element of the feedback mechanism is modelled by its result: the periodic shedding (or release) of vortices from the origin of the shear layer. Then various characteristics of the feedback cycle can be studied.

Typical examples of application of the above mentioned technique are those of Curle (8) and of Rossiter (3), that were able to derive formulas for the frequency of oscillation and explained the jumps it presents, by simulating the shear layers by successions of point vortices released from the origin of an edge-tone system or from the upstream lip of a cavity, correspondingly. In these models the succession of the vortices is "frozen". However, for the study of the other basic element of the feedback mechanism, i.e. the generation of the periodic pressure fluctuations at the reattachment edge, the kinematics of the vortices and their dynamic effects must be considered.

For the above task appropriate modelling of the flow is necessary. The replacement of the finite size vortices by single point (discrete) vortices is an approximation that has been applied successfully in many vortex/surface interactions. Then the techniques of complex variables allow the calculation of the trajectories of the discrete vortices. These trajectories are qualitatively similar to those of the centroids of the finite size vortices (Saffman & Baker, 9), unless the vortices pass very close or impinge on the surface (Rockwell & Knisely, 6). Some typical examples of application of this method are reviewed by Saffman & Baker.

The necessity of concidering or not the finite-area of the vortices in a vortex surface interaction has been addressed recently by the present author (Panaras, 10). Simulating the vortex/airfoil interaction by both techniques he found that for relatively large distances of the interacting vortex from the surface of the airfoil the single point-vortex technique provides results similar to those of the finite-area method. However, when the distance of the vortex from the surface of the airfoil is small its shape is distorted and the induced pressure pulses have smaller amplitude than the ones induced by an equivalent point vortex. In the limit, where the vortex impinges on the leading edge of the vortex, it is split into two and the time-dependent pressure pulses even take negative values at some parts of their period.

For the specific case of the impinging shear layers, Conlisk & Rockwell (11) were the first to apply the technique of the point vortices for the successful calculation of the pressure fluctuations induced on a corner by a single line vortex or by patterns of vortices, similar to those observed experimentally. Also, the present author applied this technique for studying the effect of the geometry of the reattachment edge on the amplitude of the pressure pulses induced by a single point vortex (Panaras, 12). Furthermore,he has studied the case of the interaction of a succession of discrete vortices with surfaces, that simulate an edge-tone or a cavity-type flow, and he has shown that some critical features of the instability cycles can be explained by the dynamic effects of the vortices (Panaras, 13). In the latter case the finite-area of the interacting vortices has been considered. To this purpose, the classical technique involving sheets of point vortices is used, properly modified. In the present paper the work of the author in the simulation of shear layers impinging on edges will be reviewed.

2. DESCRIPTION OF THE MODEL

The method of complex transformations will be used in the present work. The curve that defines the geometry of any particular edge in the z-plane will be transformed, by means of a transformation function $z=f(\lambda)$, into a segment of the horizontal axis in the transformed λ-plane. Then, it is easy to estimate the velocity potential. For the application of the method, the simulated vortical structures will be released periodically from the "origin" of the flow at a predetermined frequency. If each vortical structure is composed of N discrete vortices, each of Γ strength, the complex velocity potential at a

point λ in the transformed plane, is:

$$F(\lambda) = U_\infty \lambda + \frac{i\Gamma}{2\pi} \sum_{n=1}^{N} \ln(\lambda-\lambda_n) - \frac{i\Gamma}{2\pi} \sum_{n=1}^{N} \ln(\lambda-\bar{\lambda}_n) \tag{1}$$

The velocity field induced on a point z in the physical plane is given by:

$$u(z)-iv(z) = \frac{dF}{d\lambda} \frac{1}{f'(\lambda)} = \left[1 + \frac{iK}{2\pi} \sum_{n=1}^{N} \frac{1}{\lambda-\lambda_n} - \frac{iK}{2\pi} \sum_{n=1}^{N} \frac{1}{\lambda-\bar{\lambda}_n}\right] \frac{1}{f'(\lambda)} \tag{2}$$

In equation (2), $f'(\lambda)$ is the first derivative of the function, the velocities have been non-dimensionalized on U_∞, the lengths on an appropriate length a, and $K=\Gamma/aU_\infty$.

For the calculation of the velocity of a vortex located at a point z_j Routh's rule must be used leading to:

$$u_j - iv_j = \left[1 + \frac{iK}{2\pi} \sum_{\substack{n=1 \\ n\neq j}}^{N} \frac{1}{\lambda_j-\lambda_n} - \frac{iK}{2\pi} \sum_{n=1}^{N} \frac{1}{\lambda_j-\bar{\lambda}_n}\right] \frac{1}{f'(\lambda_j)} - \frac{iK}{4\pi} \frac{f''(\lambda_j)}{[f'(\lambda_j)]^2} \tag{3}$$

The trajectory of any vortex in the flow will be estimated by solving numerically, at successive time steps, Δt, the equations:

$$\frac{dx_j}{dt} = u_j(x_j, y_j)$$

$$\frac{dy_j}{dt} = v_j(x_j, y_j) \tag{3a}$$

Since the velocity components u_j, v_j are given in terms of the variable λ_j inversion of the transformation $z=f(\lambda)$ is necessary. In some of the transformations that will be used this inversion is straightforward, but in some others a numerical solution will be applied.

For the estimation of the periodic pressure fluctuations induced on an edge by a succession of vortices, the following pressure coefficient, that contains only the effect of the vortices and not of the parallel stream, will be applied:

$$c_p = \frac{(p_k - p_\infty) - (p - p_\infty)}{q_\infty} = (u^2+v^2) - (u_k^2 + v_k^2) - \frac{\partial\varphi}{\partial t} \tag{4}$$

Equation (2) is used for the calculation of the velocity components u, v, assuming that there is no vortex in the flow ($K=0$), while the components u_k, v_k include the vortex term ($K\neq 0$).

The term $\partial\varphi/\partial t$ in equation (5) denotes the non-dimensional unsteady potential function:

$$\varphi = R(\lambda) + \frac{K}{2\pi}\left[\sum_{n=1}^{N} \arg(\lambda-\bar{\lambda}_n) - \sum_{n=1}^{N} \arg(\lambda-\lambda_n)\right] \tag{5}$$

The time-dependent pressure coefficient will be calculated on some specific points along the various edges that will be studied.

3. INTERACTION OF A VORTEX WITH AN EDGE OF VARIABLE GEOMETRY

3.1 Suppression of cavity-type oscillations

The term "cavity-type" used in this work applies to bodies similar to those shown in figure 2. They are characterized by the existence of a planar or an axisymmetric mixing layer, which envelops the separation area formed between the leading and the trailing edge. The possibility of suppressing, or even eliminating, the self-induced oscillations of the shear layer by various techniques in a common characteristic of cavity-type bodies. All the bodies of figure 2 are included in the classification of Rockwell & Naudascher (7) except for the axisymmetric concave body: however, one of the two modes of instability that have been observed when the high-speed flow about a concave body is unsteady is similar to the classical oscillation of the cavity flows (Panaras 14). The techniques which have proved successful for the suppression of the oscillation of the flow about a cavity or about a concave body are similar.

In the case of the cavities, the majority of the experimental work concerns appropriate modifications of the geometry of the rectangular cavity. These modifications have been applied to the leading or to the trailing edge of the cavity, or to both. The rounding of the lip or the use of ramps or offsets (figure 3) are the main changes to the trailing edge tested. The tests have been performed in incompressible or supersonic flows. All of these modifications have attenuated, to an extent, the amplitude of oscillations; the use of offsets being the least successful. The most comprehensive studies are those of Ethembambaoglu (15), Franke & Carr (16) and Heller & Bliss (17). Rossiter (3) has found that installation of leading-edge spoilers is very effective in reducing the magnitude of the pressure fluctuations.

The problem considered in this paper is closely related to the shear-layer oscillations between the main stream and the plenum chamber of an open jet of a ventilated (slotted or perforated) wind tunnel. Mabey (18) demonstrated how the shear-layer oscillations could be attenuated, either by covering the slots with flat perforated screens or by rounding the downstream corner of the plenum chamber at the entry to the diffuser.

To conclude, according to the experimental evidence, the self-induced oscillations of the flow about a body similar to one of those shown in figure 2, may be attenuated if:

(a) The shoulder of the reattachment edge is rounded or, if sharp, has a small inclination angle or even lies below the leading edge (for cavities).

(b) The shear layer is tripped by means of spoilers, sand, etc.

Concerning the role of the tripping, it will be assumed in this paper that, by affecting the state of the otherwise laminar shear layer, the large-scale vortices formed have less energy. Indeed as Roshko (19) points out, much of the evidence suggests that any important effects of Reynolds number appear indirectly through conditions affecting transition rather than through the direct action of viscosity on the developing turbulent structure. Browand & Latigo (20), studying the effect of the initial boundary layer upon the downstream growth of the turbulent mixing layer between two streams, concluded that if the mixing layer is tripped by a wire its large-scale structures are relatively suppressed. Kibens (21) also observed the absence of highly energetic discrete vortices in the shear layer which envelops the potential core of a jet, if the shear layer is turbulent. Finally, Chandrsuda et al. (22) mention that recent experiments strongly suggest that the Brown-Roshko structures will not form if the initial mixing layer is turbulent.

In the next section a simple, incompressible and two-dimensional model will be described for the study of the interaction of a discrete vortex with a reattachment edge. The shape of the edge will be variable. Thus, the effect of the geometrical parameters which, if they are of proper value, stabilize the otherwise oscillating shear layer,will

be studied. Considering the existence of a common mechanism that induces the shear-layer oscillation, it is assumed that the results of the present analysis are applicable, qualitatively, to all the cavity-type bodies of figure 2.

3.1.1 Interaction of a vortex with a ramp

For the study of the interaction of a vortex with a ramp of angle α (figure 4) the following Schwarz-Christoffel transformation (Spiegel, 23) may be used:

$$z = C\int_0^{\lambda} \frac{g^{2\alpha/\pi}}{(1-g^2)^{\alpha/\pi}}\, dg + ib \tag{6}$$

The value of C can be expressed in terms of the gamma function using the fact that $z=a$ when $\lambda=1$. It is found that:

$$C = \frac{(a-bi)(\pi)^{\frac{1}{2}}}{\Gamma(\frac{\alpha}{\pi}+\frac{1}{2})\Gamma(1-\frac{\alpha}{\pi})} \tag{7a}$$

Considering various properties of the gamma function and setting $\delta=\alpha/\pi$, it can be shown that:

$$C = b\,\frac{\Gamma(\frac{1}{2})\Gamma(\delta)}{\pi\Gamma(\frac{1}{2}+\delta)}\, e^{-i\alpha} = \frac{b}{\pi}\, B(\tfrac{1}{2},\delta)e^{-i\alpha} \tag{7b}$$

If $g=\lambda t^{\frac{1}{2}}$ and z is non-dimensionalized by b, the transformation (6) becomes:

$$z = \frac{B(\frac{1}{2},\delta)}{2\pi}\, e^{-i\alpha}\, \lambda^{(1+2\delta)} \int_0^1 t^{(\delta-\frac{1}{2})}\, (1-\lambda^2 t)^{-\delta}\, dt \tag{8}$$

For the calculation of this integral the hyporgeometric Gauss series included in the tables of Abramowitz & Stegun (24) are used. This series is defined by the equation:

$$F(d,e;\, f;\, h) = \frac{\Gamma(f)}{\Gamma(e)\Gamma(f-e)} \int_0^1 t^{e-1}(1-h^{(f-e-1)}(1-ht)^{-d}\, dt \tag{9}$$

The hypergeometric series is valid for $Re(f) > Re(h) > 0$ and for all values of h, except for a cut along the real axis from 1 to ∞. Its expression depends on the value of $|h|$:

for $|h| \leq 1$:

$$F(d,e;f;h) = 1 + \frac{de}{f1!}\, h + \frac{d(d+1)e(e+1)}{f(f+1)2!}\, h^2 + \ldots \tag{10}$$

for $|h| \geq 1$:

$$F(d,e;f;h) = \frac{\Gamma(f)\Gamma(e-d)}{\Gamma(e)\Gamma(f-d)}\, (-h)^{-d}\, F(d,d+1-f;d+1-e;\tfrac{1}{h}) + \frac{\Gamma(f)\Gamma(d-e)}{\Gamma(d)\Gamma(f-e)}\, (-h)^{-e}\, F(e,e+1-f;e+1-d;\tfrac{1}{h}) \tag{11}$$

For the application of the hypergeometric series on the transformation (8) the following equivalence is used:

$$d = \delta, \quad e = \delta+\tfrac{1}{2}, \quad f = \delta+\tfrac{3}{2}, \quad h = \lambda^2$$

The final result, after several manipulations, is:

for $|\lambda| \leq 1$.

$$z = i + \frac{B(\frac{1}{2},\delta)}{\pi}\, e^{-i\alpha}\lambda^{(1+2\delta)}\left[\frac{1}{1+2\delta} + \sum_{n=1}^{\infty} \frac{\delta(\delta+1)\ldots(\delta+n-1)}{n!\,(2n+1+2\delta)}\, \lambda^{2n}\right]; \tag{12}$$

For $|\lambda| \geq 1$:

$$z = \frac{B(\frac{1}{2},\delta)}{\pi}\, \lambda\left[1 - \sum_{n=1}^{\infty} \frac{\delta(\delta+1)\ldots(\delta+n-1)}{n!\,(2n-1)}\, \frac{1}{\lambda^{2n}}\right]. \tag{13}$$

For the numerical calculation of the above series for any value of the angle parameter δ it is sufficient to consider only a few terms. The transformations are very accurate everywhere except at the region of $|\lambda| = 1$. Also, the derivatives are easily estimated. These transformations are developed for the first time in this work:

If $a \to 0$, $\alpha \to \frac{\pi}{2}$, and (6) is reduced to:

$$z = i - i \int_0^{\lambda} \frac{q\,dq}{(1-q^2)^{\frac{1}{2}}} = (\lambda^2-1)^{\frac{1}{2}}. \qquad (14)$$

This equation has also been used because of its simplicity.

For the inversion of the transformation, the complex and the real part are separated and then the resulting system of equations is solved numerically by applying the method of Newton described in the algorithm (2.13) of Conte & de Boor (25). Difficulties in finding the zeros of the system of equations have been experienced at some points near the origin of the axis for $\alpha > 60°$.

A typical example of the application of the present method to the calculation of the interaction of a discrete vortex with a ramp is shown in figure 5. The dashed line denotes the trajectory of the vortex, while the numbered solid lines indicate the value of the pressure coefficient at the correspondingly numbered points of the ramp.

It is observed in figure 5 that, as the vortex approaches the ramp, the induced pressure on its surface increases, initially very slowly, and then it rises rather abruptly when the vortex reaches the vicinity of the ramp. After reaching the maximum value the pressure pulse on each point starts to fall. The amplitude of the pressure pulses is quite small at the base of the ramp, but it becomes very large at its shoulder.

The small discontinuities observed in some curves are due to the shifting of the calculation from one branch of the transformation function (equation 13) to the other (equation 12). This shifting takes place at the point $|\lambda_0| = 1$, where the transformation is not very accurate.

3.1.2 Interaction of a vortex with an ellipse

The ellipse is quite an appropriate geometrical figure for the study of the interaction of a vortex with a curved surface. It is easily transformed into a piece of straight line on the λ-plane by using an intermediate transformation into a circle on the q-plane (figure 6).

The intermediate transformation of the ellipse into the circle, non-dimensionalized by b, is:

$$z = p\left(q + \frac{q}{q}\right), \qquad (15)$$

where:

$$p = \frac{A+1}{2A}, \quad q = \frac{A-1}{A+1} A^2, \quad A = \frac{a}{b}.$$

The transformation of the circle into the straight line is:

$$\lambda = \frac{1}{2}\left(q + \frac{1}{q}\right). \qquad (16)$$

Then the required transformation function $z = f(\lambda)$ and its derivatives are found to be:

$$z = p\left[\lambda + \sqrt{(\lambda^2-1)} + \frac{q}{\lambda + (\lambda^2-1)^{\frac{1}{2}}}\right]; \qquad (17)$$

$$f'(\lambda) = \frac{p}{q-\lambda}\,\frac{q^2-q}{q}; \qquad (18)$$

$$f''(\lambda) = p\frac{(g^2-2g\lambda+g)}{(g-\lambda)^3} \quad . \tag{19}$$

The numerical calculation of a point z_n, is easily done in steps, separating the real from the imaginary part, if the corresponding point λ_n, in the λ-plane, is known.

3.2 Application of the method

The various parameters that have been found experimentally to affect the behaviour of the flow about a cavity-type body will be examined in this section, by using the mathematical model described previously. These parameters are: the shape of the reattachment edge; the initial y-coordinate; and the strength of the vortex.

According to Conlisk & Rockwell (11) the range of the non-dimensional strength of vortices generated in cavity flows in laboratory experiments is K=0.1-0.6. These values will be used in the present work.

3.2.1 Effect of the shape of the edge

The optimization of the shape of the reattachment edge has been found to be the most effective means of suppressing the self-excited oscillations. A ramp of small angle is a very efficient shape in this sense. In figures 5 and 7 the trajectories of a vortex of strength K=0.5 and the induced pressure fields along ramps of 30°and 90°angles, respectively, are shown.

When comparing figures 5 and 7 one may see that, if the ramp angle increases, the trajectory of the vortex approaches the edge and the induced pressure pulses at the shoulder increase abruptly. Thus, for α = 90° the amplitude of the pressure pulse at point 5 of the ramp is almost an order of magnitude higher than the amplitude at the equivalent point of a ramp with α = 30°. It is noted here that, according to the experimental evidence, the flow about cavities equipped with reattachment ramps of α = 30° is steady, while the flow about regular rectangular cavities oscillates.

In all cases shown in the aforementioned figures, the amplitude of the pressure pulses is significant only at the edge of the ramp, while it has low values at its base. This feature suggests that for the suppression of the self-excited oscillations of the flows about the bodies shown in figure 2, it is sufficient to optimize only the lip of the reattachment surface and not its base. This rule has already been empirically applied in various experimental studies.

The small value of the width of the pressure pulses at the lip of the edge is another remarkable feature of the pressure field (figures 5,7). For example it is seen in figure 7 that, if the vortex lies upstream of the edge at a distance equal to its height (x = -1.0), the induced pressure is reduced to half of its maximum value. If the vortex lies further upstream, at x = -2.0, its contribution to the pressure pulses is only one-sixth of the maximum value. Thus, the contribution of a vortex to the induced pressure field at the edge is reduced very abruptly when its distance from the edge is increased. If a row of vortices is considered, it seems then that a small spacing or wavelength λ is required for the production of discrete pulses. In this case the mean value of the pulses will be greater, because of the contribution of the other vortices.

For the study of the effect of a curved edge on the amplitude of the induced pressure pulses, two cases of vortex-ellipse interactions are shown in figures 8,9 for ratio of ellipse axis equal to 1.0 and 3.0. In both cases the strength of the vortex is K=0.5.

It is remarkable that, though in these figures a rather broad range of curvature of the lip of the reattachment surface is represented, nevertheless the amplitude of all the pressure pulses is very small compared to the ones of the rectangular cavity (figure 7).

Their maximum value is about equal to the one observed on the ramp of $\alpha = 30°$.

3.2.2 Effect of geometrical offsets

The lowering of the trailing edge of a rectangular cavity is one technique effective to some degree in attenuating the shear-layer oscillations, though not so successful as the use of ramps or the rounding of the edge. Ethembabaoglu's (15) experimental data lead to an estimation of a 30% reduction of the cavity pressure fluctuations for a 20% offset of the leading edge.

For studying this effect here, the initial vertical distance of the vortex is used as a parameter. The results of such a calculation are shown in figure 10. It is observed that the amplitude of the pressure pulses depends strongly on this parameter. More specifically, if the vortex initially lies below the lip of the edge ($y_0 < 1.0$) the pressure amplitude is greater than when it lies above the lip ($y_0 > 1$). It is noted in figure 10 that the rate of change of the amplitude of the pressure is higher for values of $y_0 < 1$.

The curves of figure 10 indicate that the forcing mechanism has small intensity when, according to the experimental evidence, the amplitude of the oscillations is small. It is also seen that, in the case of the rectangular cavity, the level of the forcing function does not reach the low values observed in the oscillation-free case of the ramp of 30°, even if the offset distance of its leading edge takes very high values ($y_0 = 1.4$).

However, it is evident that, if the trailing edge has the shape of a ramp, the application of offset may have a more profound effect on the suppression of the oscillations.

3.2.3 Effect of the strength of the vortices

The strength of the interacting vortices is a basic parameter of the present model. Its effect on the induced-pressure pulses is shown in figure 11 for the case of the vertical plate ($\alpha = 90°$). It is observed that, if the strength of the vortices is small ($K = 0.10$), the pressure pulses have the same order of magnitude as those induced on an oscillation-free configuration (a small-angle ramp or an ellipse) but with vortices of much higher strength.

As has already been mentioned in §3.1, it may be assumed that small values of the strength of the discrete vortices may simulate the existence of spoilers in an appropriate position of a rectangular cavity or of a concave axisymmetric body. These mechanisms have proven quite effective in reducing the oscillations. The results of figure 11 seem to enforce the hypothesis concerning the role which the spoilers play in the reduction of the oscillations. Still, comprehensive laboratory measurements are required to validate this evidence.

3.3 Discussion and conclusions

The strong dependence of the pressure pulses, that are generated by the vortex-edge interaction, on the specific shape of the edge is the main conclusion of the present analysis. More specifically, it has been found that the induced pressure pulses on ramps of small angle or ellipses have very small amplitude, even for large values of the strength of the interacting vortices. On the other hand, the pressure amplitude on steep ramps is very large.

Also, it has been shown experimentally that the flow about the cavity-type bodies shown in figure 2 is steady when their trailing edge has the shape of a ramp of small angle or when it is rounded, while the flow is oscillating when the ramp angle is large.

The above comparison indicates that, for the establishment of sustained oscillations in a cavity, the existence of a periodic feedback force of certain value is neces-

sary. To explain this, resource to the experimental evidence is required. To our knowledge no one has studied experimentally the effect of the geometry of the reattachment edge of a cavity on the development of the structure of the shear layer.

However, detailed studies have been performed on the influence of sound excitation of variable amplitude, at a discrete frequency, on enhancing the organization of a free-shear layer. Experimental evidence seems to support the view that similarity exists between these types of flow. This similarity was discovered by Rockwell & Knisely (6) when they compared the velocity spectra with and without insertion of the reattachment edge of a cavity, to those measured by Miksad (26) in a non-impinging shear layer with and without application of sound at a discrete frequency.

Clear evidence of the role of the level of acoustic forcing in the development of a laminar low-speed shear layer has been provided by Freymuth (27). He has discovered that, the lower the level of forcing, the longer is the length of the shear layer required for the growth of the instabilities to the saturation limit and, consequently, for the appearance of organized vortices.

A similar conclusion was reached very recently by Gharib (28). One of the objectives of his investigation was to study the receptivity of a cavity shear layer to externally imposed disturbances, for a cavity length less than the one required for the onset of self-sustained oscillations. His flow-visualization pictures showed that, while in the oscillation mode periodic vortices are produced near the reattachment edge, in the case of the steady flow no vortices are observed. Gharib applied variable forcing at various frequencies. Spectral analysis of the response-velocity fluctuations indicated that the level of shear-layer response at all the frequencies increased with the forcing power. But, when the forcing reached a threshold level, resonance appeared at the forcing frequency in which the shear-layer satisfies the phase criterion ($L=\lambda n$, λ: wave length, n:mode number). When he increased the length of the cavity, Gharib observed that the resonance peak appeared at a lower forcing level, an indication that the threshold level decreases as the length of the cavity increases.

Gharib (28) concludes that it is logical to propose that, as the cavity length increases, the threshold level decreases to such an extent that a flow background frequency, which satisfies the phase criterion and has sufficient amplitude, will initiate the self-sustained oscillation.

It is concluded then that, in view of the present analysis, it seems that the oscillations are initiated and sustained by the periodic pressure pulses induced by the vortex-edge interaction, provided that the geometry of the edge is such that the amplitude of the pressure pulses is sufficient.

4. INTERACTION OF A SUCCESSION OF VORTICES WITH AN EDGE

In this section a model will be presented for the simulation of interactions similar to those shown in figure 1, where the interacting shear layer is transformed in well developed vortices. According to the experimental evidence, when a vortex approaches an edge or a corner, it may pass above the surface, or it may inpinge on it and be split into two. Modelling of the latter possibility is not easy by any step or block transformation that can be used for the simulation of a cavity-type flow. That, because while, in a real cavity flow (figure 1) the vortices pass above a "dead air" region, in a numerical simulation the vortices will be embedded within a parallel stream that extends down to the horizontal axis; hence, even if the simulated succession of vortices initially lies very near this axis, still no splitting of the vortices will happen (figure 12b). On the contrary, if an edge is used as the impingement surface of the model, splitting of the vortices is possible, because any element of a vortex that lies below the horizontal axe will pass below the edge (figure 12a).

For the forementioned reasons, an edge will be used primarily in the present model, as an impingement surface, while a step will be used in a limited number of applications, for demonstrating the global character of the mechanism that induces the feedback pressure waves.

The appropriate modelling of the Kutta condition, which requires finite values of the pressure in the vicinity of the tip of an edge, is another numerical difficulty. This may be accomplished by releasing additional vorticity at the tip; a procedure that is rather difficult in practice. Recently, Kaykayoglu & Rockwell (29), based on their experimental results, according to which the pressure amplitude is maximum at the tip, suggest that inviscid modelling should not incorporate a leading-edge Kutta condition. Instead, a singularity at the tip would seem to be most representative of the real conditions. In the present work the issue of the Kutta condition is overcome by selecting an edge of finite thickness as an impingement surface.

Concerning the modelling of the impinging vortices, an array of discrete vortices will be used for the simulation of their finite-area. Initially, each vortex will be represented by a disturbed vortex sheet of finite thickness composed of four rows of discrete vortices. The origin of this technique goes back to Rosenhead (30) and to Acton (31), who have studied the stability of a semi-infinite vortex sheet. The present author (Panaras, 10) applied this technique for the study of a vortex/airfoil interaction. He has shown that the deformation of the vortices, due to the interaction with the surface, and their possible split, if they impinge on the leading edge, can be efficiently simulated by this technique.

The modelling of the secondary vortices, which may be formed along the edge, if the primary vortices are strong enough to separate the boundary layer, is another critical issue. It is very difficult to treat numerically this secondary shedding, as a truly self-generated phenomenon (Rockwell, 4). This feature of the real flows will not be included in the present model. Considering the fact that when a secondary vortex appears, it is nested within the primary vortex (Rockwell et al, 32), it is expected that the impact of this approximation will not be significant in the present case, where the induced pressure fluctuations will be estimated only in one point. For applications involving the distribution of the pressure fluctuations along the surface of the edge, the impact of this approximation may be serious.

A symmetrical Joukofski airfoil will be used for studying the vortices/edge interaction. The following successive transformations transform the flow about a symmetrical airfoil into the flow about a line segment on the λ-plane (figure 12a):

$$z = (g+b) + l^2/(g+b) \tag{20}$$

$$\lambda = g+a^2/g \tag{21}$$

where l and b are parameters that define a particular airfoil and a is the radius of the basic circle into which the airfoil is transformed at the g-plane. The radius a will be used for the non-dimensionalization of the various length parameters. The particular airfoil used in this work is defined by the parameters: l=0.9, b = 0.1.

The main parameters for the application of the present model are: the distance, L, between the point of release of the distributed vorticity str..ctures and the edge, the spacing, λ, of the released vortices, and the vertical offset of the edge relative to the centroids of the vortices. The distance L simulates the length of the shear layer before the impingement. In all the cases the vortices will be released one by one from the initial point (-L, offset), with a spacing corresponding to the relation: λ=Ln, where n is the mode number.

In most of the cases a typical non-dimensional length equal to L=5 will be used. Also, a standard value K=0.45 will be given to the non-dimensional strength of the vortical structures. This particular value has been selected because in this case, at the time the released vorticity distributions reach the edge, their rolling up has been completed and they have been transformed into rounded vortices.

4.1 Effect of the offset distance

For examining the effect of the offset distance of the edge on the amplitude of the pressure pulses that are induced on it, four cases of interaction are shown in figure 13 for the successive values: offset = -0.4, -0.2, 0, 0.4. The mode number in this case is n=2. In figure 13a, the offset of the vortices is such that they just pass above the upper surface of the airfoil without touching it. In figure 13b the vortices impinge on the edge and a part of them passes below the edge. In figure 13c the centroids of the vortex structures lie on the horizontal axis, so they are split into two equal parts when they impinge on the leading edge of the airfoil. In figure 13d the vortices pass below the edge.

Referring to figure 13a, for explaining the data shown in each figure, the wavy curve depicts the time-dependent pressure fluctuation at a point A of the leading edge of the airfoil. A part of the pressure fluctuation is shown, that corresponds to the time required for a released vortical structure to reach the leading edge of the airfoil. Also, in each figure the level of the zero-value of the pressure coefficient is given, plus the maximum amplitude of the pressure waves. In all the figures a "picture" of the vortices is shown at the time the calculation of the pressure coefficient terminates. The mark of the origin of the flow in this and all the other figures is schematic; there is no upstream plate in the flow.

A review of the evolution of the vortical structures in the various cases shown in figure 13, shows that the present model simulates very efficiently the real phenomenon. The rolling-up of the shear layer, the formation of the rounded vortices, their clockwise rotation, their deformation when they approach the edge, and their split if they impinge on the edge, are quite similar to the corresponding features of the laboratory vortices shown in figure 1. In addition, it is seen in figure 13b, c that the discrete vortices are moving tangentially at the trailing edge. Thus, it is not necessary to release additional vorticity at the tip of the trailing edge for fulfilling the unsteady Kutta condition. This subject is covered with more details in another paper (Panaras, 10).

Concerning the pressure fluctuations, it is observed that when the vortices are not split (figure 13a), they have the shape of smooth pressure waves that follow the frequency of the vortices. When the vortices split (figure 13b,c), peaks appear in the pressure fluctuations. The greater the part of each vortex, that passes below the surface of the edge, is, the more profound the change of the shape of the pressure waves becomes. Also, it is noted that the split of the vortices affects also the level of the mean pressure, which gradually falls to zero. At the last case where the vortices pass below the edge, the pressure fluctuations are negative. If these pressure waves are compared to those of figure 13a, it is seen that they have higher amplitude and a phase difference equal to π.

4.2 Effect of the spacing of the vortices

For studying the effect of the spacing of the vortices, in figure 14, the case of figure 13a is repeated but for mode numbers n=3,4. Comparison of these figures shows that when the spacing is increased, the mutual interaction forces of the vortices become greater. This is indicated by the change of the shape of the vortices. Besides, the smaller the spacing of the vortices is, the smaller the amplitude of the pressure waves becomes,

while the mean pressure is increased. The observed decrease of the pressure amplitude for increasing values of the mode number is very rapid. Between the 3rd and 4th modes the maximum pressure amplitude is reduced to a half. When the vortices pass below the edge, the pressure waves follow the same tendency (figure 15a). The pressure fluctuations remain almost invariant only when the vortices are symmetrically split upon impinging on the edge (figure 15b).

The above results are probably related to the fact that in a self-oscillating shear layer, there is a specific limit of the maximum mode of oscillation that can be established, for a constant length. It seems that this limit exists because, as the number of mode is increased, the amplitude of the feed-back force induced on the downstream edge becomes less than the one required for the generation of the large-scale vortices.

4.3 Effect of other parameters

The effect of the length of the shear layer on the amplitude of the pressure waves induced on an edge, is a basic parameter of the self-oscillating shear layers. For studying this effect, results of calculation are shown in figure 16 for a length L=2.5 and the 2nd mode. It is seen in this figure that whether the vortices pass above or below the edge, the amplitude of the pressure waves is smaller than the amplitude in the case of the greater length (L=5). No significant change in the amplitude is observed only when the vortices are split into two equal parts. If these results are extrapolated to the oscillating shear layers, they indicate, qualitatively, the following tendency: for the establishment of a specific mode of periodic oscillation, the shear-layer length should be greater than a minimum limit. The greater the mode number is, the greater the required shear-layer length becomes. This tendency is in agreement with the experimental evidence.

It is of practical importance to investigate the effect of jets or mixing layers to adjacent surfaces. For this, in figure 17 a case of relatively large offset distance is shown. It is seen that when the spacing of the vortices is relatively large (figure 17a), a significant vertical elongation of their shape is observed. This elongation is due to the strain imposed on the vortices by the non-uniform flow field. However, no elongation at all is observed when the vortices are closely spaced (figure 17b). Evidently, in this case the effect of the local velocity field has been offset by the mutual interaction forces of the vortices. Concerning the pressure fluctuations, they are seen to have the shape of smooth waves. While the mean value of these fluctuations is large, their amplitude is very small and it becomes almost insignificant when the spacing of the vortices is reduced. In view of these results it seems that a surface adjacent to a shear-layer feels a constant pressure, but for the appearance of a fluctuating pressure, the vortices must pass very near the surface.

For the completeness of the analysis, some examples of calculation are shown in figure 18 with the vortices impinging on the sharp edge of the airfoil. Both, the evolution of the vortices and the variation of the pressure fluctuations, at a point near the tip of the sharp edge, are observed to be very similar to the case of the finite thickness edge; the amplitude being higher in the latter case. However, the total force may be higher on the surface of a sharp edge, due to the large values of the induced pressure at the tip.

4.4 Interaction with a corner

For the simulation of a cavity-type flow, the following transformation, that transforms a step into a line (figure 12b), will be used:

$$z = f(\lambda) = \left[(\lambda^2-1)^{\frac{1}{2}} + \cos^{-1}\lambda\right] h/\pi \qquad (22)$$

In order to keep the velocity at the infinite on the transformed plane equal to the corresponding one on the physical plane, the value:h=π is given to the step height. Also, for the non-dimensionalization of the various lengths of the equations of section 2, the step height will be used.

The transformation (22) has been selected because the separation of the variables, as well as the calculation of the first and of second derivative are easily done. As it has been mentioned in section 2, for the estimation of the induced velocity field it is necessary to invert the equations:

$$x = F(\xi,\eta) \qquad y = G(\xi,\eta) \tag{23}$$

This inversion has been done numerically, by applying the Newton method described by Conte & de Boor (25).

As it has been mentioned in section 2, it is not possible to simulate numerically the observed tearing of a vortex when it impinges on a corner. Thus, in the present section only the case of the convection of a succession of vortices above the corner will be examined. In figure 19, calculations similar to those of figures 13a and 14a are shown. A comparison shows that the pressure fluctuations induced on the corner are similar to those induced on an edge. Thus, in the corner flow, also, smooth pressure waves are induced. Their amplitude decreases, while their mean value increases when the spacing of the vortices is decreased. Besides, comparison of the development of the vortices with the experimental ones shown in figure 1, indicates that in this case also,the model simulates efficiently the real phenomenon.

4.5 Discussion and conclusions

The applications of the present model in the previous sections, demonstrate its efficiency in simulating the basic features of the interaction of a shear layer with an edge or a corner. The stages of evolution of the vortices, from the initial state of a piece of distributed vorticity to the formation of rounded vortices that deform when they pass close to the interacting surface or are split, when they impinge on it, are quite similar to the corresponding stages of evolution of the laboratory vortices observed in the real shear-layer/surface interactions.

The time-dependent pressure fluctuations, that are induced on a point of the interacting surface, have the shape of smooth waves, when the vortices do not come in contact with the surface, or present subharmonics when the vortices impinge on the surface and are split. Comparison of the calculated pressure disturbances with available experimental data is necessary.

Appropriate data for such a comparison are that of Rossiter (3) and of Dunham (33), who have measured the time histories of the pressure fluctuations at a point within a cavity. In figure 20, the data of Dunham and some of the cases that Rossiter includes in his work are shown. For making easy the comparison, some of the cases of figures 13, 14 have been run again with different scales. These theoretical predictions are shown in figure 21. The similarity of the theoretical predictions with the experimental evidence is very clear in these figures. This similarity apart from validating the present model, enforces the hypothesis that the feedback force which excites a shear layer so that large vortices appear, is generated at the edge by the vortices/edge interaction.

Appropriate parametric application of the present method indicates that the amplitude of the pressure fluctuations depends strongly on the length of the succession of vortices,upstream of the edge, and on the frequency of emission of the vortices. This amplitude becomes smaller when the spacing of the vortices is decreased while the length remains constant, or when the length is decreased and the mode of emission of the vortices

($n=L/\lambda$) is constant. Besides, as it has been mentioned in the introduction, there is strong evidence that, for the excitation of a mixing layer to the level required for the onset of self-sustained oscillations, the amplitude of the applied feed-back force has to be greater than a threshold amplitude. These observations are useful in understanding the following features of a self-oscillating impinging shear-layer: when the length of the shear layer is constant there is a specific limit of the maximum mode of oscillation that can be established; on the other hand, when the shear-layer length is increased, a critical value is reached, above which the next mode appears.

A close examination of the various cases presented in this paper shows that though a vortex spacing, λ, conforming to the equation:$n=L/\lambda$ has been assumed for their estimation, the actual periodic cycles, m, of the pressure induced on the edge, during the motion of one specific vortex from the origin of the flow to the edge, are less than the mode number, n. The relation: $m=L/\lambda-\varepsilon$ is valid in any particular mode of oscillation. The constant ε approximately is equal to: $\varepsilon=1/4$. This relation is similar to the one found experimentally by Sarohia (34). The difference between the parameters n and m is due to the variation of the convection velocity of the vortices along their trajectory. These results indicate that the spacing of the generated vortices, in an self-oscillating impinging shear layer, probably is not constant, but rather, it presents a small variation.

REFERENCES

1. Rayleigh, J.W.S. The theory of sound. Dover Ed., Vol. 2, 1945.

2. Brown, G.B. 1937 The vortex motion causing edge tones. Proc.Phys. Soc. 49, 493-507.

3. Rossiter, J.E. 1964 Wind tunnel experiments on the flow over rectangular cavities at subsonic and transonic speeds. RAE Rep. and Memoranda No. 3438.

4. Rockwell, D. 1983 Oscillations of impinging shear layers. AIAA J. 21, 645-664.

5. Ziada, S. & Rockwell, D. 1982 Oscillations of an unstable mixing layer impinging upon an edge. J. Fluid Mech. 124, 307-334.

6. Rockwell, D. & Knisely, G. 1979 The organized nature of flow impingement upon a corner. J. Fluid Mech. 93, 413-432.

7. Rockwell, D. & Naudascher, F. 1979 Self-sustained oscillations of impinging free shear layers. Ann. Rev. Fluid Mech. 11, 67-94.

8. Curle, N. 1953 The mechanics of edge tones. Proc. Roy. Soc. ser. A, Vol. 216, p. 412.

9. Saffman, R.G. & Baker, G.R. 1979 Vortex interactions. Ann. Rev. Fluid Mech. 11, 95-122.

10. Panaras, A.G. 1986 Numerical modelling of the vortex-airfoil interaction. AIAA J. (to appear).

11. Conlisk, A.T. & Rockwell, D. 1981 Modeling of vortex-corner interaction using point vortices. Phys. Fluids 24, 2133-2142.

12. Panaras, A.G. 1985 Pressure pulses generated by the interaction of a discrete vortex with an edge. J. Fluid Mech., Vol. 154, 445-462.

13. Panaras, A.G. 1986. Shear layer-edge interaction: simulation by finite area vortices, Under preparation.

14. Panaras, A.G. 1981 Pulsating flows about axisymmetric concave bodies. AIAA J. 19, 804-806.

15. Ethembabaoglu, S. 1973 On the fluctuating flow characteristics in the vicinity of gate slots. Division of Hydraulic Engineering, University of Trondheim, Norway.

16. Franke, M.E. & Carr, D.L. 1975 Effect of geometry on open cavity flow-induced pressure oscillations. AIAA paper 75-492, AIAA 2nd Aero-Acoustics Conf., Hampton, Va., March 24-26.

17. Heller, H.H. & Bliss, D. 1975 The physical mechanism of flow-induced pressure fluctuations in cavities and concepts for their suppression. AIAA Paper 75-491, AIAA 2nd Aero-Acoustics Conf., Hampton, Va., March 24-26.

18. Mabey, D.G. 1971 Flow unsteadiness and model vibrations in wind tunnels at subsonic and transonic speeds. ARC CP 1155.

19. Roshko, A. 1976 Structure of turbulent shear flows: a new look. AIAA J. 14, 1349-1357.

20. Browand, F.K. & Latigo, B.O. 1979 Growth of the two-dimensional mixing layer from a turbulent and non-turbulent boundary layer. Phys. Fluids 22, 1011-1019.

21. Kibens, V. 1980 Discrete noise spectrum generated by an acoustically excited jet. AIAA J. 18, 434-441.

22. Chandrsuda, C., Mehta, R.D., Weir, A.D. & Bradshaw, P. 1978 Effect of free-stream turbulence on large structure in turbulent mixing layers. J. Fluid Mech. 85, 693-704.

23. Spiegel, M.R. 1964 Complex Variables. Schaum's Outline Series. McGraw-Hill.

24. Abramowitz, M. & Stegun, I.A. 1970 Handbook of Mathematical Functions. New York: Dover.

25. Conte, S.D. & De Boor, C. 1972 Elementary Numerical Analysis. An Algorithmic Approach. McGraw-Hill.

26. Miksad, R.W. 1972 Experiments on the nonlinear stages of free-shear transition. J. Fluid Mech. 56, 695-719.

27. Freymuth, P. 1966 On transition in a separated laminar boundary layer. J.Fluid Mech. 25, 683-704.

28. Gharib, M. 1983 The effect of flow oscillations on cavity drag, and a technique for their control. Ph.D. thesis, California Institute of Technology.

29. Kaykayoglu, R., and Rockwell D. 1985 Vortices incident upon a leading edge: instantaneous pressure fields. J. Fluid Mech., Vol. 156, 439-461.

30. Rosenhead, L. 1932 The formation of vortices from a surface of discontinuity. Proc. Roy.Soc. A134, 170-192.

31. Acton, E. 1976 The modelling of large eddies in a two-dimensional shear layer. J. Fluid Mech. Vol. 76, 561-592.

32. Rockwell, D., Kaykayoglu R., Sohn D., Kuo C.H. 1985 An assessment of some vorticity field-leading edge interactions. Winter Annual Meeting of ASME.

33. Dunham, W.H. 1962 Flow-induced cavity resonance in viscous compressible and incompressible fluids. Report ARC-73, Fourth Symposium on Naval Hydrodynamics, Vol. 3, ONR, 1057-1081.

34. Sarohia, V. 1977 Experimental investigation of oscillations in flows over shallow cavities. AIAA J. Vol. 15 984-991.

ACKNOWLEDGEMENT

The author wishes to thank Prof. D. Rockwell for his help in providing valuable data from his comprehensive investigation of the impinging shear flows.

1. Experimental examples of vortex/edge interactions (courtesy of Prof. D. Rockwell).

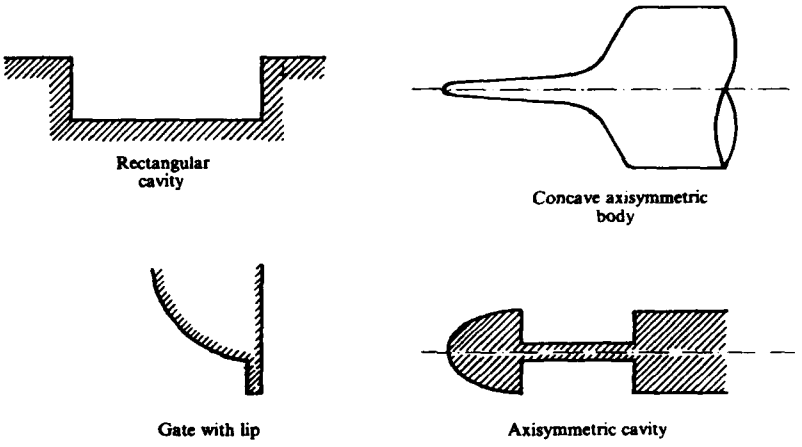

2. Cavity-type bodies.

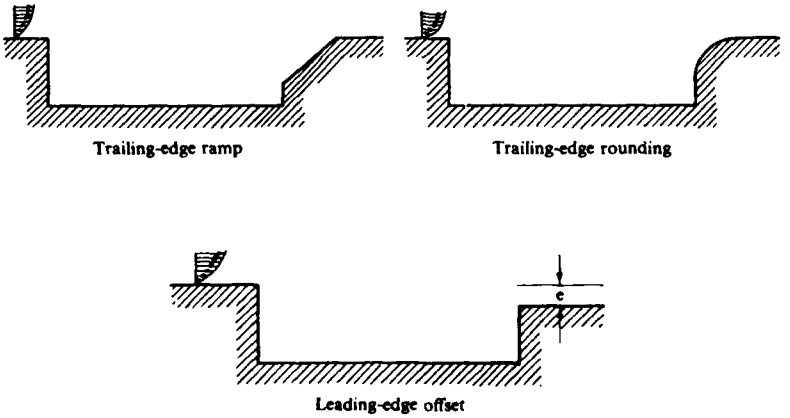

3. Geometrical variations of cavities for attenuation of oscillations.

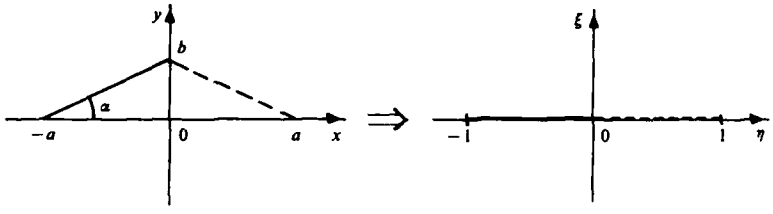

4. Transformation of a ramp.

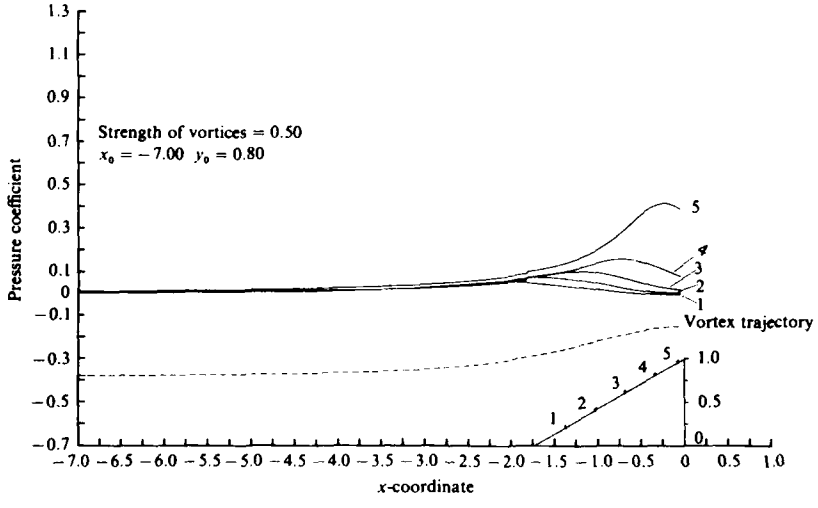

5. Pressure pulses along a ramp of 30^0.

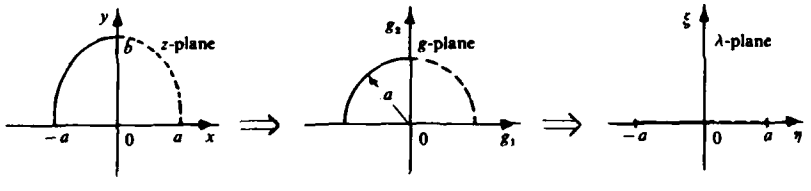

6. Transformation of an ellipse.

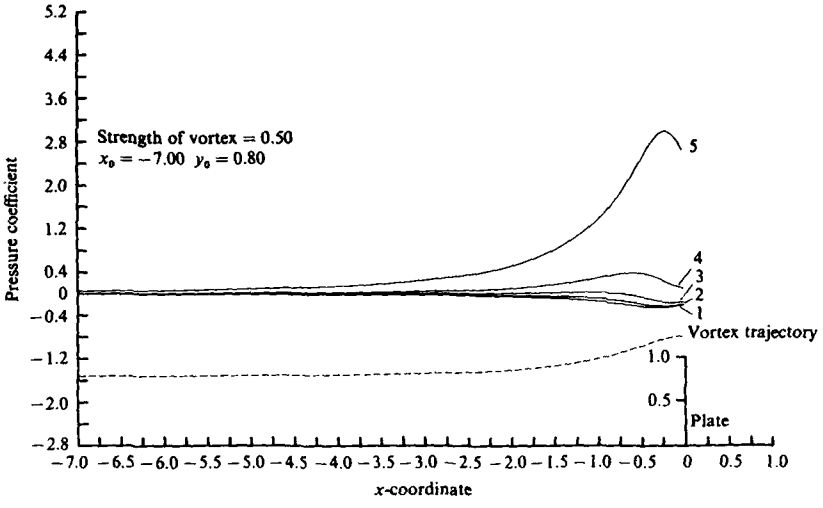

7. Pressure pulses along a ramp of 90^0.

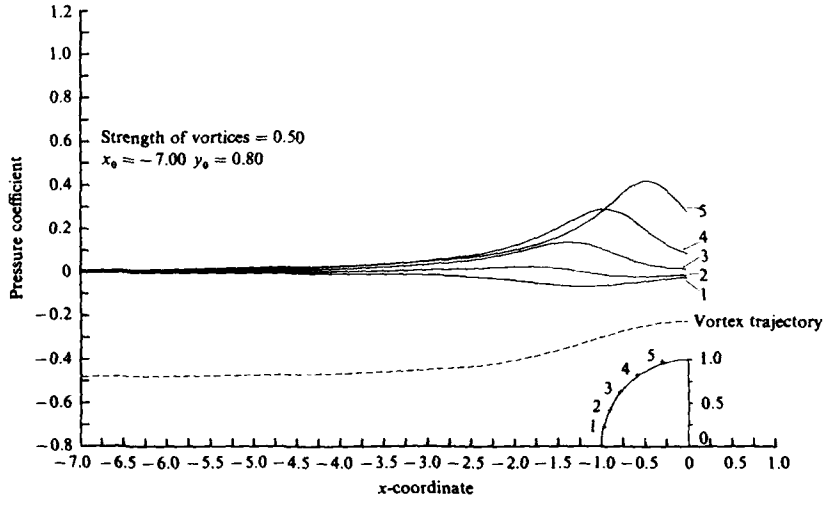

8. Pressure pulses along a circle.

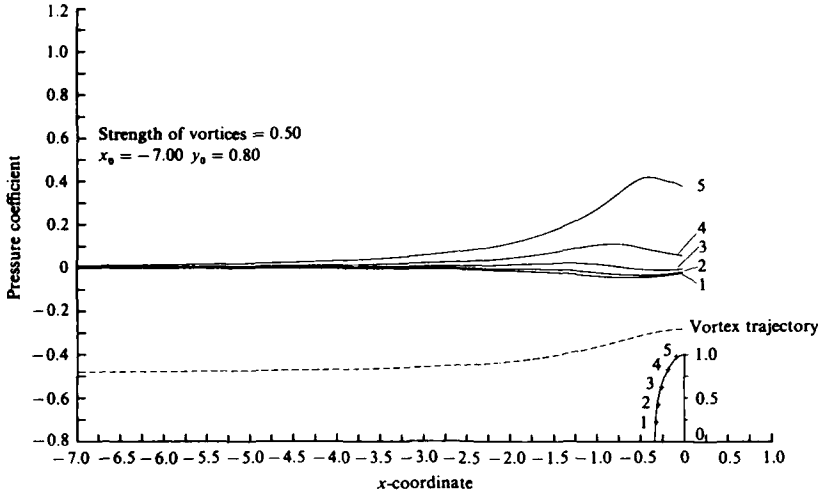

9. Pressure pulses along an ellipse, ratio of ellipse axes=3.0.

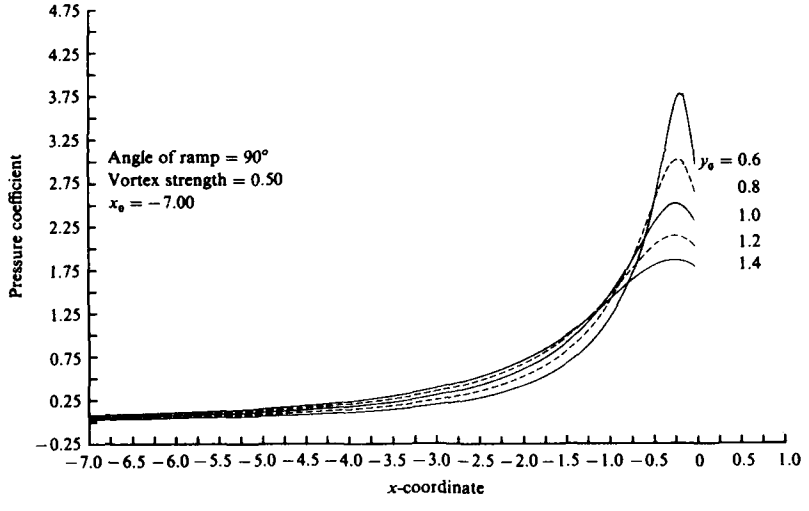

10. The effect of the initial vertical distance of the vortex from the edge on the amplitude of the pressure pulses, for ramps of 90^0.

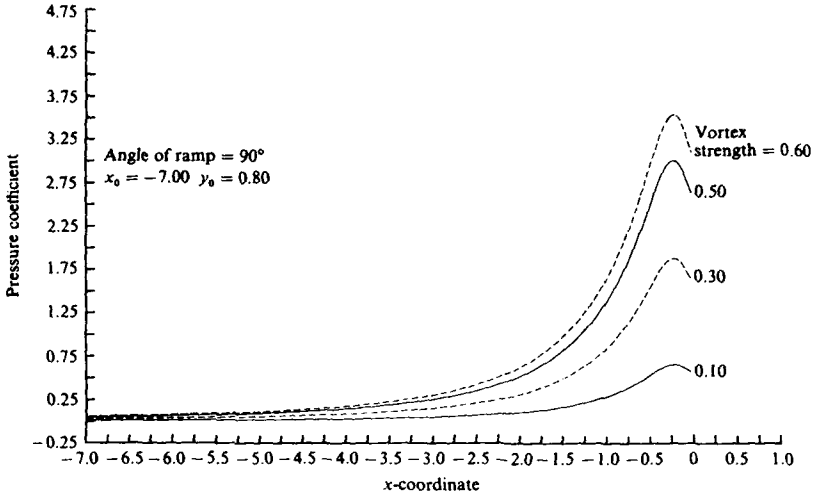

11. The effect of the strength of the vortices on the amplitude of the pressure pulses, for ramps of 90^0.

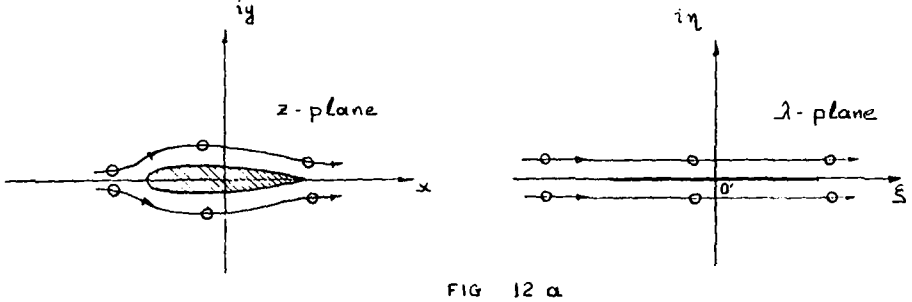

FIG 12 a

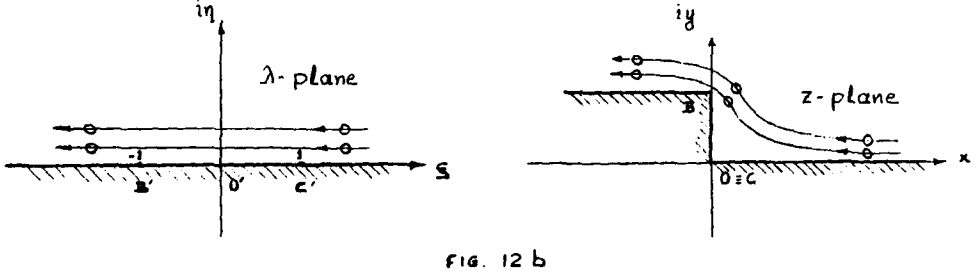

FIG. 12 b

12. models of vortices/edge interaction.

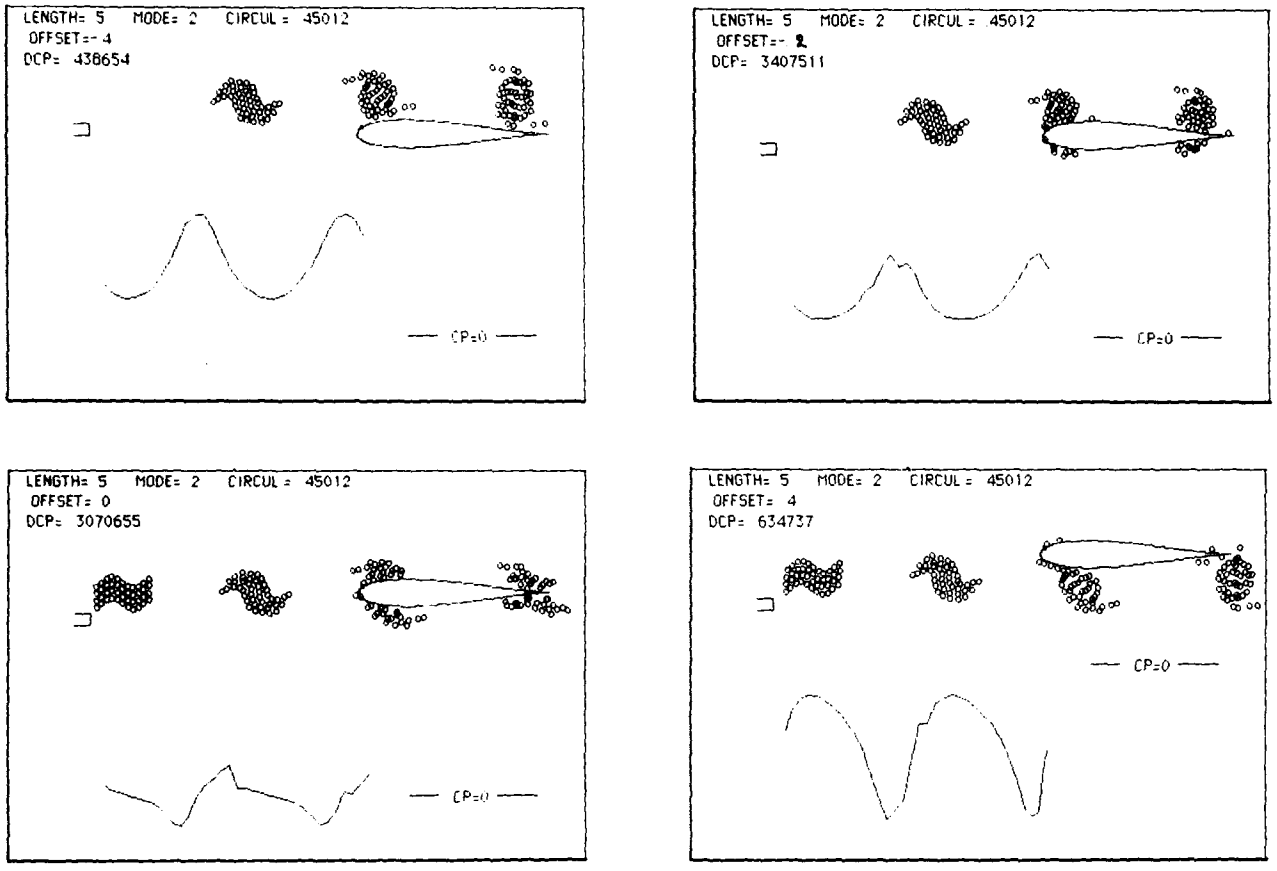

13. The effect of the offset distance on the interaction.

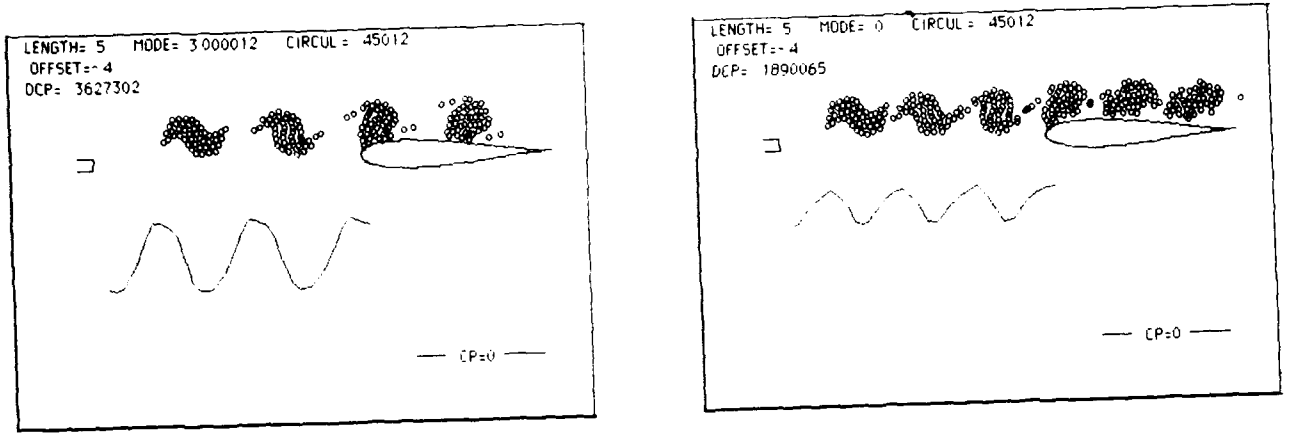

14. The effect of the spacing of the vortices. Flow above the edge.

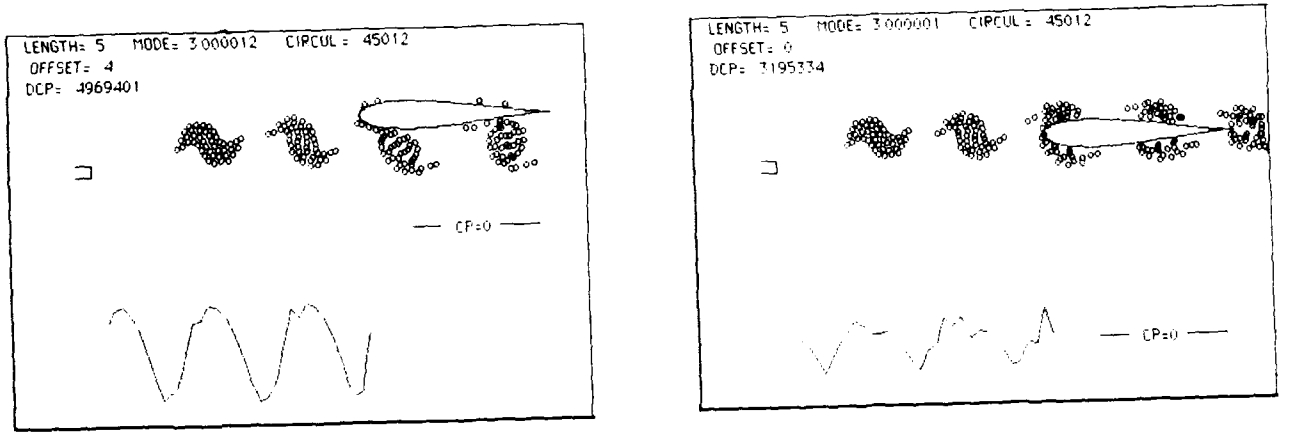

15. The effect of the spacing of the vortices. Impingement on the edge.

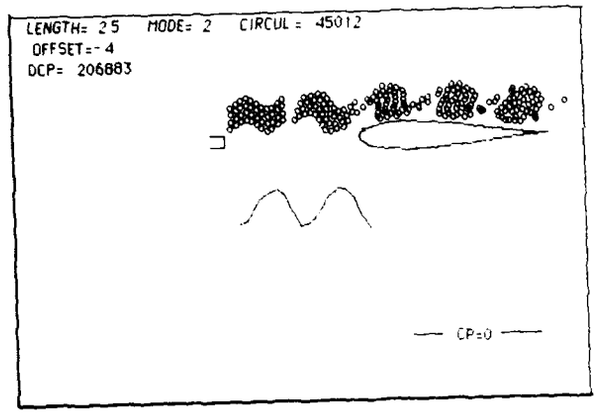

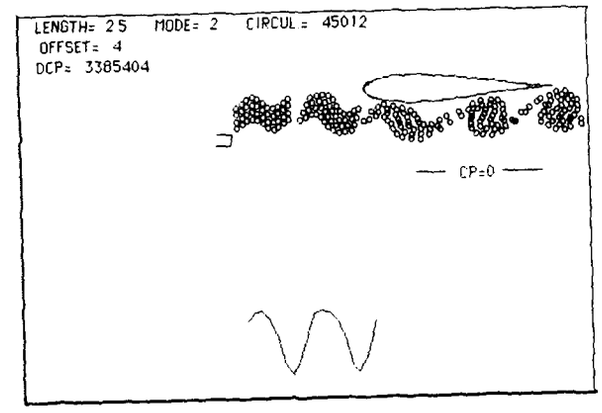

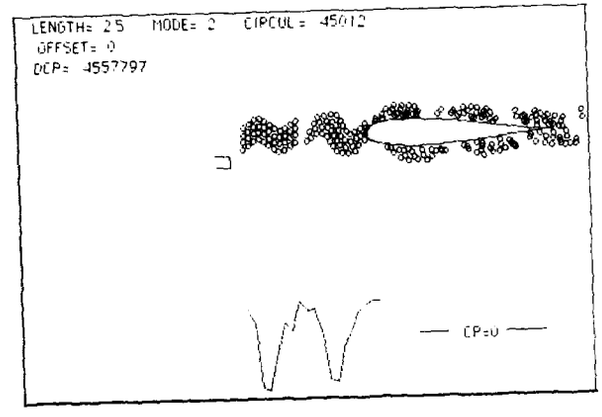

16. The effect of the length of the succession of the vortices.

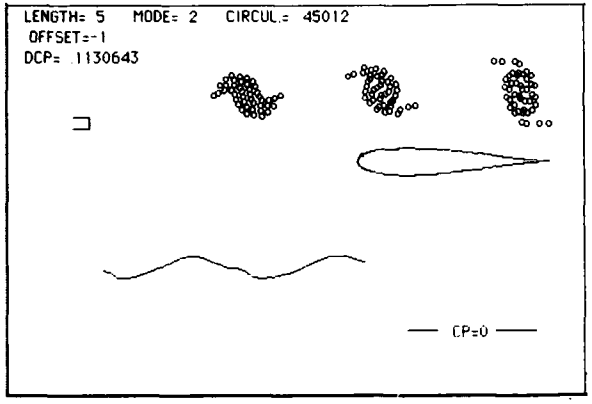

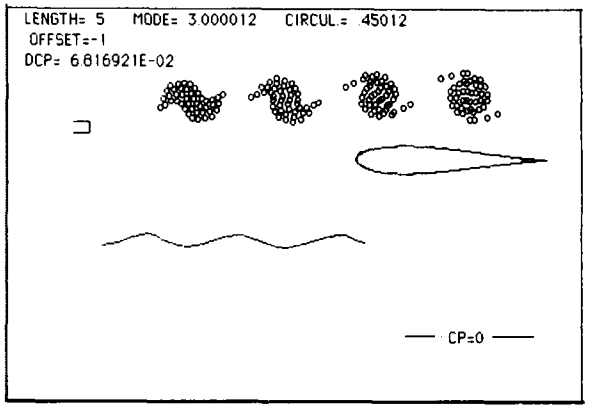

17. Simulation of the effect of mixing layers on adjacent surfaces.

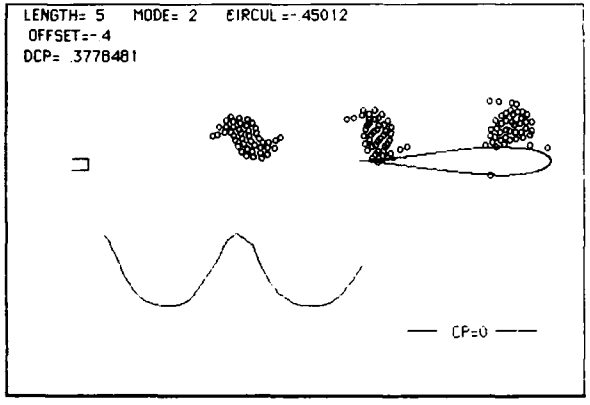

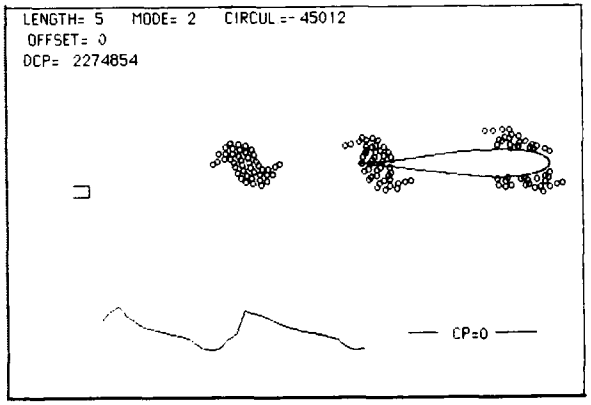

18. Impingement on the sharp edge of the airfoil.

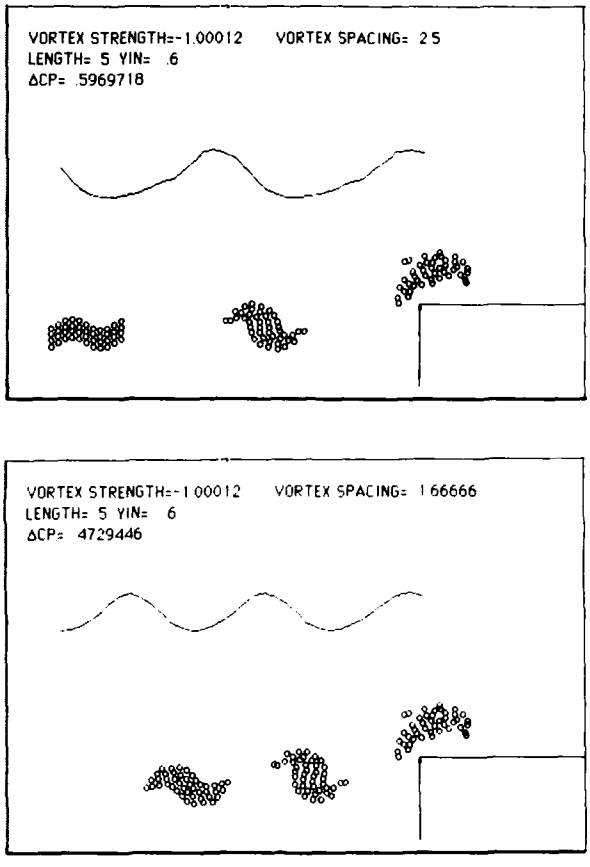

19. Vortex/corner interactions. Effect of the vortex spacing.

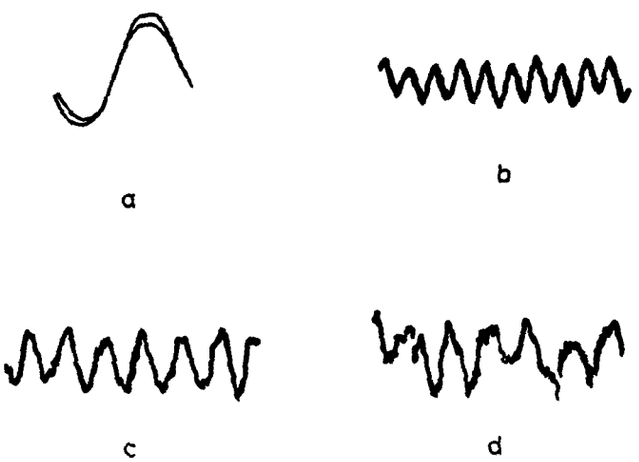

20. Experimentally measured pressure fluctuations, (a): Dunham(1962), (b), (c), (d): Rossiter(1964)

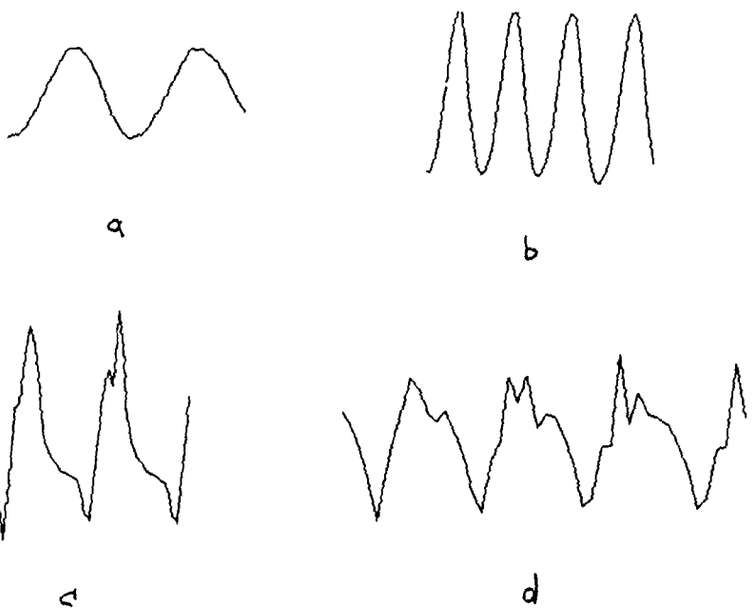

21. Calculated pressure fluctuations for comparison with experimental data.

VORTEX DYNAMICS-SURVEY OF THE ACTIVITY IN ITALY

by
M. GERMANO
Department of Aerospace Engineering
Polytechnic of Torino
C.so Duca degli Abruzzi 24
10129 TORINO, Italy

SUMMARY

The activity in modelling time variant flows using vortex dynamics is at present very limited in Italy. Moreover the contributions are principally in fundamental areas or in areas outside the aeronautical field.

1. INTRODUCTION

The current work on vortex dynamics in Italy is presented. Such work is mainly conducted in Universities and can be divided in theoretical, computational and experimental work. At the Universities of Roma and Trento theoretical work is in progress on the approximation of 2-D Navier-Stokes equations by vortex methods [1,3-6] . At the University of Genova unsteady axisymmetric separated flows are studied [7-9] and at the University of Pisa a computational work is conducted concerning the steady wake of missiles [11-12] . An accurate experimental work on the non steady periodic wake of a marine propeller is carried out in the Italian Navy recirculation water tunnel by means of a laser doppler velocimeter [13] and finally at the Polytechnic of Torino work is in progress on the intrinsic equations of a filament vortex [17] . In the following such activities are presented in detail.

2. UNIVERSITIES OF ROMA AND TRENTO

In the Departments of Mathematics of these Universities a joint group of researchers is particularly active in studying the vortex methods from a mathematical point of view. Their main interest is the connection between the equations governing the motion and the vortex theory, and their attention is particularly devoted to proving that the Navier-Stokes equations may be approximated by vortex methods. Their investigations are mainly limited to two dimensional flows, but recently they are considering vortex models in three dimensions. In paper 1, following ideas that are at the basis of the well known numerical method of Chorin [2], they show that the two dimensional Navier-Stokes equations may be interpreted as a field equation for a system of vortices on which a stochastic perturbation related to the viscosity is acting. Such an approximation has been widely investigated for numerical purposes, and the authors provide precise connection between the Navier-Stokes equations and such methods. In particular they consider a system of N vortices interacting via a smoothed potential g_ε different from the logarithmic potential g in an ε-sphere around the origin and subjected to a stochastic perturbation. In the limit $N \to \infty$ and when the cut off $\varepsilon \to 0$ they show that this system converges to the solution of the Navier Stokes equation, once the initial data of the vortex system approach the initial data of the Navier Stokes equation at time zero. Similar results have been obtained for bounded flows, and the generation of vorticity near the boundary has been considered in ref.3, where a mathematical justification of the fact that the boundary behaves as a singular source of vorticity is given. Related studies are devoted to the general properties of the vortex dynamics. The evolution of a two dimensional, incompressible, ideal fluid in which the vorticity is concentrated in small disjoint regions of the physical space is given in ref.4. There it is proved that at least for short times the evolution of the centers of vorticity of each blob can be described by a vortex model. In ref.5 and 6 the motion of a system of vortices in bounded domains is considered, and the results are extended to systems of particles interacting via a long range potential, like the Coulomb particle systems.

3. UNIVERSITY OF GENOVA

De Bernardinis (Institute of Hydraulics, University of Genova) and Graham and Parker (Imperial College, London) have studied unsteady axisymmetric separated flows around disks and through orifices using vortex dynamics [7]. The research is stimulated by the physiological importance of these flows, (genesis of atherosclerosis, detection of arterial stenoses), but the general interest of the model adopted is due to the fact that the shed vortex sheet is represented by sequences of discrete vortex rings. Characteristics problems of the extension to the axisymmetric flows of the vortex models are a much more complicated interaction between vortices, the possibility of vortex stretching and the existence of the self induced velocity on a vortex ring. Theoretical results are obtained for an oscillating disk starting from rest and for an oscillatory flow through an orifice in a pipe. Numerical predictions are compared with experimental results and the conclusion is that the method predicts the dominant features of the flow accurately. In another paper [8] the classic problem of the evolution of a vortex pair generated by pushing fluid down a semi-infinite channel by means of an impulsively started piston is examined. The strength and the separation of the two fully developed vortices and the formation of the secondary pair due to the sudden stop of the piston motion is studied in detail and compared with experimental results. Another interesting investigation of three-dimensional vorticity was computed by Dhanak and De Bernardinis with reference to the evolution of an elliptic vortex ring [9]. The authors follow numerically different elliptic configurations using a cut-off approximation for the velocity at the vortex and in particular they are able to calculate the time in which the initial elliptic ring would break into two smaller rings formation. The last stage evolution of an aircraft trailing vortex system [10] is discussed following these computations.

4. UNIVERSITY OF PISA

At the University of Pisa the group of Dini, Psarudakis and Vagnarelli is particularly active in the determination of the non linear aerodynamic missile loads in three-dimensional subsonic regime flow. The studies are by now limited to steady situation and are based on the vortex lattice method. In this method a horse-shoe vortex is associated with each element of the lifting surface and the wake is composed by free vortex segments that separates from the edges. The wake is relaxed by an iterative process and particular criteria are used to assure the method convergence, do more stable results and reduce the computer time in relation to the vortex segment number. In paper 11 a numerical computer program is developed for the preliminary missile design phase and some results are presented concerning the wake geometry of a rectangular wing and of a delta wing, Figs.1-2, and the wake geometry of the wing-body-tail configuration, Fig.3. The influence of the fuselage on wings has been studied in more detail in paper 12, and the results obtained are satisfactory as compared with theoretical and experimental results by other authors.

5. CEIMM (Centro Esperienze Idrodinamiche Marina Militare) and UNIVERSITY OF ROMA

The group of Accardo, Cenedese and Milone is applying a phase sampling procedure to the analysis of the non steady and periodic field in the near wake of a marine propeller [13]. The experiments are carried out in the Italian Navy recirculation water tunnel and the results obtained by means of a laser doppler velocimeter give a detailed an accurate description of the vortex sheet from the blade trailing edge. The measurements are extended to the mean values, the standard deviations, the skewness and the kurtosis of the velocity components. The presence of the tip-vortex can be clearly observed in Fig.4.

6. POLYTECHNIC OF TORINO

At the Polytechnic of Torino work is in progress on the intrinsic equations of a vortex filament. These equations describe the filament evolution with reference to the curvature and the torsion of the vortex axis. They were first obtained by Da Rios [14] in 1906, were studied in detail by Levi-Civita [15] in 1932 and were finally rediscovered independently by Betchov [16] in 1965, as related by Germano [17]. In the same paper Germano rederives these equations as a particular case of the motion of an unextensible curve. He

is presently trying to incorporate in these equations the effects due to the viscosity and to the eventual different section of the vortex tube along the filament.

7. CONCLUDING REMARKS

We have attempted to present the activities related to vortex dynamics in Italy. These activities are presently scattered in different directions and not well organized in order to coordinate the mutual interests. Anyway it seems possible that in a case of a Symposium related to this topic some contributions can be expected from Italy.

REFERENCES

1) C. Marchioro, M. Pulvirenti "Hydrodynamics in two dimensions and vortex theory". *Commun. Math. Phys. 84*, 483 (1982).

2) A.J. Chorin "Numerical study of slightly viscous flow". *J. Fluid Mech. 57*, 785 (1983)

3) G. Benfatto, M. Pulvirenti "Generation of vorticity near the boundary in planar Navier-Stokes flows". *Commun. Math. Phys. 96*, 59 (1984)

4) C. Marchioro, M. Pulvirenti "Euler evolution for singular initial data and vortex theory". *Comm. Math. Phys. 91*, 563 (1983).

5) C. Marchioro, E. Omerti "Time evolution of an infinite number of vortices in a strip". *J. of Statistical Phys. 33*, 133 (1983).

6) D. Dürr, M. Pulvirenti "On the vortex flow in bounded domains". *Commun. Math. Phys. 85*, 265 (1982).

7) B. De Bernardinis, J.M.R. Graham, K.H. Parker "Oscillatory flow around disks and through orifices". *J. Fluid Mech. 102*, 279 (1981).

8) P. Blondeaux, B. De Bernardinis "On the formation of vortex pair near orifices". *J. Fluid Mech. 136*, 111 (1983).

9) M.R. Dhanak, B. De Bernardinis "The evolution of an elliptic vortex ring". *J. Fluid Mech. 109*, 189 (1981).

10) S.C. Crow "Stability theory for a pair of trailing vortices". *AIAA J.8*, 2172 (1970).

11) D. Dini, P. Psarudakis, F. Vagnarelli "Non linear discrete vortex method for use of computer programmes for preliminary missile design phase". AGARD Symposium "Missile System Flight Mechanics", CP 270, London, England 21-24 May (1979).

12) D. Dini, P. Psarudakis, F. Vagnarelli "Influenza della fusoliera su ali a caratteristiche aerodinamiche non lineari in missili subsonici". *L'Aerotecnica Missili e Spazio 58*, 203 (1979).

13) L. Accardo, A. Cenedese, R. Milone "Analisi del campo fluidodinamico nella scia di un'elica". VIII Congresso Nazionale AIDAA, Torino, Settembre (1985).

14) L.S. Da Rios "Sul moto d'un liquido indefinito con un filetto vorticoso di forma qualunque". *Rend. Circ. Mat. Palerm 22*, 117 (1906).

15) T. Levi-Civita "Attrazione Newtoniana dei tubi sottili e vortici filiformi". *Ann. R. Scuola Normale Sup. Pisa*, Serie II, I, 1-54 (1932).

16) R. Betchov " On the curvature and torsion of an isolated vortex filament". *J. Fluid Mech. 22*, 471 (1965).

17) M. Germano "Sulla riscoperta delle equazioni del Da Rios concernenti il moto di un filetto vorticoso". VII Congresso Nazionale AIDAA, Napoli, Ottobre (1983).

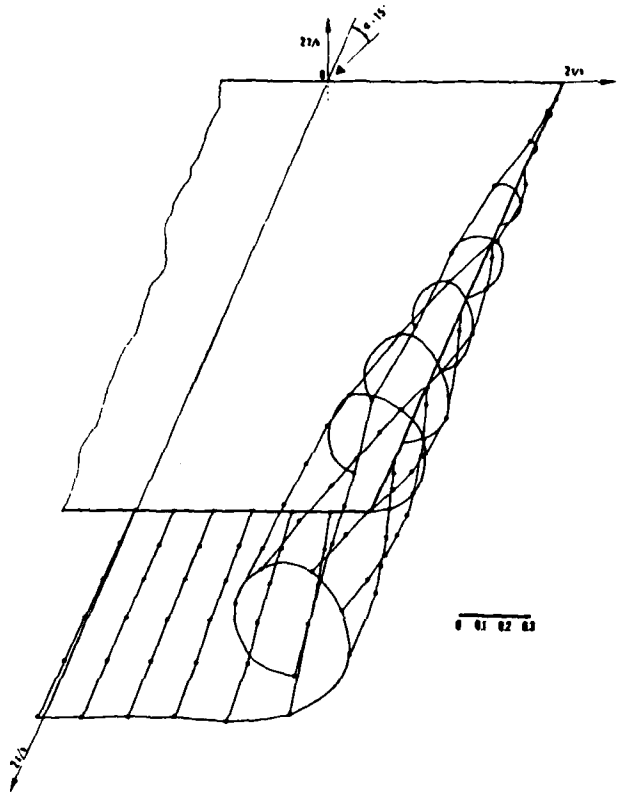

Fig. 1 - Wake geometry and wake nodes position (•) of an AR = 1 rectangular wing. (Ref. 11)

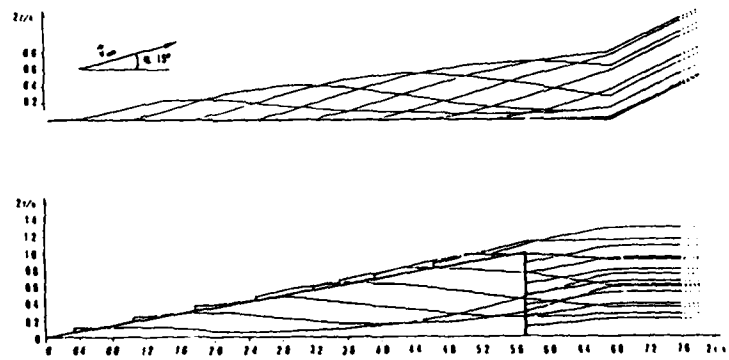

Fig. 2 - Wake geometry of a delta wing of AR = 0.7 at $\alpha = 15°$.(Ref. 11)

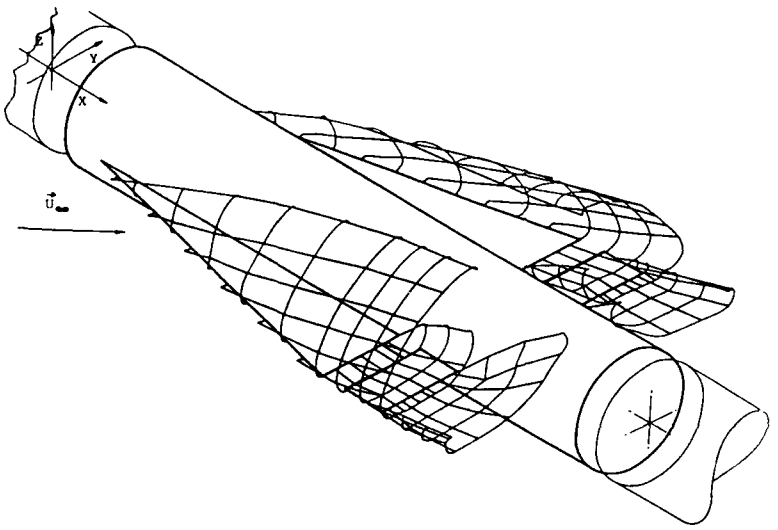

Fig. 3 - Wake geometry of the wing - body - tail configuration at $\alpha = 20°$. (Ref. 11)

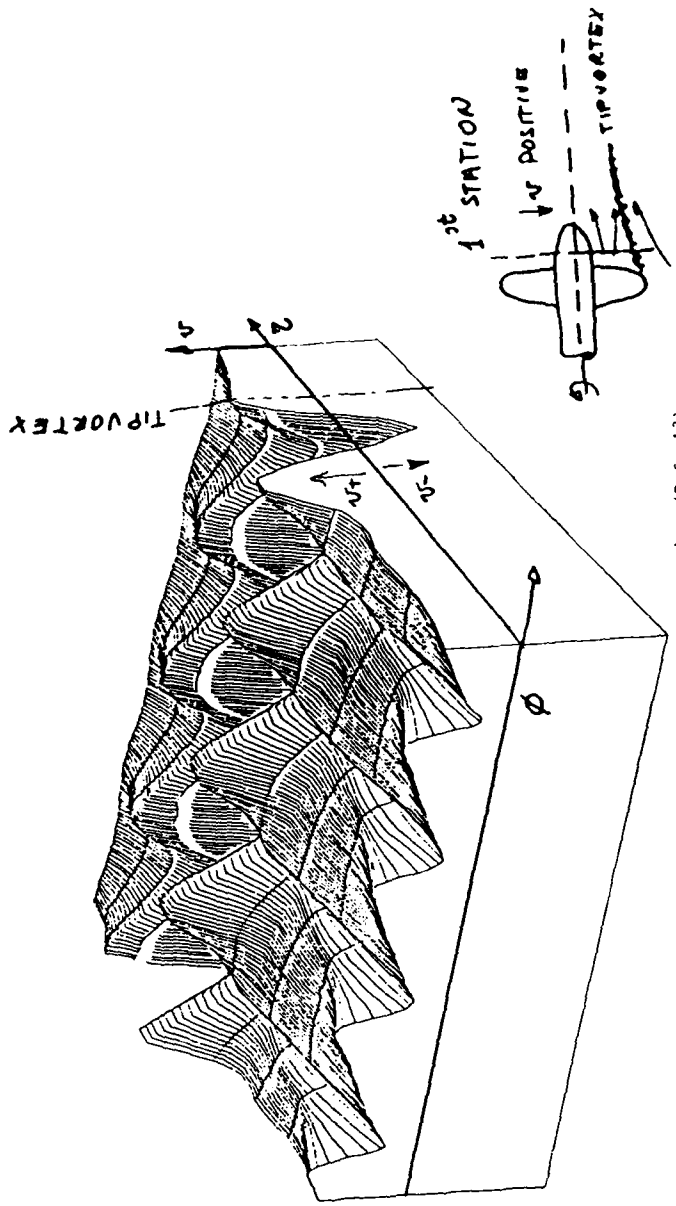

Fig. 4 - Radial velocity component at the first station. (Ref. 13)

MODELLING OF TIME-VARIANT FLOWS USING VORTEX DYNAMICS-ACTIVITIES IN THE NETHERLANDS

by
H.W.M. Hoeijmakers
National Aerospace Laboratory NLR
Anthony Fokkerweg 2, 1059 CM Amsterdam
The Netherlands

SUMMARY

Activities in the Netherlands in the area of simulating low-speed flows using vortex elements are summarized. Aspects of some of the methods developed are highlighted and plans for future work are indicated.

1. INTRODUCTION

In the area of computational fluid dynamics vortex methods have been used for the past decade or so for simulating incompressible, inviscid and also slightly viscous high-Reynolds-number flow in both two and three space dimensions (Ref. 1,2). In thise Lagrangian type of methods the vortical flow structures are followed as they evolve in physical space. The use of the physically relevant quantity of vorticity provides a key to direct interpretation of the numerical results. In addition, vortex elements are only required in regions where the vorticity is non-zero. Furthermore the vorticity is not spread by numerical diffusion, i.e. the vortical flow regions are fitted rather than captured as is the case in finite-volume Euler codes.

A disadvantage of the Lagrangian approach is its operational count, which is $O(N^2)$ where N is the number of vortex elements. However, in some cases the operational count can be reduced considerably by the introduction of an underlying Eulerian grid. On the other hand, the present-day supercomputers tend to alleviate the computational burden sufficiently to warrant the direct approach as well. A further disadvantage is that in case vortex sheets or contours of finite areas of constant vorticity are followed the topology may become very complicated, requiring a correspondingly complex logic in the computer code.

In this contribution to the Round Table Discussion we summarize the current work in the Netherlands on vortex methods for simulating time-variant flow. When appropriate we will discuss some of the details of the work as well as indicate the direction for future work.

2. SUMMARY OF ACTIVITIES IN THE NETHERLANDS

In the Netherlands there are several places where there is interest in the simulation of (time-variant) incompressible flow using vortex elements. This section provides a list of the various places and a short description of their interest.

Delft University of Technology

At the Department of Aerospace Engineering some work is done, on fundamental aspects of flows with vortices. Furthermore, exploratory surveys of flow fields involving vortices have been carried out (e.g. Ref. 3 and 4) and are subject of future work. The experimental investigations may provide a basis for comparison with computational results.

At the Laboratory for Aero- and Hydrodynamics a student has been involved in simulating shear layers using a discrete vortex method, but this line of research has not yet been pursued further.

At the Department of Applied Mathematics Prof. Hermans and his students have looked into some of the aspects of the vortex method under development at MARIN, see section 3.

Technical University Eindhoven

At the Department of Technical Physics one is looking into the feasibility of starting the development of a vortex method for the flow through T-shaped ducts.

Shell/KSLA, Amsterdam

Here one is interested in simulating confined flows, e.g. mixing layers. Currently one is evaluating a 2D vortex method to judge its applicability to industrial type of flows.

Netherlands Organisation for Applied Scientific Research (TNO)

At the IWECO institute one is involved in predicting the characteristics of the flow about submerged objects shedding vortex wakes.

At the Institute of Applied Geoscience (DGV) a formulation based on Clebsch variables has been developed for the flow involving rotation (Ref. 5).

Maritime Research Institute Netherlands (MARIN)

At MARIN work is carried out to develop a vortex method for the prediction of the dynamic forces on bluff bodies with vortex shedding in high-Reynolds-number flow. The intended applications include simulating the flow about off-shore structures, rod bundles, manoeuvring ships and ship propulsion. In section 3 of this report the main features of the method, described in Refs. 6 and 7 are briefly described.

National Aerospace Laboratory (NLR)

At NLR methods are being developed for predicting the evolution of vortex wake structures (Ref. 8 and 9) as well as the vortex flow about oscillating strake-wing configurations. Some details of this work are described in section 4 of the present report. Also, the work carried out in the area of aero-acoustics involves the study of vortex shedding due to incident sound waves (e.g. Refs. 10 and 11).

At still other institutes and research departments there is interest in simulating flows with vortices, a.o. at Fokker where the prediction of the aerodynamics of missile configurations involves flows with vortices.

3. ACTIVITY AT MARIN

At the Maritime Research Institute Netherlands (MARIN) v.d. Vegt and Huijsmans (Refs. 6 and 7) are developing a method for simulating the flow about bluff bodies with vortex shedding. Some aspects of the method are being investigated by Prof. Hermans and his students at the Delft University of Technology.

The method is based on the fractional step method put forward by Chorin (Ref. 12) and uses vortex blobs to represent the vorticity field. In Chorin's scheme the governing equations are solved in two steps, the convection step which represents the inviscid vorticity convection as well as the creation of vorticity and the diffusion step which represents the viscous part of the flow problem.

3.1 The convection step

In the convection step the Euler equations

$$\vec{\nabla}.\vec{u}^{E} = 0 \tag{3.1a}$$

$$\frac{\partial \omega^{E}}{\partial t} + (\vec{u}^{E}.\vec{\nabla})\,\omega^{E} = 0 \tag{3.1b}$$

with $\omega^{E} = (\vec{\nabla} \times \vec{u}^{E}) \cdot \vec{e}_z$ are solved subject to the following boundary conditions:

$$\vec{u}^{E}.\vec{n} = \vec{u}_B \cdot \vec{n} \text{ at } S \tag{3.2a}$$

$$\vec{u}^{E} \to \vec{U}_\infty(t) \text{ at } |x| \to \infty \tag{3.2b}$$

where S is the surface of the body, $\vec{n}$ is the normal to the body surface, $\vec{u}_B$ is the motion of the body and $\vec{U}_\infty$ is the velocity far upstream of the body. The solution is obtained by introducing the stream function ψ (such that $\vec{u}^{E} = \vec{\nabla}\psi \times \vec{e}_z$) which is split into two parts, i.e.:

$$\psi = \psi^{P} + \psi^{H} \tag{3.3}$$

Here ψ^{P} represents the shed vorticity field in the unbounded domain, i.e. ψ^{P} satisfies

$$\nabla^2\psi^{P} = -\omega^{E} \tag{3.4}$$

subject to the far-field boundary condition given in Eq. (3.2b). In Eq. (3.3) ψ^{H} represents the flow due to the presence of the body in the flow field, i.e. ψ^{H} satisfies

$$\nabla^2\psi^{H} = 0 \tag{3.5a}$$

subject to the stream surface condition at the solid surface, as given in Eq. (3.2a), which becomes

$$(\vec{\nabla}\psi^{H} \times \vec{e}_z).\vec{n} = (\vec{u}_B - \vec{\nabla}\psi^{P} \times \vec{e}_z).\vec{n} \quad \text{at } S \tag{3.5b}$$

and the far-field condition

$$\vec{\nabla}\psi^{H} \times \vec{e}_z \to 0 \text{ for } |\vec{x}| \to \infty \tag{3.5c}$$

The vorticity field consists of a large number of overlapping, individual vortex blobs of fixed circular shape with vorticity distribution

$$\omega^{E}(\vec{x},t) = \sum_k \Gamma_k \gamma_k(|\vec{x}-\vec{x}_k(t)|) \tag{3.6}$$

where Γ_k is the circulation of the k-th vortex blob, located at $\vec{x}_k$, and γ_k is the vorticity distribution inside the blob, taken here as a Gaussian distribution.

3.2 The diffusion step

In the diffusion step the vortices are diffused using a random walk with Gaussian probability distribution with zero mean and standard deviation of $\sqrt{2\nu\Delta t}$.

3.3 The computational procedure

The computational procedure is started at t=0 by impulsively setting the fluid in motion. Then the following sequence of steps is executed:

1. Compute ψ^{H} by solving Eqs. (3.5a-c) using a first order panel method based on the formulation of the Dirichlet boundary condition for the flow inside the body.
2. Create 2NP vortices at the body surfaces. The strength of the new vortices is such that in the mean the no-slip condition is satisfied, i.e.:

$$\omega^{E} = (\vec{\nabla}\psi^{H} \times \vec{e}_z) \cdot \vec{t} \tag{3.7}$$

   where $\vec{t}$ is the tangent vector to the surface. Here NP denotes the number of panels used to discretize the boundary S.
3. Do the first diffusion step with time step $\frac{1}{2}\Delta t$. In this step the newly created vortices that wander into the body, on the average NP vortices, are removed. The vortices created earlier that move inside S are reflected back into the flow field.

4. Carry out the convection step with time step Δt, i.e. *solve for* ψ^P. *For this* Buneman's (Ref. 13) variational formulation for point vortices has been extended to vortex blobs. The variational formula used is

$$J(\psi^P,\vec{x}_k) = \iiint \tfrac{1}{2}\,|\vec{\nabla}\psi^P|^2\,dxdydt - \sum_k \Gamma_k\Big(\iiint \gamma(|\vec{x}-\vec{x}_k|)\psi^P\,dxdydt + \tfrac{1}{2}\int \vec{x}_k \times d\vec{x}_k\Big) \qquad (3.8)$$

Variation of ψ^P and $\vec{x}_k$ then yields Eq. (3.4) for ψ^P while one finds for $\vec{x}_k$:

$$\frac{d\vec{x}_k}{dt} = \iint \gamma(|\vec{x}-\vec{x}_k|)(\vec{\nabla}\psi^P \times \vec{e}_z)\,dxdy \qquad (3.9)$$

where the integration is over the area of the vortex blob. Eq. (3.9) shows that the vortex blobs are convected *with the* vorticity weighted velocity.
The variational problem is solved in Fourier space. For the latter a computationally efficient procedure has been developed involving an interpolatory cubic-spline approximation for the trigoniometric functions which facilitates the use of FFT for the summations. The operational count of this step amounts to $N+m\log_2 m$, where N is the number of vortex blobs and m the number *of Fourier components*.
In this step the force on the body is computed using a formulation which just involves the vorticity and velocity of the flow field and does not require the explicit computation of the pressure.
5. Do the second diffusion step with time step $\frac{1}{2}\Delta t$, bouncing the vortices that move into the body.
Next the whole procedure is repeated, starting at step 1.

3.4 Example of application

Figure 1 shows a comparison of the calculated flow field with the results of flow visualisation experiments for a circular cylinder in steady free stream . The Reynolds number based on the cylinder diameter is 31,700. The computation was carried out using 512*512 Fourier components for the vorticity field and 64 panels for discretizing the contour of the cylinder. The computation took about 2 hours CPU time on the Cray-1S computer and involved up to 15,000 vortex blobs. Recently the efficiency of the code was improved considerably, reducing CPU-time requirement by nearly an order of magnitude.
As illustrated in figure 1 the general characteristics of the measured and computed flow pattern compare quite well. This was also the case for the vortex-shedding frequency while the prediction of drag and lift time histories were quite reasonable.

3.5 Future work

Future work will be the further validation and evaluation of the above described method for 2D flow. This will include the application to the "lock-in" phenomenon.
Extension of the method to three space dimensions is underway. The latter code will be applied to the flow about a cylinder to investigate the development of 3D disturbances in the initially 2D flow field.

4. ACTIVITY AT NLR

At the National Aerospace Laboratory (NLR) a method has been developed for computing the evolution of wake structures. This method will be described in section 4.1 and 4.2.

Another activity that will start soon is the development of a method for predicting the aerodynamic characteristics of oscillating wings with leading-edge vortex separation. The interest for the latter work came from the current experimental investigation in the flow about an oscillating, generic, strake-wing configuration. The method to be developed, will be an extension of the methods developed earlier for the flow about steady configurations with leading-edge vortices, see section 4.3.
Some of the above activities have been carried out in cooperation with the Department of Aerospace Engineering of the Delft University of Technology.

4.1 2D-time-dependent vortex wakes

For transport type of aircraft in cruise condition the precise shape of the wake has in general only a small effect on the lift and pressure distribution on the wing. In most current computational methods it is therefore common practise to assume a rigid wake of some suitable shape. For aircraft in landing configuration, fighter aircraft and also for missile configurations, where in addition to the tip vortex other vortices may develop, often a more accurate description is required. The method to be described provides a tool to obtain an insight in the development of the wake topology in the vicinity of the aircraft.

For the Reynolds and Mach numbers involved the flow may be considered inviscid and irrotational with embedded regions of rotational flow, i.e. vortex sheets and vortex cores. Two types of vortex cores occur, single-branched cores at wing tips and double-branched ones at initially smooth portions of the vortex sheets. For the present purpose we are interested in the simulation of the flow outside the vortex cores itself. This warrants the introduction of an approximate model where for the outer flow field the vortex core is represented by an isolated vortex/feeding sheet combination (see Fig. 2).

Under the assumption that the variations in streamwise direction are much smaller than the ones in the cross-flow plane the originally three-dimensional steady problem is re'uced to a two-dimensional time dependent problem in the cross-flow (Trefftz) plane. This is accomplished by replacing the streamwise coordinate x by $U_\infty\tau$ where U_∞ is the component of the free stream along the x-axis and τ is a time-like coordinate. The resulting problem is an initial value problem describing the motion of a two-dimensional vortex system (built-up out of vortex-sheet segments, see Fig. 3) as it is convected by the velocity field composed of the cross-flow-plane free-stream velocity $\vec{v}_\infty$ and the velocity it induces upon itself, i.e.

$$\frac{d}{d\tau}\vec{x}(t;\tau) = \vec{v}_\infty + \frac{\vec{e}_x}{2\pi} \times \Sigma\Big(-\int_{C_v} \frac{\vec{R}}{|\vec{R}|^2}\frac{d}{d\eta}\rho(\eta)d\eta + \delta_v^N \frac{\vec{R}_v^N}{|\vec{R}_v^N|^2}\rho_N - \delta_v^1 \frac{\vec{R}_v^1}{|\vec{R}_v^1|^2}\rho_1\Big) \qquad (4.1)$$

with $\vec{R} = \vec{X}(t;\tau) - \vec{X}(\eta;\tau)$, $\vec{R}_v^N = \vec{X}(t;\tau) - \vec{X}_v^N(\tau)$ and $\vec{R}_v^1 = \vec{X}(t;\tau) - \vec{X}_v^1(\tau)$ and the summation is over all segments. In Eq. (4.1) the sheet vorticity is expressed in terms of the doublet distribution (= circulation) along the vortex sheet segment C_v, which position is given by $\vec{X}(t;\tau)$. The parameter $\delta_v^N = 1$ in case the last point on vortex sheet segment C_v is connected to a vortex, positioned at $\vec{X}_v^N(\tau)$, while $\delta_v^N = 0$ otherwise. Similarly $\delta_v^1 = 1$ in case the first point of segment C_v is connected to a vortex at $\vec{X}_v^1(\tau)$ and $\delta_v^1 = 0$ otherwise. The initial conditions of the problem are the position of the vortex sheet(s) and the circulation along it at $\tau = 0$. The method developed, designated VOR2DT, can handle quite general multiple segmented vortex sheet systems with single and double-branched vortices. A second-order panel method using quadratic doublet distributions on curved panels is used for the discretization of the integral in Eq. (4.1). The subdivision into panels of the vortex sheet is done through an adaptive curvature-dependent panel scheme that decreases the panel width in regions of high curvatures, enabling the accurate description of rolling-up portions of the sheet. For the time-like integration a simple Euler scheme is used with the time step restricted such that any panel does not change its position more than a fraction of its width.

The computational procedure also features options to split segments, to cut a vortex sheet to a specified length or attitude of the feeding sheet, to monitor quantities like circulation and center of vorticity that, possibly, are invariants of the motion, etc.

4.2 *Example of application of VOR2DT*

The example considered here is the wake of a transport aircraft with a deployed part-span flap. This is a case where the trailing vorticity changes sign along the wing span, resulting in counter-rotating vortex cores. In Fig. 4a results of the present method at three points in time are compared with ones of the so-called cloud-in-cell method of Ref. 14. Although there appear many small-scale structures in the latter the global structures agree fairly well. First, one observes the appearance of the tip vortex, followed by the evolution of a double-branched vortex approximately at the position of the outboard edge of the flap. Finally, a second double-branched vortex is formed at the inboard edge of the flap.

In Fig. 4b the results of the present method at a much later point in time are compared with the ones from the finite-difference solution of the Navier-Stokes equations in vorticity/stream function formulation (Ref. 15). The results agree surprisingly well, the vortex cores have about the same position in space and a similar shape. In both results no further vortices have formed and the outboard flap-edge vortex has gained most in strength, its circulation is about twice the circulation of the tip vortex as well as the inboard flap edge vortex. The latter is of opposite sign compared to the other two vortices.

Figure 4c shows the results of continuing the computation to still longer times. It illustrates that the present method continues to produce smooth results, in spite of the circumstance that the strength of the vortex sheet has diminished quite considerably and by this time most of the vorticity has amalgamated in the vortex cores.

More examples of applications, including one where there is an indication of the ill-posedness of the initial-value problem are given in Ref. 9.

4.3 Leading-edge vortex flow

For simulating the flow about steady wings with leading-edge vortices two types of potential flow method have been developed (Ref. 16).

- a panel method for general configurations with rolled-up vortex sheets attached to prescribed fixed separation lines, based on the slender-body approximation (VORSBA),
- a panel method for the 3D flow about thin wings with leading-edge vortex sheets (VORSEP).

A typical result of the VORSBA program for a unit-aspect-ratio delta wing is shown in Fig. 5, where the computed vortex sheet and vortex core position is compared with total-pressure contours obtained in a wind-tunnel experiment at the Delft University of Technology.
Fig. 6 shows a typical result of the 3D vortex sheet method; the computed vortex sheet shape for a 65 deg swept wing at 10, 15 and 20 deg incidence. A detailed comparison of results of the VORSEP method with the ones of the Euler code for incompressible flow developed at FFA, Sweden can be found in Ref. 17.

The flow about double-delta wings and strake-wing configurations is more complex, e.g. Ref. 3. It involves a primary vortex core, originating at the leading edge of the strake and a secondary double-branched vortex core, originating at the kink in the leading edge. An example of the simulation of the flow about a double-delta wing is shown in Fig. 7, which compares the result of the VORSBA method with the result of a discrete-vortex method (Ref. 18). In the discrete-vortex method two distinct centers of roll-up evolve and instabilities occur before the last station is reached. In the panel method result the kink in the leading edge causes a dent (region with curvature of opposite sign) in the vortex sheet. Seen in downstream direction the dent, representing the double-branched vortex, travels along the sheet towards the vortex core, just like observed in experiments. Clearly, for larger discontinuities in the leading-edge sweep, when the secondary vortex is stronger, a double-branched vortex model is required to obtain an even more accurate simulation of the flow.

4.4 Future work

Future work will be the further evaluation of the VOR2DT method. We are also considering the extension of the method to:

- periodic vortex systems. This will enable the simulation of the temporal development of mixing layers, waves and other interfaces.
- contour dynamics (e.g. Ref. 19). This is required to study the behaviour of finite areas of vorticity, for example, occurring during the final stages of inviscid vortex wake roll-up. The advantage of the contour-dynamics approach is that it provides a solution of the Euler equations not afflicted with numerical diffusion, so that it is ideally suited for the long-time evolution of vortical structures.

Future work will also include the extension of the methods for leading-edge vortex flow to oscillating wings, as well as improving the present methods by including double-branched vortex cores and possibly finite-area vortex cores.

5. CONCLUDING REMARKS

- Clearly, in the Netherlands there is interest in the modelling of time-variant flows using vortex elements. Work in this area is being considered or in progress at various research laboratories, technical universities and industry.
- At present most of the methods are still under development, or their feasibility to specific applications is investigated.
- An FDP activity on this topic would certainly be welcomed by the workers in this field and probably attract active participation from the Netherlands.

6. REFERENCES

1. Leonard, A., "Vortex Methods for Flow Simulation", Journal of Computational Physics, Vol. 37, 1980, pp. 289-335.
2. Leonard, A., "Computing Three-Dimensional, Incompressible Flows with Vortex Elements", Annual Review of Fluid Mechanics, Vol. 17, 1985, pp. 523-559.
3. Verhaagen, N.G., "An Experimental Investigation of the Vortex Flow over Delta and Double-Delta Wings at Low Speed", Paper 7 of AGARD-CP-342, 1983.
4. Verhaagen, N.G., Kruisbrink, A.C.H., "The Entrainment Effect of a Leading-Edge Vortex", AIAA Paper 85-1584, 1985.
5. Zijl, W., "Solution of Surface Water Flow Equations Using Clebsch Variables", Water Resources Research, Vol. 20, No. 11, November 1984, pp. 1650-1658.
6. Vegt, J.J W. van der, Huijsmans, R.H.M., "Numerical Simulation of Flow around Bluff Bodies at High Reynolds Numbers", Paper presented at 15th Naval Hydrodynamics Symposium, August 1984, Hamburg, Also Report Z50457, Maritime Research Institute Netherlands (MARIN), August 1984.
7. Vegt, J.J.W. van der, Boom, W.C. de, "Numerical Simulation of Flow about Circular Cylinders at High Reynolds Numbers", Report Z50551, Maritime Research Institute Netherlands (MARIN), January 1985.
8. Hoeijmakers, H.W.M., Vaatstra, W., "A Higher-Order Panel method Applied to Vortex-Sheet Roll-Up", AIAA Journal, Vol. 21, April 1983, pp. 516-523.
9. Hoeijmakers, H.W.M., "Computational Vortex Flow Aerodynamics", Paper 18 of AGARD-CP-342, 1983.
10. Rienstra, S.W., "Sound Diffraction at a Trailing Edge", Journal of Fluid Mechanics, Vol. 108, 1981, pp. 443-460.
11. Rienstra, S.W., "Acoustic Radiation from a Semi-Infinite Annular Duct in a Uniform Subsonic Mean Flow", Journal of Sound and Vibration, Vol. 94, No. 2, 1984, pp. 267-288.
12. Chorin, A.J., "Numerical Study of Slightly Viscous Flow", Journal of Fluid Mechanics, Vol. 57, No. 4, 1973, pp. 785-796.
13. Buneman, O., "Variationally Optimized, Grid-Insensitive Vortex Tracing", Springer-Verlag, Lecture Notes in Physics, Vol. 35, 1974, pp. 111-116.
14. Baker, G.R., "The Cloud-in-Cell Technique Applied to the Roll-Up of Vortex Sheets", Journal of Computational Physics, Vol. 31, 1979, pp. 76-85.
15. Weston, R.P., Liu, C.H., "Approximate Boundary Condition Procedure for the Two-Dimensional Numerical Solution of Vortex Wakes", AIAA Paper 82-0951, 1982.
16. Hoeijmakers, H.W.M., "Methods for Numerical Simulation of Leading-Edge Vortex Flow", paper presented at ICASE/NASA Langley Workshop on Vortex Dominated Flows, July 1985. Also NLR MP 85052 U.
17. Hoeijmakers, H.W.M., Rizzi, A., "Vortex-Fitted Potential Solution Compared with Vortex-Captured Euler Solution for Delta Wing with Leading-Edge Vortex Separation", AIAA Paper 84-2144, 1984.
18. Peace, A.J., "A Multi-Vortex Model of Leading-Edge Vortex Flows", International Journal of Numerical Methods in Fluids, Vol. 3, 1983, pp. 543-565.
19. Zabusky, N.J., Hughes, M.H., Roberts, K.V., "Contour Dynamics for the Euler Equations in Two Dimensions", Journal of Computational Physics, Vol. 30, 1979, pp. 96-106.

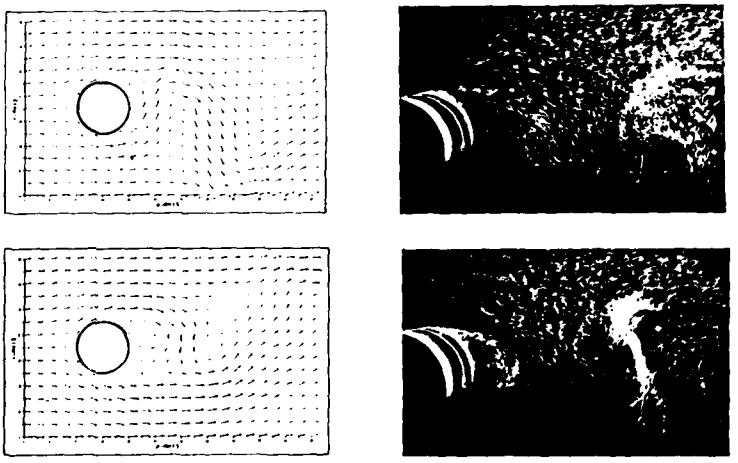

Fig. 1 Comparison of computed and observed flow field around circular cylinder at Reynolds number of 31,700 (Ref. 7)

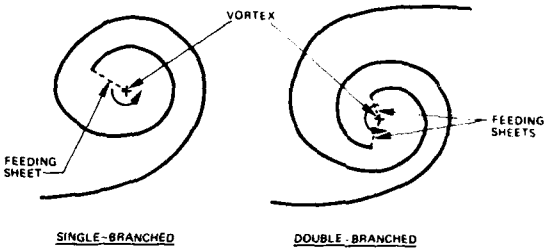

Fig. 2 Isolated vortex/feeding sheet(s) core model

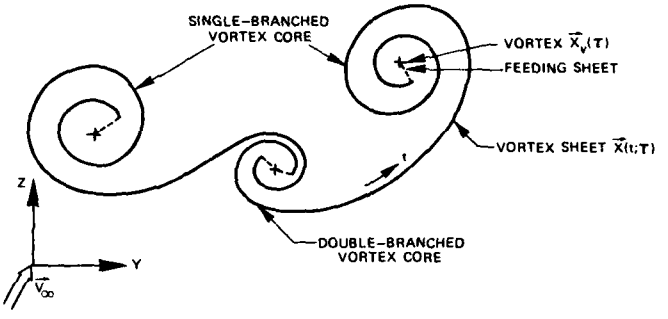

Fig. 3 Vortex sheet model in Trefftz plane for initial roll-up

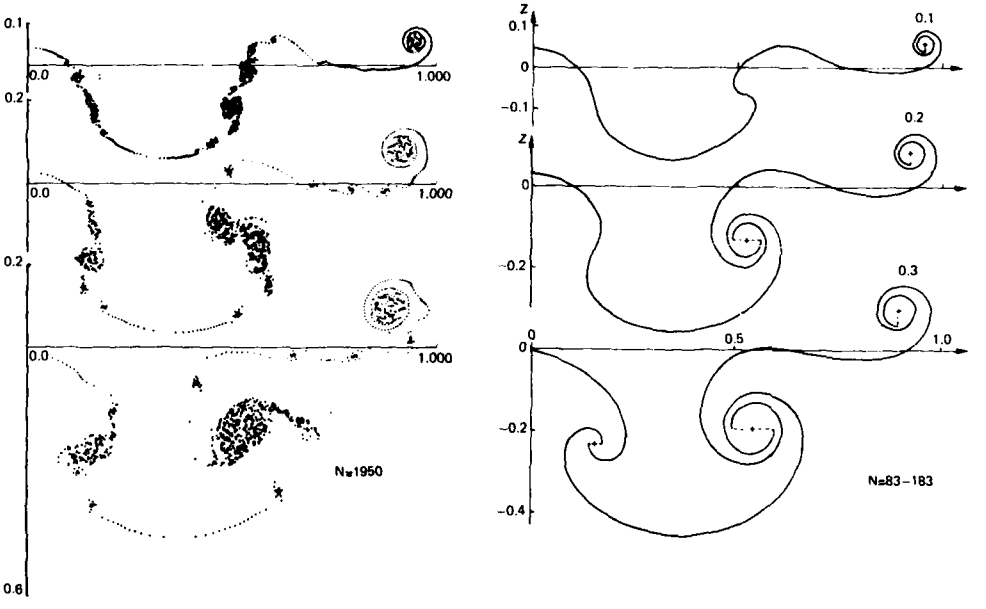

(i) CLOUD-IN-CELL METHOD
BAKER, REF. 14

(ii) PANEL METHOD
VOR2DT REF. 8

Fig. 4a Wake behind wing-body with deployed flap

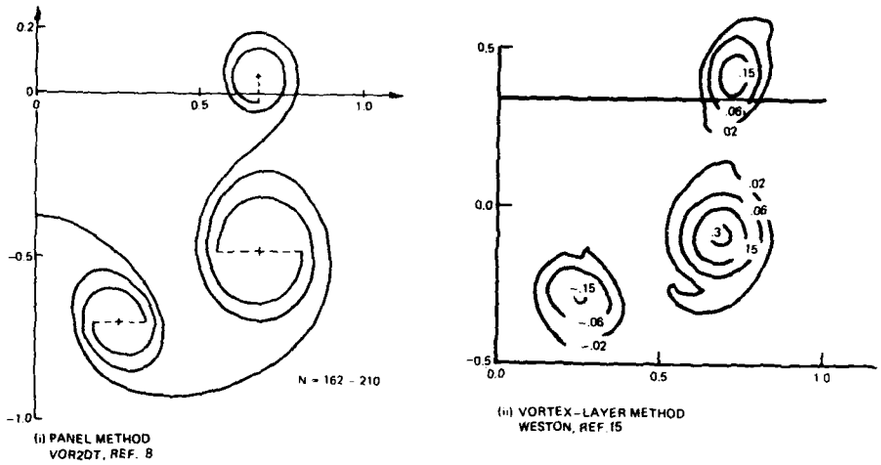

Fig. 4b Wake behind wing-body with deployed flap, $\tau \approx 1.0$

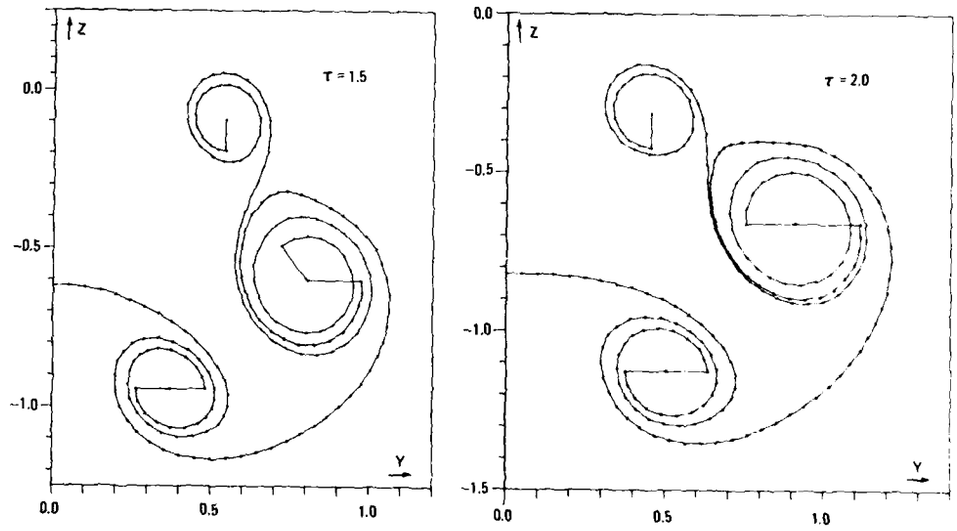

Fig. 4c Wake behind wing-body with deployed flap, VOR2DT results

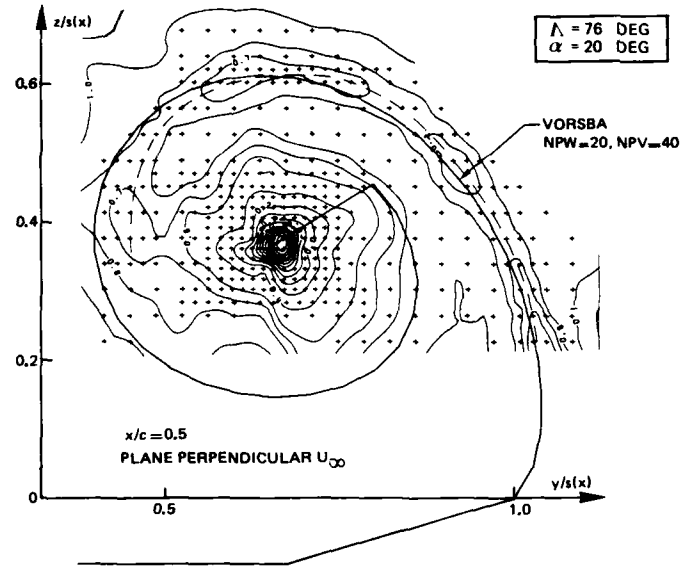

Fig. 5 Comparison of measured total pressure contours (Delft University of Technology) and computed (VORSBA) vortex sheet geometry

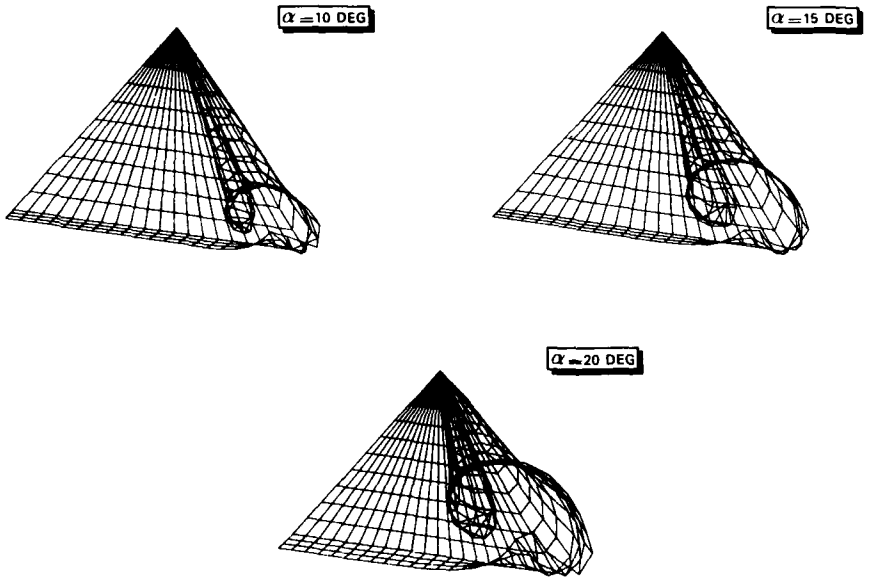

Fig. 6 Computed 3D vortex sheet geometry (VORSEP) for 65-deg swept delta wing

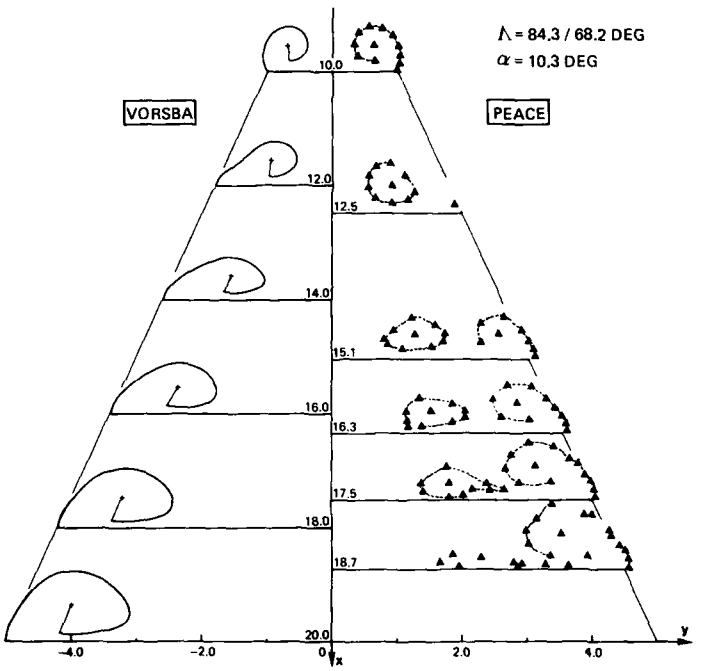

Fig. 7 Computed vortex sheet geometry for double delta wing. Comparison of panel method and discrete-vortex method

FLOW MODELS USING VORTEX DYNAMICS - WORK IN THE UNITED KINGDOM

by
D.J. Maull
University Engineering Department
Trumpington Street
Cambridge CB2 1PZ
UK

SUMMARY

A review is given of work in the United Kingdom on vortex dynamics. This method of modelling separated flows is applied to unsteady flow around aerofoils, bluff bodies, boundary layers and pollution studies. Many applications are given and some of the difficulties in using the method described.

INTRODUCTION

The representation of a flow field by identifiable regions of vorticity embedded in an otherwise irrotational flow is one of the oldest models of fluid flow. Thus we have the boundary layer approximation of Prandtl, the wing vortex system of Lanchester and the wake and drag of a body presented by von Karman. A solution of the Navier-Stokes equations will, of course describe the entire flow field but at the moment solutions at high Reynolds numbers are limited and it is at these high Reynolds numbers that models involving vortex dynamics can offer some advantages. The time taken to convect a distance ℓ with velocity v is ℓ/v and during that time diffusion, due to viscosity ν, will take place over a distance $(\nu\ell/v)^{\frac{1}{2}}$, thus the Reynolds number is a direct measure of the importance of convection compared with diffusion. It is therefore at high Reynolds numbers, where the convection of vorticity is much more important than its diffusion, that vortex dynamics calculations have their most useful and meaningful applications.

Vortex dynamics is undoubtedly a popular subject and therefore to bring this review down to a manageable size, consistent with a short presentation, some rather arbitrary decisions have had to be made as to what subject areas should be omitted. The main omission is a discussion of the three-dimensional flows present for instance in the vortex flow over slender bodies. They have been omitted mainly because they have been reviewed extensively in two excellent papers in the last few years by Smith (1) and (2). Papers published before 1974 have usually been omitted since they have been referred to in a review paper by Clements and Maull (3). Subsequent review papers have been presented by Graham (4) and (5) and a discussion of the method within the framework of computational fluid mechanics has been given by Roberts and Christiansen (6).

Most of the applications of this method have been to two-dimensional flows where, in the absence of viscosity, the vorticity equation is simply $\frac{Dw}{Dt} = 0$. The problems in applying the equation then arise in (a) the means of injecting vorticity into the flow (the Kutta condition); (b) the efficiency of the schemes for tracking the vortices (Biot-Savart law or vortex-in-cell methods); (c) schemes for reducing the number of vortices (amalgamation of vortices); (d) prevention of unrealistic velocities (use of vortices with cores); (e) prediction of forces; (f) the possible inclusion of viscous effects and (g) the probability that the flows that are being calculated contain, in reality, three-dimensional effects.

The review will start with a case of unseparated, unsteady flow with a non-linear vorticity wake and progress to cases where there is a strong interaction between two, initially distinct vortex sheets, including problems of interest to the offshore industry where the free stream is periodic. Other topics will include the representation of axisymmetric jets, the dispersion of pollutants and free surface problems.

APPLICATIONS

(1) Unsteady, attached flow about an aerofoil

In this case, vorticity is only shed from one point, the trailing edge, and the most important part of the calculation is centred around the modelling of the trailing-edge flow. Basu and Hancock (7) represent the wake vorticity immediately adjacent to the trailing edge by a sheet of vorticity whose length and inclination are subsequently calculated as part of the solution. An interesting result of this calculation is that the inclination of the sheet agrees with that proposed as a Kutta condition by Maskell (8). Vorticity further down the wake is represented by discrete vortices. The method has been applied to an aerofoil suddenly changing incidence, entering a gust and oscillating. The oscillating aerofoil has also been studied by Vezza and Galbraith (9) who used a similar representation at the trailing edge and a comparison of their results with experiment is shown in Figure 1, where it can be seen that the experimental lift loop has been reasonably well predicted.

For the starting flow round an aerofoil it is questionable whether in the early part of the motion that a planar vortex sheet is a good representation of what is likely to be

a spiral vortex sheet. This is modelled by Graham (10) as a concentrated vortex joined to the aerofoil trailing edge by a cut and it is argued that this is a better representation when the flow is dominated by rapid changes round the trailing edge compared with convection due to the free stream.

(2) Unsteady, separated flow from a single edge

A purely oscillatory flow, with zero time mean, can occur under waves and the prediction of forces on bodies in these conditions is of interest to the offshore industry. The flow is characterised by the Keulegan-Carpenter number $(K_C) = 2\pi a/D$, a being a free-stream particle displacement and D a typical dimension of a body in the flow. Thus if the Keulegan-Carpenter number is small any vortices formed from one edge will not have time to interact with vortices from another edge before the flow reverses, although subsequent vortices from a single edge will interact.

This type of flow has been considered by Graham (11) and is shown in Figure 2. He shows that for a flat plate the drag coefficient is given by $C_D = A\, K_C^{-1/3}$ (see Figure 3), but that A is over predicted by about 40%. In this calculation a multi-vortex model was used but with a single plane sheet element next to the body edge. Thus the representation at the separation point is similar to that used in (7) and (9).

Another problem where vortex shedding from two edges may not interact significantly is the case of the shedding from the keel of a rolling barge. In this case vortex shedding from the keel, particularly if it is sharp, will produce damping in roll which cannot be calculated other than by using vortex dynamics. This damping has been calculated by Downie, Bearman and Graham (12) using the method of Graham (11) for placing the vortices into the flow near the sharp edges. A similar calculation has been presented by Brown and Patel (13) where now the most recent vorticity shed in the calculation is not placed as a sheet, as is done by Graham, but as a discrete vortex at a fixed point near to the shedding edge with a strength proportional to the square of velocity at that point.

Another example of separation from a sharp edge is given by Evans and Bloor (14) for the starting flow through a sharp-edged orifice. In this case the most recent shed vortex is placed at a point, h, above the edge of the orifice. The vortex strength is taken as proportional to u^2, where u is the velocity at h, and h is calculated by ensuring that the flow leaves the orifice edge smoothly. This method, and others, of satisfying the Kutta condition will be discussed later. Results from (14) are shown in Figure 4 which agrees reasonably well with photographs of the starting flow through an orifice.

(3) Steady, separated flow from a single edge

All vortex dynamics calculations are time-marching so it could be hoped that a calculation such as (14) above, if left long enough, would settle down to a fairly steady pattern. Lewis (15) considered a similar problem to (14) and found that the large recirculating region downstream of the plate continued to grow with time with all vortices being swept into it. This is obviously incorrect and the resulting calculation of drag showed increasing large fluctuations as the time developed. Burton (16), however, did what seemed to be the same calculation and showed very little fluctuation of drag, indeed the drag coefficient agreed very well with experiment for the mean drag of a body shedding alternate vortices.

Summers, Hanson and Wilson (17) and (18) have also done a similar calculation for the flow over a building shape. In this case vortices do travel downstream in fairly well defined clusters. The difference between their calculation and those of (15) and (16) is that allowance is made for vortices to have reduced strength when approaching a surface by diffusing opposite sign vorticity into the flow from the surface.

(4) Interacting separated flow

Most of the work on vortex dynamics has been in this area since it does present a method of calculating complicated vortex shedding problems in two dimensions. It is now accepted that the Strouhal number for vortex shedding from sharp-edged bodies is reasonably well predicted. A recent calculation of vortex shedding from wedge and squares by Stansby (19) shows, in most cases considered, that the Strouhal number was over-predicted by about 25% which is somewhat less accurate than earlier calculations for longer bodies.

A more difficult body to deal with is one, such as the circular cylinder, where the separation points are not fixed. Immediately the question arises as to what to do about the separation points: do you make an inspired guess, do you use experimental data (which seems somewhat pointless since the object is probably to predict some experimental data) or do you perform a boundary layer calculation at the same time as the vortex dynamics calculation? All of these methods have been used including modelling of the boundary layer using vortex dynamics.

Virtually all of the calculations over-predict the drag and produce flow patterns which indicate vortices rolling up too near to the base of the body. It is clear that these effects are due to the fact that the vortices produced by the method are too strong and so various methods have been introduced to build into the calculation some form of vortex decay. Thus Smith and Stansby (20) and (21) use $\Gamma(t^*) = \Gamma_o \exp(-q/t^*)$ and

Ali and Narayanan (22) use $\Gamma(t^*) = \Gamma_o(1 - \exp(\beta/t^*)$ where t^* is non-dimensional time and q and β are constants. In (22) the problem considered is that of a circular cylinder near a plane boundary and β is a function of the gap between the cylinder and the boundary. The effect of different values for q are seen in Figure 5 (from (20)) where the variation in q produces little variation in drag coefficient which is about 1.2 for q of 0.05 and 0.10 compared with 1.3 for $q = 0$. However, as can be seen, the higher value of q eventually stops all oscillation of the lift coefficient and presumably no vortex street is formed. It is somewhat peculiar that a non-zero time mean lift is generated. The use of a decay law is usually justified on two counts; that real vortices diffuse and that most experiments involving separated regions contain three-dimensional effects which reduce the induced velocity at a point compared with a two-dimensional model. The velocity field of a viscous, laminar vortex is given by

$$v = \frac{\Gamma_o}{2\pi r}\,(1 - \exp(-r^2/4\nu t))\ ,$$

v being the velocity at radius r due to a vortex which at time $t = 0$ had strength Γ_o. Thus the velocity field of the laminar vortex can be quite different from the velocity field of the vortices with time delay mentioned above particularly near the vortex centre. If two potential vortices become too close they will tend, obviously, to move with very high unrepresentative velocities and this is usually stopped by either giving the vortices a core with a linear velocity distribution or by amalgamating vortices if they become too close.

An example of using discrete vortices not only in the wake but also in the boundary layer is given by Stansby and Dixon (23) where molecular diffusion is represented by a random walk where the Reynolds number is introduced via a random walk with Gaussian distribution. The results are encouraging giving drag and Strouhal number in broad agreement with experiment.

Stansby (24) uses a much simpler, empirical, criteria for separation on a circular cylinder and again produces a reasonable prediction for Strouhal number and an underestimate for drag.

Porthouse and Lewis (25) assume for a circular cylinder that separation is fixed and a random walk is used on the shed vortices. These calculations show an increase in Strouhal number with Reynolds number (via the random walk).

Large-scale separation from an aerofoil is another form of bluff body flow which has been calculated by Vezza and Galbraith (26). In this case the separation point is fixed and the flow started by suddenly putting the aerofoil up to the stalled incidence. The vortices are given a constant vorticity core and vortices are coalesced if they become too close. An example of the excellent agreement with experiment is shown in Figure 6. A stalling aerofoil has also been studied by Lewis and Porthouse (27) and (28) who also include stalled flow in a cascade of aerofoils.

The rapid deployment of a spoiler is another example of a large-scale separated region on an aerofoil. This has been studied by Tou and Hancock (29) and experimental adverse lift effects have been confirmed over a range of aerofoil angle of incidence and spoiler angle.

An unusual application of the discrete vortex method is given by Soliman, Smith and Cheeseman (30) for the calculation of a circulation control circular cylinder. The results predicting the lift-coefficient as a function of jet momentum are reasonably good but some vortex decay has had to be used to bring the results in line with experiment.

The interaction of the wakes from two bodies in a flow produces a further complication. Two circular cylinders across the main stream have been studied by Stansby (24) and the large-scale features of the calculated wakes agree broadly with experiment although the prediction of the forces is less satisfactory. Kamemoto and Bearman (31) have presented a calculation for the interaction of two flat plates across the stream and produce flow patterns which look convincing but there are no experimental results for comparison.

(5) Unsteady free stream

Of particular interest to the offshore petroleum industry is the prediction of the forces on bodies in an oscillatory free stream, usually, but not exclusively, with a zero time mean velocity. One paper (11) has already been mentioned in this area for low Keulegan-Carpenter number flows where the separated shear layers may not interact. At higher numbers significant interaction can occur with obviously more complicated flow patterns. Early calculation by Stansby (32) for a circular cylinder with fixed separation points under-predicted the drag coefficient at low Keulegan-Carpenter numbers and over-predicted at high numbers. The inertia coefficient was under-predicted over the range. The lift force will contain harmonics of the free stream frequency depending upon the Keulegan-Carpenter number and these are shown in another calculation by Stansby (33). Instead of using the Biot-Savart law as in (32) to calculate the vortex velocities, Stansby (34) used the vortex-in-cell method for the same problem again with fixed separation points. Now the root-mean-square of total force agrees well with experiment but the individual drag and inertia coefficients show large discrepancies between calculation and experiment. A more advanced method using a random walk simulation for viscous effects is presented by Stansby and Dixon (23) showing again a fair prediction of the root-mean-square force but only a moderate prediction of the drag and inertia coefficients.

Ali and Narayanan (35) have calculated the unsteady flow past a circular cylinder on a plane surface and whilst the results agree reasonably well with high Reynolds number full-scale experiments they do not agree with more detailed low Reynolds number laboratory experiments.

Another example of an oscillatory free stream is given by Clements (36), in this case dealing with the question of the effect on vortex shedding of oscillations superimposed upon a uniform steady stream. He shows that vortex shedding can lock on to longitudinal free stream oscillations at double and four times the normal shedding frequency and that the drag is increased in these regions.

Oscillatory flow over sand ripples can also be dealt with using discrete vortices. Two papers, Longuet-Higgins (37) and Smith and Stansby (38) deal with the problem. In (37) conformal transformation is used for the ripples and a viscous dissipation is introduced by allowing the core of a vortex to increase with time. The results show the same trend for drag coefficient with the ratio of free stream particle excursion to ripple wave length as that of experiment but there is some indication that the calculation might be going unstable as time progresses. A vortex-in-cell method is used in (38), together with a random walk, for the oscillatory flow over a sinusoidally rippled bed. Figure 7 shows a comparison with experiment for the velocity at a point above the bed showing good agreement as long as the vortices decay with time. In this case the circulation must decay by 55 % in its first quarter cycle for good agreement.

(6) Vortex interactions

A model of the Kelvin-Helmholtz instability has been studied by Bromilow and Clements (39) taking into account surface tension and density changes across the interface. It is shown that a high order form of rediscretization of the vortex sheet is required to give good agreement with analytical predictions.

In (40) Bromilow and Clements have presented some calculations for the interaction of two and three vortices of different strengths showing the possibility, in a single shear layer, of rapid stretching and tearing of the vortices.

Acton (41) also studied the rolling up of a single sheet and found that to adequately represent vortex pairing the sheet had to be given some thickness.

In an attempt to investigate the effect of free stream turbulence on a shear layer, Kiya, Ohyama and Hunt (42) performed an experiment on the effect of an isolated vortex on a shear layer and modelled this by means of a discrete vortex calculation. The calculation showed the basic features of the experimental flow particularly the early stages of the interaction and assisted in understanding the complicated flow.

Waves on a free surface can be represented by a vortex sheet and this has been studied by Stansby and Slaouti (43) together with the interaction of the wave with a body under the surface. The results look encouraging and show none of the instability found by other authors.

N point vortices on the vertices of a regular polygon are stable for $N < 7$, neutrally stable if $N = 7$ and unstable if $N > 7$. Dhanak (44) examined the effect of a finite core on the stability and found that now the arrangement was still stable for $N < 7$ but unstable for $N \geq 7$.

As a vortex is convected past a flat plate at zero incidence to the flow, lift is generated on the plate and vorticity shed off the trailing edge which can interact with the main vortex. This interaction, with the plate placed above a plane wall, has been studied by Acton and Dhanak (45) and is a good example of a complicated flow which can be modelled by a discrete vortex calculation. Whether it is a good model, of course, depends upon the importance of viscous and three-dimensional effects in the real flow.

(7) Boundary layers

Boundary layers have been modelled using discrete vortices and a random walk to simulate viscous diffusion in some of the vortex shedding calculations previously mentioned. A more thorough modelling has been reported by Lewis and Porthouse (27) and Figure 8 shows the solution of a laminar boundary layer compared with the Blasius solution. The displacement thickness and momentum thicknesses are both predicted to an accuracy of about three per cent. Decelerating and accelerating flows have also been calculated and compared with Falkner-Skan solutions, the agreement is good for accelerating flows but less so for decelerating flows.

(8) Axisymmetric flows and ring vortices

An obvious application of discrete vortex calculations is to axisymmetric jets although it must be asked whether any jet is truly axisymmetric. The difference between two-dimensional and ring vortices is, of course, that ring vortices have a self-induced velocity which is a function of the core size and distribution, indeed zero core radius will produce an infinite self-induced velocity. The representation of an axisymmetric vortex sheet by ring vortices has been discussed by Bernardinis and Moore (46). Dhanak and Bernardinis (47) chose a particular core size and vorticity distribution in studying the evolution of an elliptic vortex ring. They showed the oscillation of the ring size in Figure 9 which agreed well with experiment.

The starting flow of an axisymmetric jet has been well predicted using ring vortices by Davies and Hardin (48). In this case the core radius was taken to be $(4\nu t R_o/R)^{\frac{1}{2}}$ where R_o was the initial value of the ring radius at time $t = 0$ and R the instantaneous radius. The calculation was taken much further in time by Davies, Hardin, Edwards and Mason (49) in order to calculate the spectrum of noise from the jet. The calculation shows that the peak Strouhal number is correctly predicted but the peak is narrower than that of experiments, probably because the model does not allow for any small scale asymmetric disturbances. The same conclusion is arrived at by Edwards and Morfey (50) and is shown in Figure 10. In this case a velocity cut-off was used to simulate the effect of a core on the velocity induced on a nearby vortex and this is discussed by Morfey and Edwards (51).

Acton (52) modelled the effect of harmonic forcing on an axisymmetric jet and produced results showing large scale eddies similar to those observed experimentally. Figure 11 gives the radial velocity development with time for an unforced jet, showing vortex pairing. Figure 12 shows the effect of forcing the jet and clearly demonstrates the enhanced pairing of vortices caused by the forcing.

(9) Pollution modelling

Sene (53) has used the method to predict void fraction profiles for the two-phase flow of air bubbles in a water mixing layer, showing good agreement with experiment. Figure 13 shows the reasonable agreement between the model and experiment for the ground level concentration of a pollutant coming from a point source behind a blunt base. In this calculation Turfus (54) used vortex decay with time, a finite core and also decay as a function of the distance of a vortex from the wall.

A two-dimensional cloud of gas instantaneously released in a flow has been modelled by Rottman, Simpson and Stansby (55). A vortex-in-cell calculation has been used together with viscous diffusion using a random walk to study the progressive deformation of the cloud. The results are in general agreement with both laboratory and large-scale field experiments.

BASIC PROBLEMS AND TECHNIQUES

In a series of papers (56,57,58,59) Moore nas studied in detail instabilities that can arise in vortex sheets. In (56) he shows that a vortex sheet will develop a singularity as an initial disturbance evolves and that unless the vortex layer which is represented by a sheet is undergoing rapid stretching then the thickness of the layer must be represented. It is well known from early calculations that discretising a vortex sheet can eventually introduce chaotic motion into the vortex paths. This is shown by Moore (57) to be due to numerically introduced disturbances which are amplified and that the instability can be reduced by using either a repositioning technique or smoothing. Both methods were tested on a circular vortex sheet. Discretization of surface waves can introduce spurious resonances as discussed in (58) and it is not clear why these resonances did not occur in the calculation of Stansby and Slaouti (43). A further discussion of these resonances is given in (59).

Two techniques are used to improve the representation of a vortex sheet that is rolling up and both of these have been discussed by Bromilow and Clements (60). If vortices become too close together then very high velocities are induced which are totally unrepresentative of the real flow. One solution is to give to each vortex a core where the velocity is reducing to zero as the centre of the vortex is approached, another solution is to simply amalgamate vortices which become too close. It is a modification of this second method that is discussed in (60) and it certainly gives a smooth rolling up on a sheet. Rapid stretching of the sheet can mean that vortices become so far apart that the representation is lost and for this reason alone some form of repositioning of the vortices should be used. One such method is given in (60).

It is evident that the discrete vortex method when applied to bluff based bodies is reasonably successful in predicting Strouhal numbers but the flow patterns produced show vortex formation that is closer to the body than that seer in experiments. One result of this is that the forces, and in particular the drag, are usually too large. To counteract this, as has already been mentioned, some workers give every vortex a decay which is a function of its age. This is sometimes justified by saying that viscous diffusion is being modelled but this cannot be the case since viscous diffusion produces a core to the vortex and leaves the far velocity field of the vortex virtually unchanged. A better representation is a vortex core which is expanding with time as used by Longuet-Higgins (37).

Most experiments on separated flows undoubtedly contain three-dimensional effects and again vortex decay is occasionally put into the calculation to allow for these effects. A preliminary assessment of these effects has been made by Graham (61) by considering the spanwise waviness of the shed vortex lines, the effect being to reduce the drag coefficient.

There appears to be no agreement as to what value of decay should be put into these calculations, indeed Stansby (19) using the same calculation method and the same decay rate shows good agreement with experiment for a wedge but not for rectangles and squares.

Whether the lack of agreement is because the calculations are two-dimensional and the experiments are largely three-dimensional cannot be easily resolved. One comparison,

however, is available between the vortex method and a two-dimensional Navier-Stokes solution. Figure 7 showed good agreement between the vortex method, with imposed vortex decay, and some experimental results. The original paper giving these experimental results also showed good agreement between these results and a Navier-Stokes solution, which seems to indicate, at least in this case, that the vortex decay was not accounting for three-dimensionality but possibly for viscous effects.

It is possible that the vorticity shed at the separation points in the calculations is greater than in practice because vorticity of the opposite sign generated in the base region is usually neglected. A scheme for considering this vorticity is presented by Stansby and Dixon (62) which introduces secondary separation of the flow in the base region.

The application of a continuous Kutta-Joukowski condition at a separation point when a discrete calculation method is being used presents some problems. If U is the velocity at the separation point then the rate of vortex shedding is $U^2/2$ and the vorticity convects away with a velocity $U/2$. If the continuous vortex sheet just downstream of the separation point is replaced by a point vortex then to satisfy the Kutta condition the separation point will be a stagnation point and $U = 0$. There are then two possibilities, either to fix the strength and the position of the last vortex which has been shed and evaluate U somewhere near the edge or to relax the Kutta condition and fix the initial position. A more satisfactory solution is to represent the initial shed vorticity as a sheet attached to the separation point as has been done in (7) and discussed, together with the point vortex representations, in Graham (63).

The size of the time step in the calculation is obviously important and most papers give some indication as to what values have been used. Kamemoto and Bearman (31) made a thorough study of this together with the effect of the initial vortex position for the flow round a flat plate. The conclusions are that the first vortex should be placed about one per cent of the base height away from the body but at the same time the non-dimensional group of vortex position divided by free stream velocity times the time step should be about 0.05.

The calculation of the force on the body is done either by using Blasius equation or by integrating the pressure distribution. Using Blasius equation implies that the total pressure in the flow is the same in all regions including the wake and therefore the drag is solely dependent upon the motion of the vortices. Putting vortex decay into the calculation may model the total pressure loss in the wake. The pressure at a separation point is the same either side of the vortex sheet and thus given that the velocities are different then the total pressure variation in the wake region can be calculated if the time derivative of velocity potential can be accurately assessed. This appears to be difficult and pressure distributions in the base region usually show greater variations than those given by experiment.

CONCLUSIONS

The modelling of high Reynolds number flows using vortex dynamics has been developed in the last few years to the point where it can give reasonable answers to complex problems. It is particularly successful in predicting some aspects of unsteady flows where large-scale vortex interactions are a main feature of the field but does not seem to be too successful in estimating forces unless some empirical input is put into the calculation. Obviously more work must be done to improve the estimation of the forces.

Further applications of the method may well be in areas where the flow is very unsteady such as where the main stream is oscillating or the body is changing shape. Recent applications to problems involving the dispersion of pollutants in separated flows are encouraging and calculations involving jets and buoyant plumes at an angle to a stream are promising. The multi-vortex model of a boundary layer and its disturbance leading to transition both show reasonable results.

The method should not be seen as a competitor to Navier-Stokes or Euler solutions but rather as a complementary method which focusses attention on large-scale structures.

ACKNOWLEDGEMENTS

I would like to thank all those who have kindly supplied me with details of their work and apologise to those whose work has been inadvertently missed out. This paper, being only one part of a larger review, has been necessarily parochial in nature and I would like to make it clear that a large part of the work cited has come about from interactions with studies in other countries.

REFERENCES

(1) Smith, J.H.B. Achievements and problems in modelling highly-swept flow separations. In Numerical Methods in Fluid Mechanics, ed. P.L. Roe, Academic Press, 1982.

(2) Smith, J.H.B. Theoretical modelling of three-dimensional vortex flows in aerodynamics. Aeronautical Journal of Roy. Aero. Soc., pp.101-116, April 1984.

(3) Clements, R.R., Maull, D.J. The representation of sheets of vorticity by discrete vortices. Prog. Aerospace Sci. 16, pp.129-146, 1975.

(4) Graham, J.M.R. Numerical simulation of steady and unsteady flow about sharp-edged bodies. IAHR Symposium on Separated Flow around Marine Structures, Trondheim, Norway, June 1985.

(5) Graham, J.M.R. Application of discrete vortex methods to the computation of separated flows. Int. Symposium on Computational Fluid Dynamics, Reading, April 1985.

(6) Roberts, K.V., Christiansen, J.P. Topics in computational fluid mechanics. Computer Physics Comm. 3, Suppl., pp.14-32, 1972.

(7) Basu, B.C., Hancock, G.J. The unsteady motion of a two-dimensional aerofoil in incompressible inviscid flow. J. Fluid Mech. 87, pp.159-178, 1978.

(8) Maskell, E.C. On the Kutta-Joukowski condition in two-dimensional unsteady flow. Royal Aircraft Est. Tech. Memo Aero 1451, 1972.

(9) Vezza, M., Galbraith, R.A.McD. A method for predicting unsteady potential flow about an aerofoil. Int. Journal Num. Methods in Fluids, 5, pp.347-356, 1985.

(10) Graham, J.M.R. The lift on an aerofoil in starting flow. J. Fluid Mech. 133, pp.413-425, 1983.

(11) Graham, J.M.R. The forces on sharp-edged cylinders in oscillatory flow at low Keulegan-Carpenter numbers. J. Fluid Mech. 97, pp.331-346, 1980.

(12) Downie, M.J., Bearman, P.W., Graham, J.M.R. Prediction of the roll damping of barges including the effects of vortex shedding. NMI Ltd. Rept. R188, 1984

(13) Brown, D.T., Patel, M.H. A theory for vortex shedding from the keels of marine vehicles. J. Eng. Math. 19, pp.265-295, 1985.

(14) Evans, R.A., Bloor, M.I.G. The starting mechanism of wave-induced flow through a sharp-edged orifice. J. Fluid Mech. 82, pp.115-128, 1977.

(15) Lewis, R.I. Surface vorticity modelling of separated flows from two-dimensional bluff bodies of arbitrary shape. J. Mech. Eng. Sci. 23, No. 1, pp.1-12, 1981.

(16) Burton, K.W. Evaluation of the vortex cloud technique for two-dimensional bluff body flows. 1985. Unpublished.

(17) Hanson, T., Summers, D.M., Wilson, C.B. Numerical modelling of wind flow over buildings in two dimensions. Int. J. Num. Methods in Fluids 4, pp.25-41, 1984

(18) Summers, D.M., Hanson, T., Wilson, C.B. A random vortex simulation of wind-flow over a building. Int. J. Num. Methods in Fluids 5, pp.849-871, 1985.

(19) Stansby, P.K. A generalised discrete-vortex method for sharp-edged cylinders. AIAA Journal, 23, No. 6, pp.856-861, 1985.

(20) Smith, P.A., Stansby, P.K. Supercritical flow around a circular cylinder by the vortex method. 1985. Unpublished.

(21) Smith, P.A., Stansby, P.K. A generalised discrete vortex method for cylinders without sharp edges. 1985. Unpublished.

(22) Ali, N., Narayanan, R. Hydrodynamic force on cylinder above plane bed. 4th Int. Symposium Offshore Mech. and Arctic Eng., Dallas, Feb. 1985.

(23) Stansby, P.K., Dixon, A.G. Simulation of flows around cylinders by a Lagrangian vortex scheme. Appl. Ocean Research 5, No. 3, pp.167-178, 1983.

(24) Stansby, P.K. A numerical study of vortex shedding from one and two circular cylinders. Aero. Quart. XXXII, pp.48-71, 1981.

(25) Porthouse, D.T.C., Lewis, R.I. Simulation of viscous diffusion for extension of the surface vorticity method to boundary layer and separated flows. J. Mech. Eng. Sci. 23, No. 3, pp.157-167, 1981.

(26) Vezza, M., Galbraith, R.A.McD. An inviscid model of unsteady aerofoil flow with fixed upper surface separation. Int. J. Num. Methods in Fluids, 5, pp.577-592, 1985.

(27) Lewis, R.I., Porthouse, D.T.C. Recent advances in the theoretical simulation of real fluid flows. N.E. Coast Inst. Eng. and Shipbuilders, pp.1-17, 1983.

(28) Lewis, R.I., Porthouse, D.T.C. A generalised numerical method for bluff body and stalling aerofoil flow. ASME Paper 82-GT-70, 1982.

(29) Tou, H.B., Hancock, G.J. A numerical study of a rapid deployment of a spoiler on a two-dimensional aerofoil. Queen Mary College, EP-1073, 1985.

(30) Soliman, M.M., Smith, R.V., Cheeseman, I.C. Modelling circulation control by blowing. In AGARD CP 365, 1984.

(31) Kamemoto, K., Bearman, P.W. The importance of time step size and initial vortex position in modelling flows with discrete vortices. Imperial College Aero Note 78-108, 1978.

(32) Stansby, P.K. An inviscid model of vortex shedding from a circular cylinder in steady and oscillatory far fields. Proc. Inst. Civ. Eng. 63, pt. 2, pp.865-880, 1977.

(33) Stansby, P.K. Mathematical modelling of vortex shedding from circular cylinders in planar oscillatory flows, including effects of harmonics and response. In Mechanics of Wave-Induced Forces on Cylinders, ed. Shaw, Pitman, 1979.

(34) Stansby, P.K. The force on a cylinder in a sinusoidal flow. ASME Paper 81-WA/FE-27, 1981.

(35) Ali, N., Narayanan, R. A discrete vortex model for wave forces on submarine pipelines. Paper submitted to ASCE 1986.

(36) Clements, R.R. On locked vortex shedding in a flow with perturbations parallel to the main stream. J. Sound Vib. 40, (4), pp.563-565, 1975.

(37) Longuet-Higgins, M.S. Oscillating flow over steep sand ripples. J. Fluid Mech. 107, pp.1-35, 1981.

(38) Smith, P.A., Stansby, P.K. Wave-induced bed flows by a Lagrangian vortex scheme. To be published in *J. Comp. Physics, 1986.*

(39) Bromilow, I.G., Clements, R.R. A discrete vortex simulation of Kelvin-Helmholtz instability. AIAA Journal 21, No. 9, pp.1345-1347, 1983.

(40) Bromilow, I.G., Clements, R.R. A numerical study of vortex interaction. J. Fluid Mech. 146, pp.331-345, 1984.

(41) Acton, E. The modelling of large eddies in a two-dimensional shear layer. J. Fluid Mech. 76, pp.561-592, 1976.

(42) Kiya, M., Ohyama, M., Hunt, J.C.R. Vortex pairs and rings interacting with shear layer vortices. To be published in J. Fluid Mech. 1986.

(43) Stansby, P.K., Slaouti, A. On non-linear wave interaction with cylindrical bodies: a vortex sheet approach. Appl. Ocean Res. 6, No. 2, pp.109-115, 1984.

(44) Dhanak, M.R. Stability of a regular polygon of finite vortices. Presented at BTMC Newcastle, 1984. Unpublished.

(45) Acton, E., Dhanak, M.R. A model of the interaction between a flow manipulator and an approaching eddy. Presented at Euromech 181 Stockholm, 1984. Unpublished.

(46) Bernardinis, B.de, Moore, D.W. A ring-vortex representation of an axisymmetric vortex sheet. Unpublished.

(47) Dhanak, M.R., Bernardinis, B.de. The evolution of an elliptic vortex ring. J. Fluid Mech. 109, pp.189-216, 1981.

(48) Davies, P.A.O.L., Hardin, J.C. Potential flow modelling of unsteady flows. Int. Conf. Num. Methods in Fluid Dynamics, 1973.

(49) Davies, P.A.O.L., Hardin, J.C., Edwards, A.V.J. A potential flow model for calculation of jet noise. AIAA Paper 75-441, 1975.

(50) Edwards, A.V.J., Morfey, C.L. A computer simulation of turbulent jet flow. Comp. and Fluids 9, pp.205-221, 1981.

(51) Morfey, C.L., Edwards, A.V.J. Energy and momentum constraints in the use of a cutoff in lumped-vortex flow models. ISVR Memo 587, 1978.

(52) Acton, E. A modelling of large eddies in an axisymmetric jet. J. Fluid Mech. 98, pp.1-31, 1980.

(53) Sene, K.J. Aspects of bubbly two phase flow. Cambridge University Ph.D. theis, 1984.

(54) Turfus, C. Stochastic modelling of turbulent diffusion near a surface. Cambridge University Ph.D. thesis, 1985.

(55) Rottman, J.W., Simpson, J.E., Stansby, P.K. The motion of a two-dimensional cloud released instantaneously in a uniform flow. To be published in J. Fluid Mech. 1986.

(56) Moore, D.W. The spontaneous appearance of a singularity in the shape of an evolving vortex sheet. Proc. Roy. Soc. Lond. A. 365, pp.105-119, 1979.

(57) Moore, D.W. On the point vortex method. SIAM J. Sci. Stat. Comput. 2, no. 1, pp.65-84, 1981.

(58) Moore, D.W. A point vortex method applied to interfacial waves. In: Vortex Motion, ed. Hornung, Müller. Vieweg and Sohn, 1982.

(59) Moore, D.W. Resonances introduced by discretization. IMA J. Appl. Math. 31, pp.1-11, 1983.

(60) Bromilow, I.G., Clements, R.R. Some techniques for extending the application of the discrete vortex method of flow simulation. Aero. Quart. XXXIII, pp.73-89, 1982.

(61) Graham, J.M.R., Naylor, P. The vortex wake of a flat plate in steady and oscillatory flow. Presented at Euromech 160, Berlin, 1982. Unpublished.

(62) Stansby, P.K., Dixon, A.G. The importance of secondary shedding in two-dimensional wake formation at very high Reynolds numbers. Aero. Quart. XXXIII, pp.106-123, 1982.

(63) Graham, J.M.R. Vortex shedding from sharp edges. Imperial College Aero. Rep. 77-06, 1977.

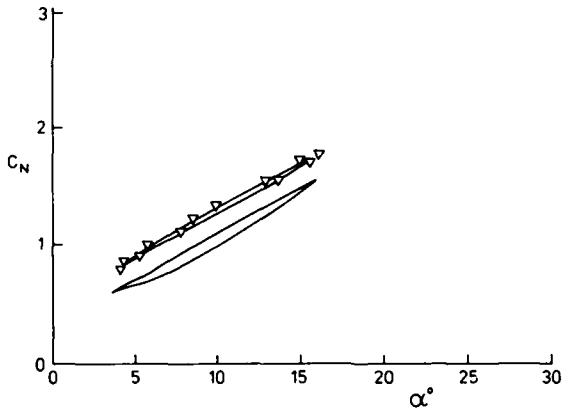

Figure 1 Normal force on NACA 23012 for $\alpha = 10 + 6\sin\omega t$
▽ , theoretical, —— experimental $R_e = 1.02 \times 10^6$

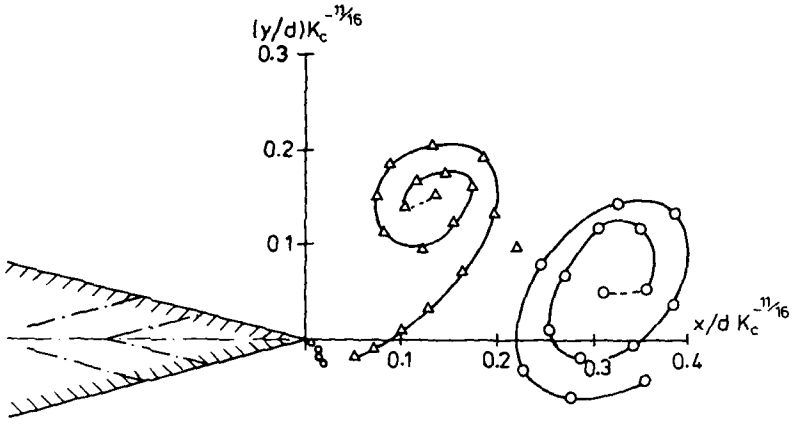

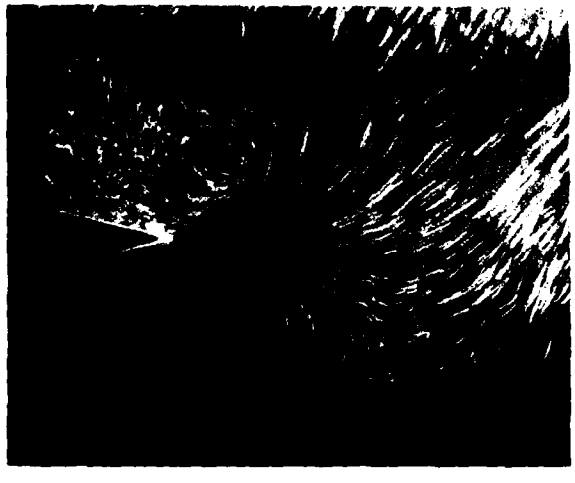

Figure 2 Oscillatory flow about a wedge corner

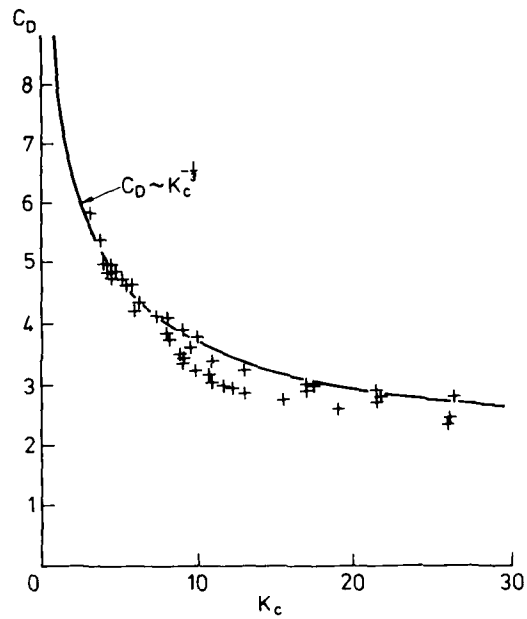

Figure 3 Drag coefficient versus Keulegan-Carpenter number for a flat plate.
+ , experimental

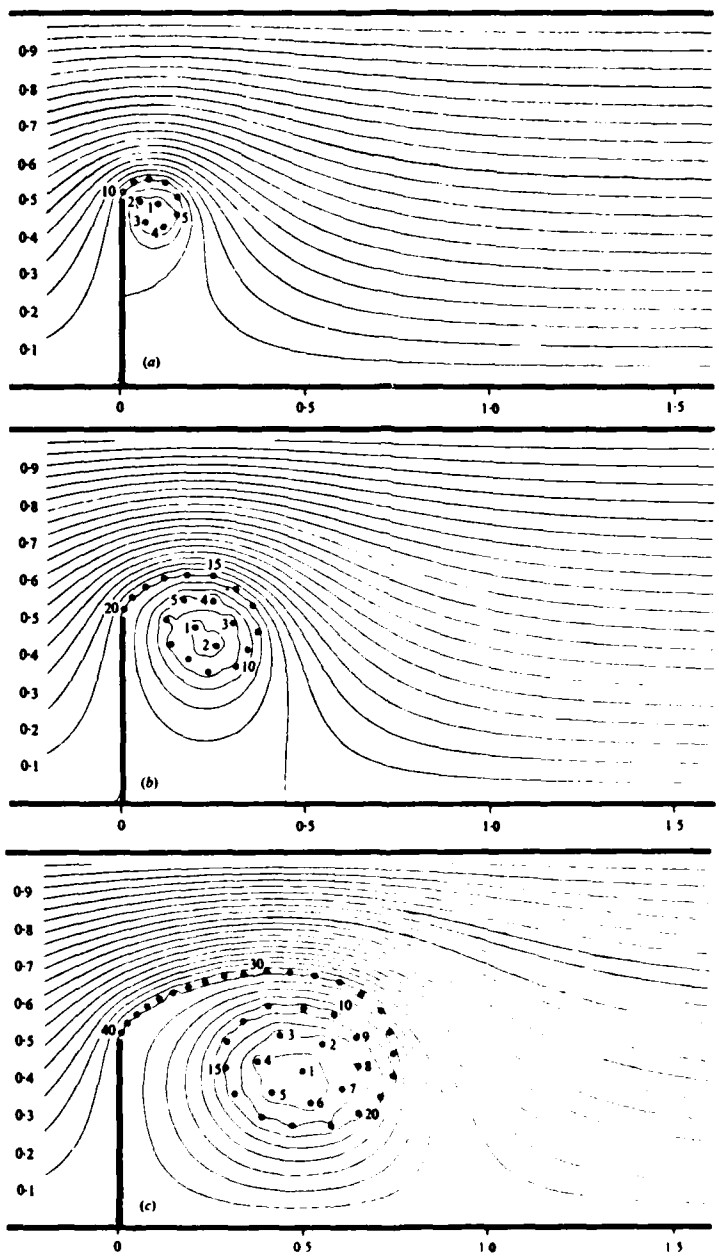

Figure 4 Starting flow past a plate

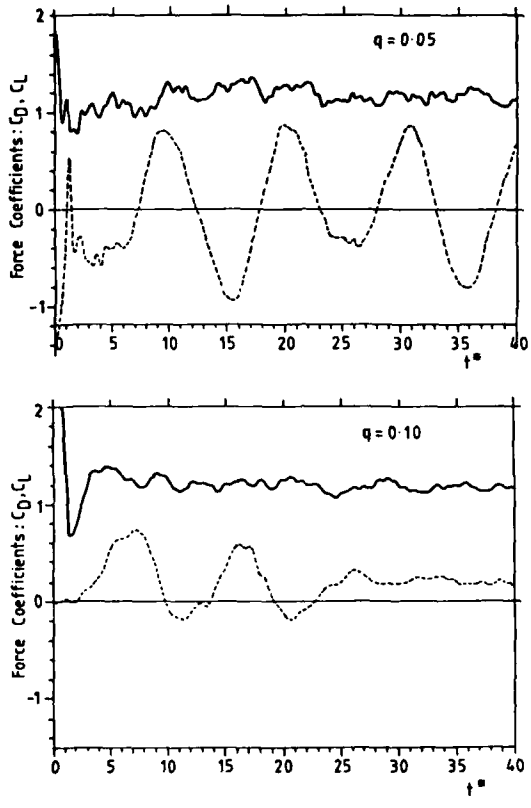

Figure 5 C_D and C_L versus non-dimensional time for a circular cylinder

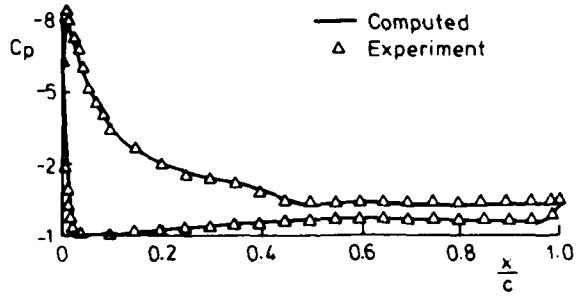

Figure 6 Chordwise pressure distribution at 20° incidence

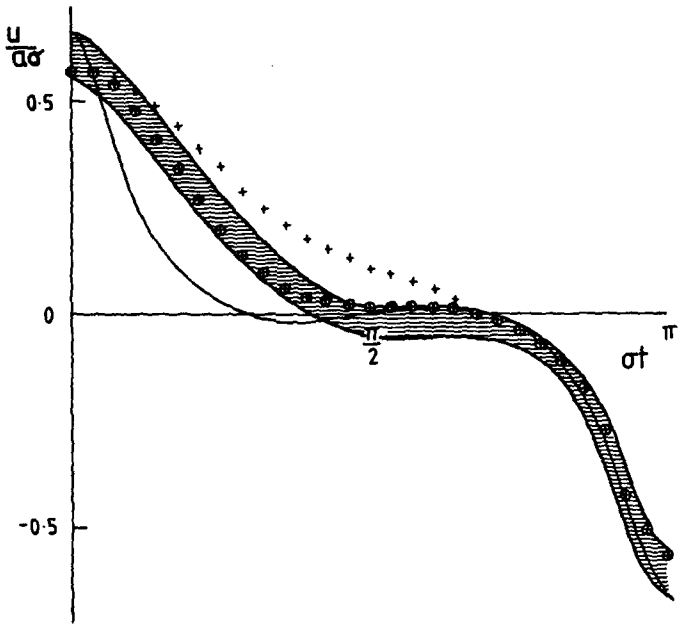

Figure 7 Velocity above an oscillating rippled bed

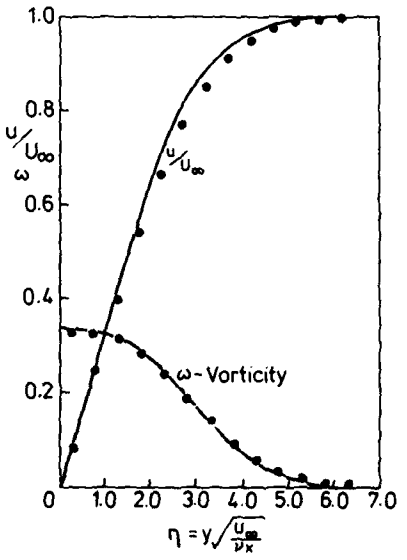

Figure 8 Flat plate boundary layer

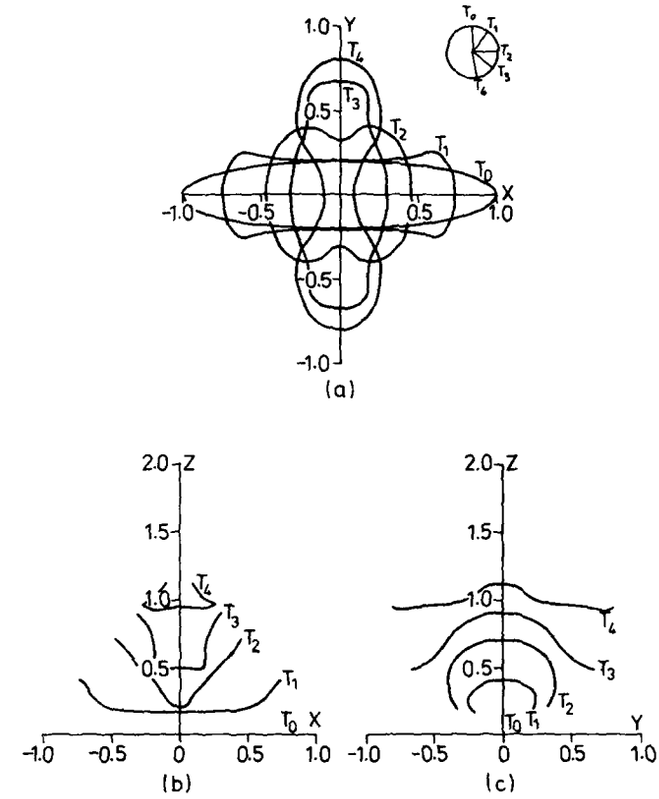

Figure 9 Deformation of an elliptic vortex

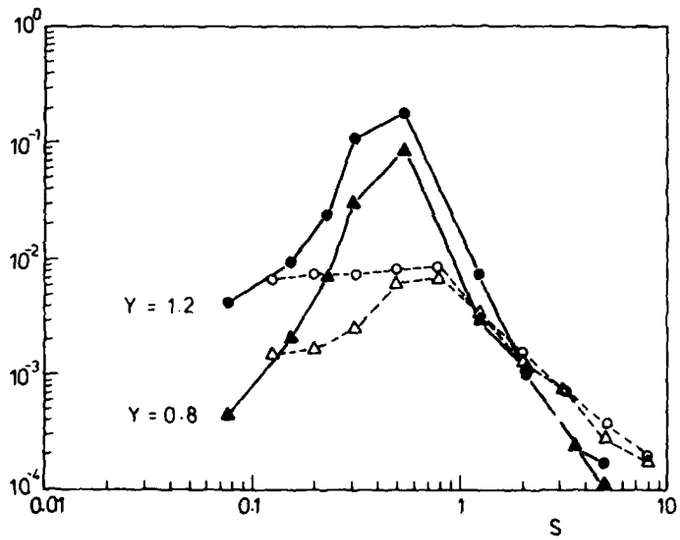

Figure 10 Radial velocity power spectra. Closed symbols model, open symbols experiment

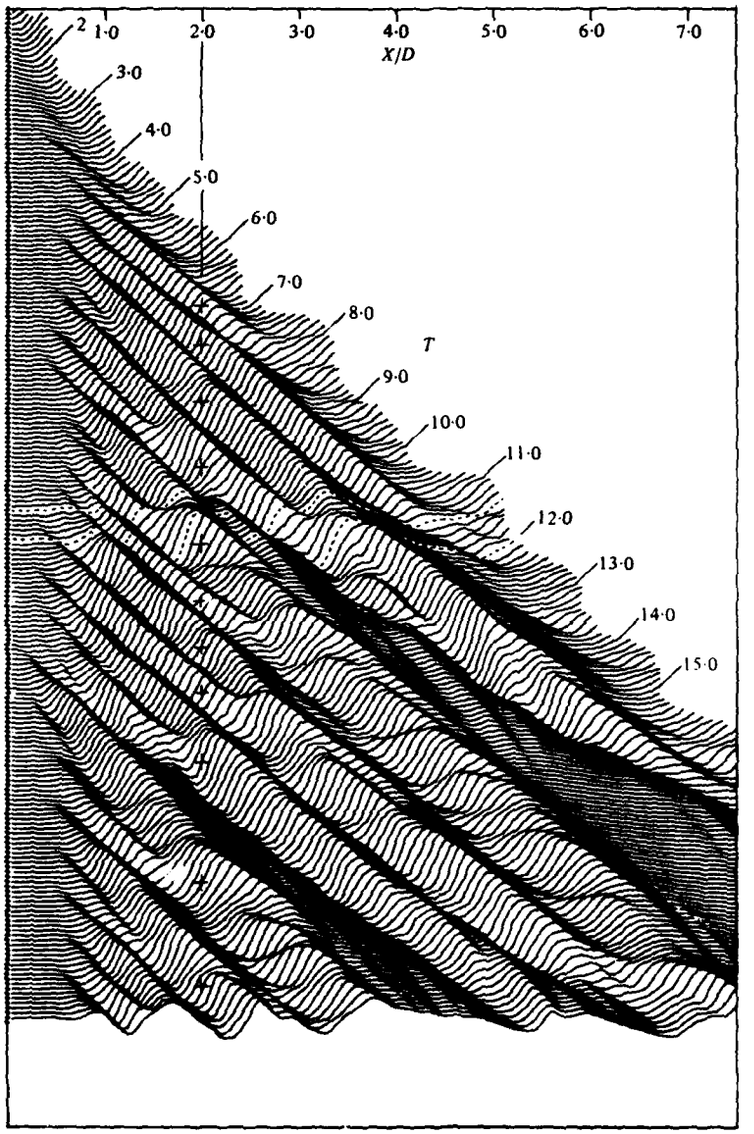

Figure 11 Axial distribution of radial velocity at equal time intervals, unforced jet

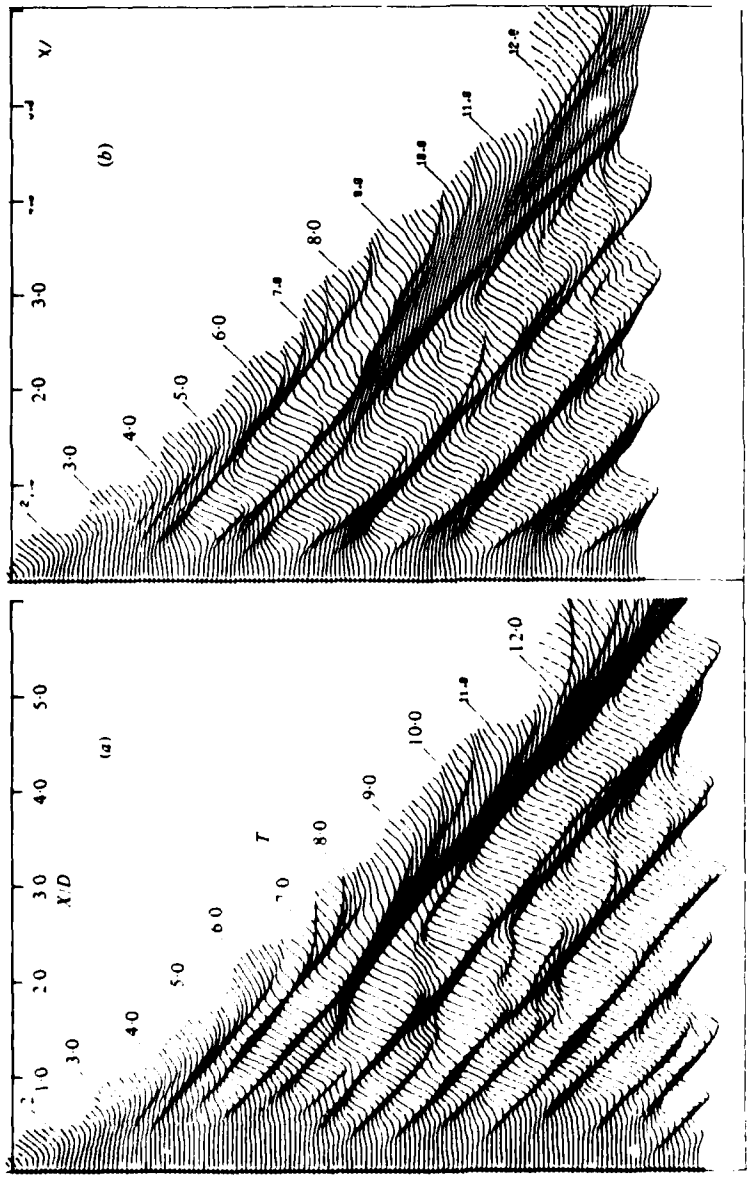

Figure 11 As Figure 10 but forced at S = 0.5 (a) A = 0.02 (b) A = 0.1

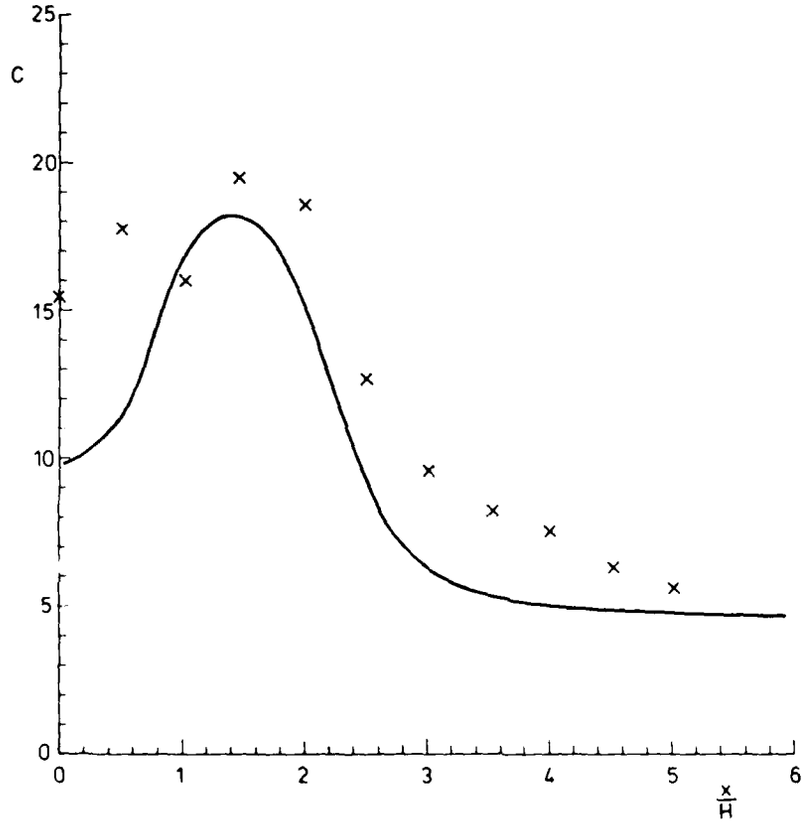

Figure 13 Ground level concentration behind a step X, experimental

Recent Activity in Vortex Methods in the United States

A. Leonard

California Institute of Technology, 301-46
Pasadena, California, 91125, USA

1. Introduction

Vortex method for flow simulation continue to have a wide-ranging appeal as a means of developing a better understanding of a complex flow and, in many cases, obtaining useful quantitative data. Part of the appeal is in the relative simplicity of the computer code that is required to do the job and, usually, in the relatively low computational cost. For example, experience has shown that some fairly complex three-dimensional flows may be simulated with a hundred or so vortex elements (sections of a vortex tube). Another aspect of the appeal is the visualization of the flow in terms of vortex dynamics, an aspect that aids in the physical understanding of the flow.

In this paper, recent activity in the United States concerning flow simulation with vortex methods is reviewed. We consider three main areas of effort: separated flows in two-dimensions (Section II), simulations using the method of contour dynamics (Section III) and three-dimensional flows (Section IV). Finally, in Section V, we cite directions for future efforts that look particularly promising.

2. Separated Flows

In many unsteady aerodynamic flows of interest the wake is characterized by the presence of time-varying, compact regions of vorticity. For constant density flows with negligible upstream turbulence, this vorticity is generated only at the no-slip boundaries of the solid surfaces. At high Reynolds number, once the vorticity separates from the boundary layer, it moves with the fluid with very little diffusion. These features suggest the use of a vortex method, in which parcels of vorticity move with the local fluid velocity, to simulate numerically the dynamics of the wake. For two-dimensional flows away from the influence of boundaries, vortex methods are reasonably well-established and methods for three-dimensional flows are developing rapidly [1].

However, to simulate separated flows two other necessary ingredients must be added:

1. Satisfy the inviscid boundary condition at the solid surface, i.e. no flow through the walls, and

2. Determine the locations of the separation points in time and the flux of vorticity into the outer flow

The first ingredient is rather easy to take care of. One can simply use a boundary integral method, one form of which is the panel method, where vortex tiles are laid along the boundary and the circulation of each tile is determined from the solution of a linear system representing the mutual influences of the tiles. For a simple geometry in two dimensions, i.e. any shape that can be transformed to a circle by a conformal map, the method of images is convenient. The second ingredient is, in general, much more difficult to satisfy. Here we have to compute the unsteady mechanics of the separating boundary layer. If we want to simulate a flow with a turbulent boundary layer we are at the mercy of available methods for these flows. However, if the boundary layer is laminar, we should, in principle, be able to compute what is required. This has been done for two dimensional flows with several levels of sophistication with some success (see Spalart, et al [2]) but more work needs to be done. For example, the following possibilities exist:

I. At the lowest level approximation, we assume the locations of the separation points or simply let a single layer of vortex elements take the place of the vortex panels representing the boundary layer. Reasonable results might be expected, for example, for shapes with sharp edges.

II. At the next level one might use an integral boundary layer method to determine when separation is allowable. If the separation criterion is not satisfied vortex elements are not permitted to leave the surface.

III. Finally the full boundary layer equations would be integrated numerically using, e.g., finite difference approximations, or by the use of vortex sheets with random walk.

A number of interesting applications have been computed recently. Spalart [3] has simulated the blockage effect of wind tunnel walls for flow past an airfoil at 90° angle of attack with blockage ratios (C/W = chord/tunnel height) between 0 and 0.2. Figure 1 shows typical snapshots of the flow. The resulting increase in drag is well represented by the expression,

$$C_{d_o} = C_d \left\{1 + a \frac{C}{W} C_{d_i}\right\}$$

with a = 0.7. C_{d_o} is the measured drag coefficient for free air. Experimental studies have recommended values of a between 0.5 and 0.96 and small disturbance theory gives a = 0.5.

In the same paper, Spalart also studied the phenomenon of rotating stall in a cascade. A number of cases were run on a cascade of five independent blades with periodic boundary conditions with two parameters varied between cases; stagger angle and angle of attack. The simulation produced the essential features of the various flow regimes and mapped the stall boundary. Typical results are displayed in Figure 2. In both of the above studies, Spalart used an integral boundary-layer solver (type II above).

Because the flow domain is grid-free, complex shapes and even multiple bodies can be treated with relative ease. For example, Couet and Spalart [4] studied the pressure traces on a bluff body located in the wake of another bluff body. The objective here was to design an accurate flow meter based on the nearly periodic shedding of the vortices behind bluff obstacles. Again, an integral boundary-layer solver was used. Figure 3 shows the instantaneous streamlines for one of the geometries that was studied. In a simulation involving a single body case, but with a complex shape, Lee and Bodapati [5] studied the flow past an airfoil with a deflected spoiler. They found good agreement between computational predictions and experimental results for large spoiler deflections but less satisfactory agreement for small deflections. In particular, the base pressure is underpredicted, apparently because of viscous and/or three-dimensional effects not accounted for in the computation. Again, integral boundary-layer methods were used for the above mentioned studies.

The use of a type I boundary layer method is exemplified by the study of Cheng, et al of a leading-edge flap [6] and Sarpkaya and Ihrig's [7] simulation of flow past rectangular prisms at angle of attack. Of particular interest in the latter study were the time-dependent forces on the prisms during the startup transient. Finally a type III approach using the random walk method, was used by Ghoniem and Gagnon [8] to study laminar flow over a backward-facing step. After filtering in time to the remove statistical fluctuations of the random walks, good comparisons were obtained with experiments for Reynolds numbers in the range 50 to 250.

3. Contour Dynamics Methods

If the vorticity field can be assumed to consist of regions or patches of constant vorticity, we can reduce the two-dimensional problem to the problem of tracking one-dimensional contours, the boundaries of the patches. Many earlier studies, using this technique, concentrated on finding rotating or translating, equilibrium states of vortex patches [9,10] with a few examples of relatively short-duration dynamic calculations [11,12]. More recently, the emphasis has has been on studying the stability of various equilibrium shapes, studying the dynamics of vortex patches in axisymmetric flow, and developing methods to extend dynamic calculations to long times.

To cite specific examples in the first group, we point to the study by Meiron, et al [13] where the linear stability of vortex streets of vortex patches was considered and to Dritschel's investigation [14] of the linear stability of corotating vortices. More recently Dritschel has studied the nonlinear evolution of corotating vorticities [15], and Shelley [16] has studied the nonlinear rollup of a finite thickness vortex sheet and has considered how the process limits to the case of zero thickness.

For axisymmetric flows, one defines the vortex patches such that the vorticity is proportional to the radial coordinate. In this case, the vorticity transport equation

$$\frac{D\left(\frac{\omega}{r}\right)}{Dt} = 0,$$

is satisfied for all interior points. Norbury [17] had computed the shapes of the cores in 1973 for a one parameter family of vortex rings, extending from Hill's spherical vortex on one end to a nearly circular shape for a ring with vanishing core area. But it was only very recently that a contour dynamics algorithm was developed. Pozrikidis [18] and Shariff, et al [19] have studied finite amplitude disturbances to Hill's vortex. In the latter study the dynamics of two vortex rings in collision and in an overtaking interaction were considered as well. See Figure 4 for an illustration of the overtaking interaction.

Building on the analysis of Kida [20], which gives the exact evolution of an elliptical vortex patch in a strain field, Melander, et al [21] have developed approximate dynamical equations for a collection of elliptical vortex patches, under the assumption that the patches remain elliptical. Thus two more degrees of freedom per vortex element are required over the circular blob approximation, aspect ratio and orientation angle, but the increased accuracy may well be worth it.

Finally, we note that Dritschel [22] has suggested and tried certain "contour surgery" algorithms that allow the simulation of evolution problems to long times at a reasonable cost. The idea is to remove thin filamentary structures that have very little influence on the future dynamics but would require considerable computational resources to maintain their identity. This pattern-recognition problem is also important for three-dimensional vortex filament and vortex sheet methods but has received only limited attention so far [23].

4. Methods for Three-Dimensional Flows

In a three-dimensional vortex method, vector elements of vorticity move at or near the local fluid velocity with the vectors strained by the local velocity gradient. In many applications, the vorticity field is well represented by isolated, thin tubes. Accurate equations for the long-wavelength dynamics of thin vortex tubes are available and form the basis for a three-dimensional vortex filament method [1]. Recently Parekh, et al [24] simulated an excited round jet in this approximation. It had been observed experimentally that dramatic changes in the structure of the jet fluid are achieved by introducing axial and orbital excitations. For this flow, the interplay between computation and ongoing laboratory experiments has led to a basic understanding of the mechanisms that govern the structure of the jet and how they might be controlled. See Figure 5 for typical experimental and computational results

In other applications, the vorticity field is a relatively smooth continuum. In this situation, vortex elements must be densely packed to represent properly the dynamics of the continuum. Recent mathematical proofs [25,26] have shown that, when properly constructed, vortex methods will produce solutions that converge to the solution of the Euler equations as the number of computational elements increases. Nakamura, et al [27] studied the three-dimensional breakdown of a vortex tube using 28 computational vortex filaments distributed over four radial zones forming a closely packed array. Upstream of breakdown the filaments were helical with pitch varying as function of radius to represent the axial and tangential velocity distributions of an experiment. Rather arbitrary three-dimensional initial perturbations eventually evolved into a nearly axisymmetric breakdown, followed downstream by a recovery and then a spiral-type breakdown. See Figure 6 for an illustration of this computational experiment. Quantitative comparisons with experiments were quite good.

In the above simulation of vortex breakdown, computed via the Biot-Savart law, a relatively large number of computational elements was required leading to very long computational times. An alternative technique available for certain types of boundary conditions, the vortex-in-cell method, may be used to compute the vortex interactions thereby significantly reducing the price of the simulation. Using the technique developed for infinite shear layers doubly periodic in the plane of the layer [28], Couet and Leonard (see [29]) studied the dynamics of perturbed Stuart vortices, obtaining new insights regarding the broadband nature of the linear instability of the pairing mode (see also Pierrehumbert and Widnall [30]) and results for the nonlinear evolution of this and other modes as well.

5. Future Directions

In the future, we expect to see vortex methods: (a) applied to increasingly complex flows, (b) extended to include a wider variety of physical phenomena, and (c) made increasingly efficient. In particular we feel that the following specific areas are ready for significant developments:

1. Compressibility effects - How does on efficiently and accurately include the effects of $\nabla \cdot \underline{u} \neq 0$ *in a vortex simulation? Steinhoff and Suryanarayanan [31], Koshigoe and Culick [32], and, Lund and Zabusky [33] have made some suggestions under various approximations.*

2. Vortex core models and vortex sheets - How does one represent the effects of a short wavelength *disturbance or a deformed core with possible axial flow without going to a multiple filament approximation.* The suggestion of Melander, et al [21], discussed above, to consider elliptical cores is an interesting possibility for two dimensional flows while Lundgren and Ashurst [34] have derived and tested approximate evolution equations for vortex filaments with time- and space-varying axial flows. *In many flows of interest, part of the vorticity field has a sheet-like structure.* Methods should be developed to represent and track sheet like structures. Eventually one would like to allow for changes in topology, reconnection or solutions, and smoothing.

3. *Three dimensional boundary layers* - *Before one can seriously consider the simulation of flow past an arbitrary three dimensional bluff body an efficient scheme for computing the unsteady behavior of a three-dimensional boundary layer must be developed*

4. *New computer architectures* - *The advent of highly concurrent computing, in which hundreds or thousands of relatively inexpensive computers work simultaneously on the same problem could very well have a major impact on fluid flow simulation in general, and on vortex simulations in particular.* Preliminary numerical experiments on a message-passing machine [35], sometimes known as the Cosmic Cube or hypercube, *have realized very high efficiencies for Biot-Savart interactions.* We expect that more complex problems, involving boundary layer calculations and boundary-integral methods, will also be well suited to such machines

6. References

1. Leonard, A., "Computing Three Dimensional Incompressible Flows with Vortex Elements," Ann. Rev. Fluid Mech., 17, 1985, 523

2. Spalart, P. R., A. Leonard and D. Baganoff, "Numerical Simulation of Separated Flows," NASA TM-84328, 1983

3. Spalart, P. R., "Two Recent Extensions of the Vortex Method," AIAA 84-0343, 1984. See also P. R. Spalart, "Simulation of Rotating Stall by the Vortex Method," J. of Propulsion and Power 1, 1985, 235

4. Couet, B., and P. R. Spalart, "Simulations of the Vortex Emission behind a Pair of Bluff Bodies by a Vortex Tracing Algorithm," Proceedings of the International ASME Conference on Modeling and Simulation, Paris-Sud, July 1-3, 1982.

5. Lee, C. S., and S. Bodapati, "Calculation of the Unsteady Flow Field of an Airfoil with a Deflected Spoiler by Vortex Method," *JIAA TR-62, Dept. Aero. and Astro., Stanford, May 1985.*

6. Cheng, H. K., R. H. Edwards and Z. X. Jia, "Simulation Studies of Vortex Dynamics of a Leading-Edge Flap," ICASE/NASA Workshop on Vortex Dominated Flows, 1985.

7. Sarpkaya, T. and C. J. Ihrig, "Impulsively-Started Flow about Rectangular Prisms: Experiments and Discrete Vortex Analysis," 1985 ASME Winter Meeting, to appear.

8. Ghoniem, A. F. and Y. Gagnon, "Vortex Simulation of Laminar Recirculating Flow," submitted for publication, 1986.

9. Deem, G. S. and N. J. Zabusky, "Stationary "V-States, Interactions, Recurrence, and Breaking," Phys. Rev. Lett. 40, 1978, 859. See also G. S. Deem and N. J. Zabusky, Stationary V-states *Interactions*, recurrence and breaking, in Solutions in Actions, Editors K. Lonngren and A. Scott, Academic Press, Inc., 1978, 277.

10. Saffman, P. G. and R. Szeto, "Equilibrium Shapes of a Pair of Equal Uniform Vortices," Phys. Fluids 23, 1980, 2339.

11. Zabusky, M. J., M. H. Hughes and K. V. Roberts, "Contour Dynamics for the Euler Equations in Two Dimensions," J. Comput. Phys. 30, 1979, 96.

12. Overman, II, E. A. and N. J. Zabusky, "Coaxial Scattering of Euler Equation Translating V-states via Contour Dynamics," J. Fluid Mech. 125, 1983, 187.

13. Meiron, D. I., P. G. Saffman and J. C. Schatzman, "The *Linear Two-dimensional* Stability of Inviscid Vortex Streets for Finite-cored Vortices," J. Fluid Mech. 147, 1984, 187.

14. Dritschel, D. G., "The Stability and Energetics of Corotating Uniform Vortices," J. Fluid Mech 157, 1985, 95.

15. Dritschel, D. G., "The Nonlinear Evolution of Configurations of Uniform Vorticity," J. Fluid *Mech.*, submitted for publication.

16. Shelley, Michael, P.D. Thesis, Department of Mathematics, University of Arizona, 1985.

17. Norbury, J., "A Family of Steady Vortex Rings," J. Fluid Mech. 57, 1973, 417.

18. Pozrikidis, C., "The Non-Linear Instability of Hill's Vortex," to appear in J. Fluid Mech., 1986.

19. Shariff, K., J. H. Ferziger and A. Leonard, "A Contour Dynamics Algorithm for Axisymmetric Flow," SIAM Fall Meeting, Phoenix, Arizona, October 20-30, 1985.

20. Kida, S., "Motion of an Elliptic Vortex in a Uniform Shear Flow," J. Phys. Soc. of Japan 50, 10, October 1981, 3517.

21. Melander, M. V., N. J. Zabusky, and A. S. Styczek, "A Moment Model for Vortex Interactions of the Two-Dimensional Euler Equations. I. Computational Validation of a Hamiltonian Elliptical *Representation*," *J. Fluid Mech.* in press.

22. Dritschel, D. G., 1985, private communication.

23. Leonard, A., "Vortex Methods for Flow Simulation," J. Comp. Phys. 37, 1980, 289.

24. Parekh, D. E., A. Leonard and W. C. Reynolds, "A Vortex Filament Simulation of a Bifurcating *Jet," Bull. Am. Phys. Soc. L8, 1983, 1353.*

25. Beale, J. T. and A. Majda, "Vortex Method I: Convergence in Three Dimensions," Mathematics of Computation 39, 1982, 29.

26. Anderson, C. and C. Greengard, "On Vortex Methods," SIAM Journal on Numerical Analysis 22, 1985, 413.

27. Nakamura, Y., A. Leonard and P. R. Spalart, "Vortex Breakdown Simulation," AIAA 18th Fluid Dynamics and Plasmadynamics and Lasers Conference, July 16-18, 1985, Cincinna i, Ohio.

28. Couet, B. and A. Leonard, "Exact Extension to the Infinite Domain for the Vortex-in Cell Method," SIAM J. Sci. Stat. Comput. 2, 3, September 1981, 311

29. Leonard, A., B. Couet and D. E. Parekh, "Two Studies in Three-Dimensional Vortex Dynamics: A Perturbed Round Jet and an Inhomogeneous Mixing Layer," Prod. Int. Symp. on Separated Flow Around Marine Structures, Trondheim, Norway, June 26-28, 1985.

30. Pierrehumbert, R. T. and S. E. Widnall, "The Two- and Three-Dimensional Instabilities of a Spatially Periodic Shear Layer," J. Fluid Mech. 114, 1982, 59.

31. Steinhoff, J. and K. Suryanarayanan, "The Treatment of Vortex Sheets in Compressible Potential Flow," AIAA 6th Computational Fluid Dynamics Conference, July 13-15, 1983, Danvers, Massachusetts, 1.

32. Koshigoe, S., V. Yang and F. E. C. Culick, "Calculations of Interaction of Acoustic Waves with a Two-Dimensional Free Shear Layer," AIAA 23rd Aerospace Sciences Meeting, January 14-17, 1985, Reno, Nevada.

33. Lund, F. and N. J. Zabusky, "Compressibility Effects in Vortex Dynamics at Constant Sound Speed," submitted for publication, 1986.

34. Lundgren, T. S. and W. T. Ashurst, "Area Varying Waves on Curved Vortex Tubes," submitted for publication, 1986.

35. Seitz, C. L., "The Cosmic Cube," Communications of the ACM 28, 1, January 1985, 22.

7 Figures

(a) (b)

Figure 1. Simulated flow at $\alpha = 90^{\circ}$ [3].

(a) Blockage ratio C/W = 0

(b) C/W = 0.2.

The body, vortices and streamlines are shown.
Dashed lines are the wall-suction distribution.
The arrow is the force vector on the airfoil.

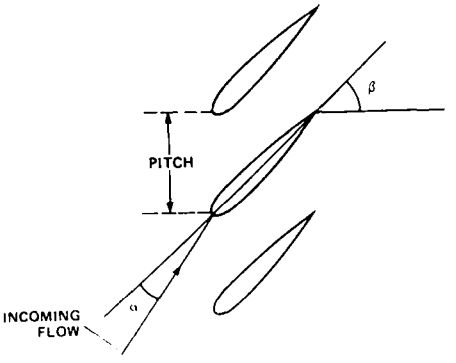

(a)

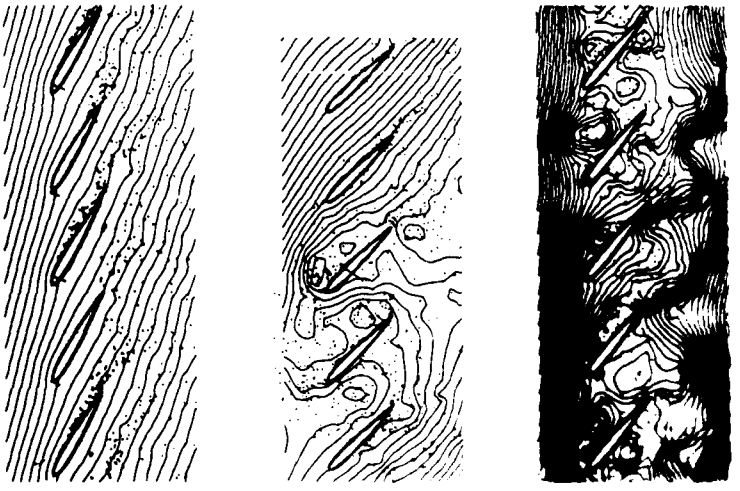

(b) (c)

Figure 2. Flow through a [illegible]

(a) Geometry [illegible]

(b) Attached flow [illegible]

(c) Rotating stall [illegible]

(d) Deep stall [illegible]

AD-A179 039 MODELLING OF TIME-VARIANT FLOWS USING VORTEX DYNAMICS (U) ADVISORY GROUP FOR AEROSPACE RESEARCH AND DEVELOPMENT NEUILLY-SUR-SEINE (FRANCE) FEB 87 2/2

UNCLASSIFIED AGARD-AR-239 F/G 20/4 NL

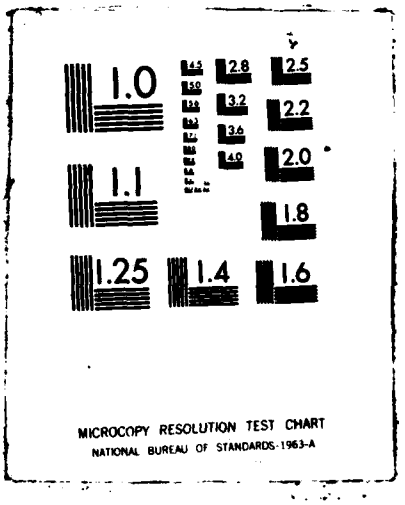
1.0
1.1
1.25
1.4
1.6
2.8
3.2
3.6
4.0
2.5
2.2
2.0
1.8
MICROCOPY RESOLUTION TEST CHART
NATIONAL BUREAU OF STANDARDS-1963-A

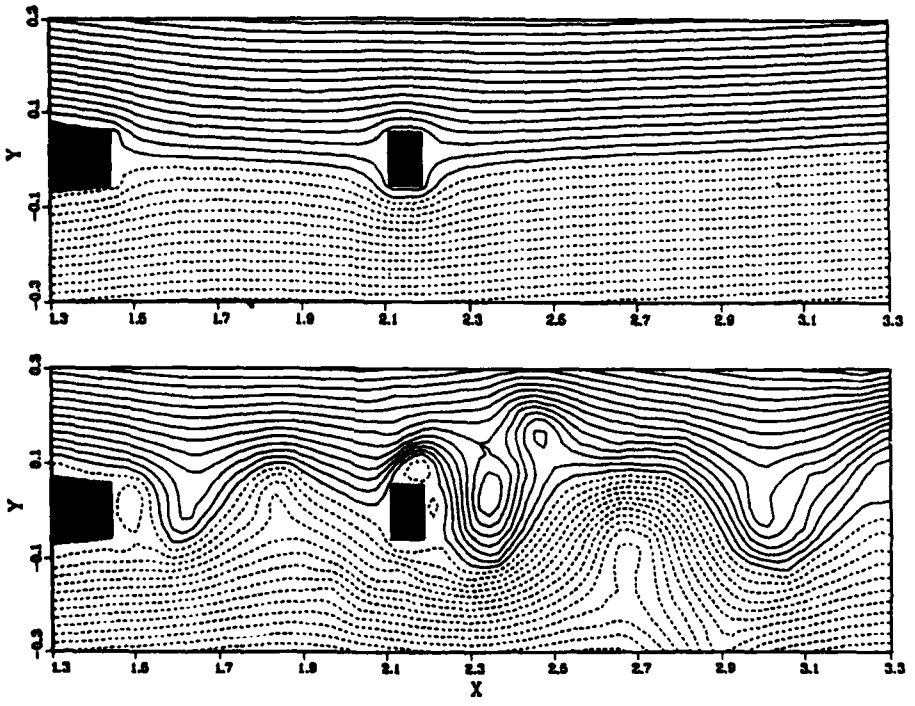

Figure 3. Vortex flowmeter [4]. Flow past a rectangle in the wake of a wedge after an implusive start.

(a) $t = 0^+$

(b) $t = 16.$

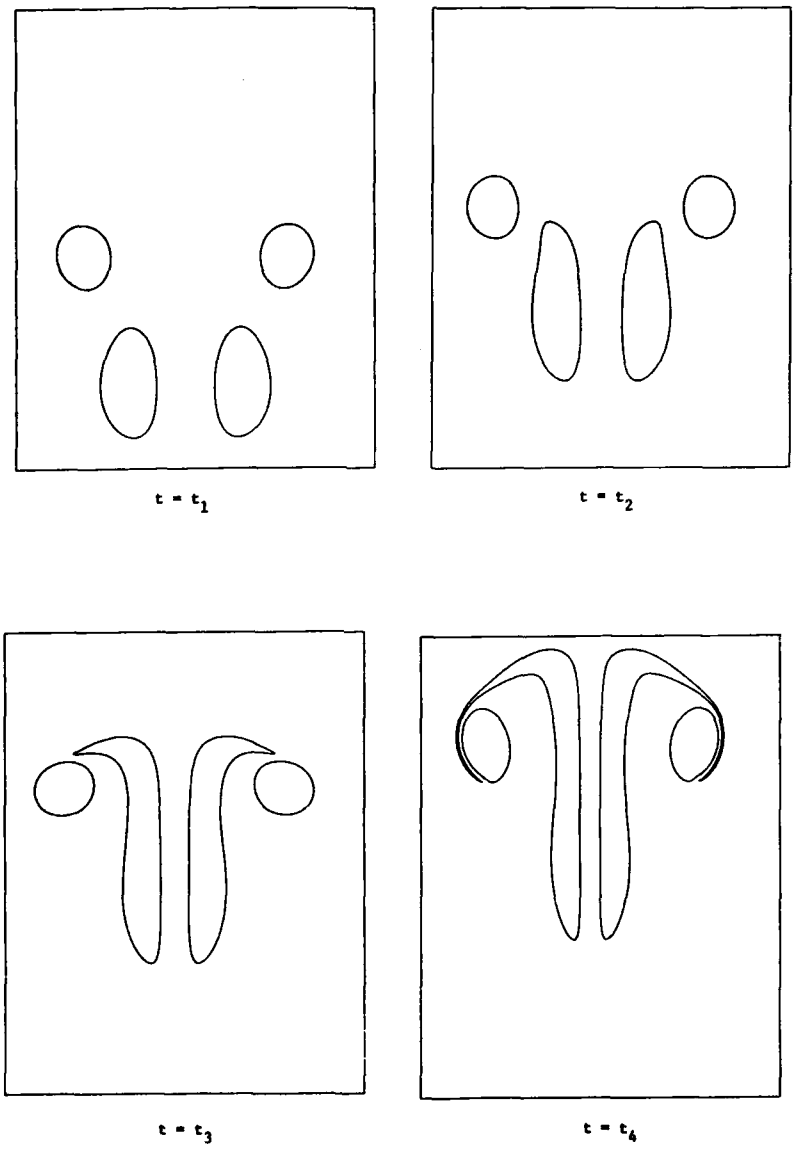

Figure 4. Contour dynamics simulation of two co-moving vortex rings in an overtaking interaction [19].

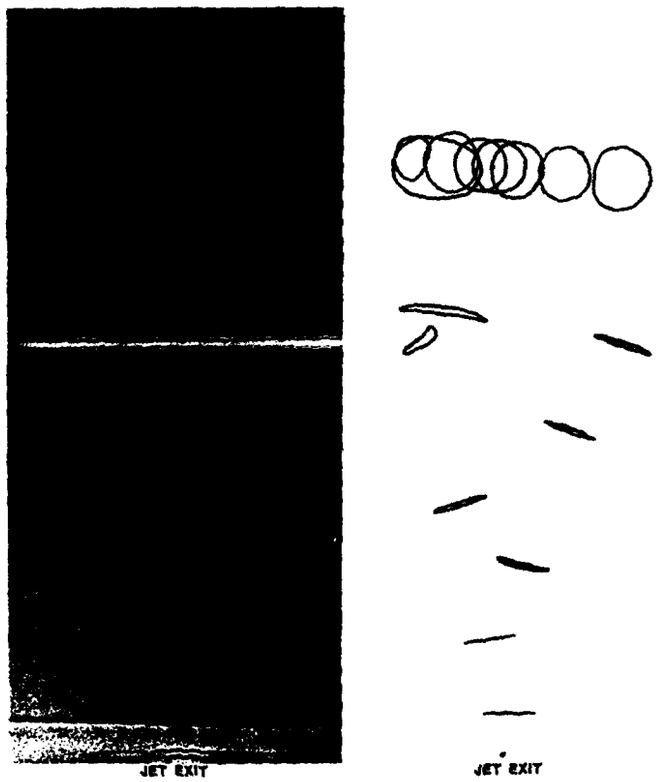

Figure 5. Bifurcation round jet, excited axially and orbitally.
(Left) Experiment of Lee and Reynolds, Bull. Amer. Phys. Soc., 28, 1983, 1362.
(Right) Vortex simulation: [1], [24]
(Top) Front views
(Bottom) Side views

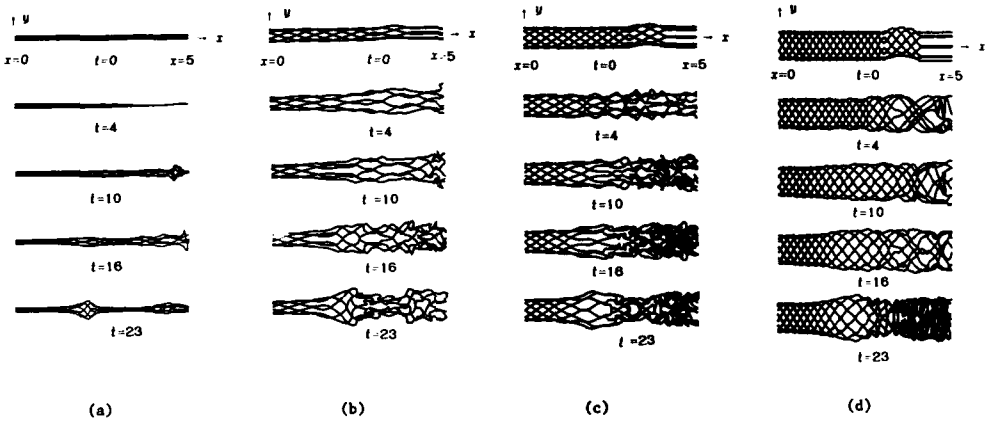

Figure 6. Simulation of vortex breakdown [27].

(a) Vortex filaments in innermost radial zone.

(b) Second radial zone.

(c) Third radial zone.

(d) Outer radial zone.

7-11

REPORT DOCUMENTATION PAGE			
1. Recipient's Reference	**2. Originator's Reference** AGARD-AR-239	**3. Further Reference** ISBN 92-835-0405-4	**4. Security Classification of Document** UNCLASSIFIED

5. Originator Advisory Group for Aerospace Research and Development
North Atlantic Treaty Organization
7 rue Ancelle, 92200 Neuilly sur Seine, France

6. Title ROUND TABLE DISCUSSION ON MODELLING OF TIME-VARIANT FLOWS USING VORTEX DYNAMICS

7. Presented at an AGARD Fluid Dynamics Panel Round-Table Discussion on Modelling of Time-Variant Flows Using Vortex Dynamics held at the Palais des Congrès, Aix-en-Provence, France, on 10 April 1986.

8. Author(s)/Editor(s)	**9. Date**
Various	February 1987
10. Author's/Editor's Address	**11. Pages**
Various	104

12. Distribution Statement This document is distributed in accordance with AGARD policies and regulations which are outlined on the Outside Back Covers of all AGARD publications.

13. Keywords/Descriptors

Fluid dynamics
Vortices
Viscous flow
Compressible flow
Mathematical models

14. Abstract

In recent years there has been a marked growth in the applications of vortex dynamics to time-varying flows, usually involving separated regions with vortical structures. The flow models are based on distributions of vortex elements which may vary in complexity.

This Report is a compilation of invited papers on the topic presented at the AGARD Fluid Dynamics Panel Round Table Discussion held in Aix-en-Provence, France, in April 1986. The papers cover current and projected developments in France, Germany, Greece, Italy, Netherlands, UK and USA. The Report provides a good overall view of the 'state of the art' of the topic, covering both the achievements and the deficiencies requiring future research.

The outstanding problems centre on how the effects of viscosity can be realistically modelled, particularly in three dimensional flow, and what might be done to deal with the effects of compressibility.

However, methods based on vortex dynamics seem particularly suited to problems involving well defined, large scale vortical flows for which they provide a more direct physical insight into the nature of the flow than other methods.

AGARD Advisory Report No.239 Advisory Group for Aerospace Research and Development, NATO ROUND TABLE DISCUSSION ON MODELLING OF TIME-VARIANT FLOWS USING VORTEX DYNAMICS Published February 1987 104 pages In recent years there has been a marked growth in the applications of vortex dynamics to time-varying flows, usually involving separated regions with vortical structures. The flow models are based on distributions of vortex elements which may vary in complexity. This Report is a compilation of invited papers on the topic P.T.O	AGARD-AR-239 Fluid dynamics Vortices Viscous flow Compressible flow Mathematical models	AGARD Advisory Report No.239 Advisory Group for Aerospace Research and Development, NATO ROUND TABLE DISCUSSION ON MODELLING OF TIME-VARIANT FLOWS USING VORTEX DYNAMICS Published February 1987 104 pages In recent years there has been a marked growth in the applications of vortex dynamics to time-varying flows, usually involving separated regions with vortical structures. The flow models are based on distributions of vortex elements which may vary in complexity. This Report is a compilation of invited papers on the topic P.T.O	AGARD-AR-239 Fluid dynamics Vortices Viscous flow Compressible flow Mathematical models
AGARD Advisory Report No.239 Advisory Group for Aerospace Research and Development, NATO ROUND TABLE DISCUSSION ON MODELLING OF TIME-VARIANT FLOWS USING VORTEX DYNAMICS Published February 1987 104 pages In recent years there has been a marked growth in the applications of vortex dynamics to time-varying flows, usually involving separated regions with vortical structures. The flow models are based on distributions of vortex elements which may vary in complexity. This Report is a compilation of invited papers on the topic P.T.O	AGARD-AR-239 Fluid dynamics Vortices Viscous flow Compressible flow Mathematical models	AGARD Advisory Report No.239 Advisory Group for Aerospace Research and Development, NATO ROUND TABLE DISCUSSION ON MODELLING OF TIME-VARIANT FLOWS USING VORTEX DYNAMICS Published February 1987 104 pages In recent years there has been a marked growth in the applications of vortex dynamics to time-varying flows, usually involving separated regions with vortical structures. The flow models are based on distributions of vortex elements which may vary in complexity. This Report is a compilation of invited papers on the topic P.T.O	AGARD-AR-239 Fluid dynamics Vortices Viscous flow Compressible flow Mathematical models

presented at the AGARD Fluid Dynamics Panel Round Table Discussion held in Aix-en-Provence, France, in April 1986. The papers cover current and projected developments in France, Germany, Greece, Italy, Netherlands, UK and USA. The Report provides a good overall view of the 'state of the art' of the topic, covering both the achievements and the deficiencies requiring future research.

The outstanding problems centre on how the effects of viscosity can be realistically modelled, particularly in three dimensional flow, and what might be done to deal with the effects of compressibility.

However, methods based on vortex dynamics seem particularly suited to problems involving well defined, large scale vortical flows for which they provide a more direct physical insight into the nature of the flow than other methods.

ISBN 92-835-0405-4

presented at the AGARD Fluid Dynamics Panel Round Table Discussion held in Aix-en-Provence, France, in April 1986. The papers cover current and projected developments in France, Germany, Greece, Italy, Netherlands, UK and USA. The Report provides a good overall view of the 'state of the art' of the topic, covering both the achievements and the deficiencies requiring future research.

The outstanding problems centre on how the effects of viscosity can be realistically modelled, particularly in three dimensional flow, and what might be done to deal with the effects of compressibility.

However, methods based on vortex dynamics seem particularly suited to problems involving well defined, large scale vortical flows for which they provide a more direct physical insight into the nature of the flow than other methods.

ISBN 92-835-0405-4

presented at the AGARD Fluid Dynamics Panel Round Table Discussion held in Aix-en-Provence, France, in April 1986. The papers cover current and projected developments in France, Germany, Greece, Italy, Netherlands, UK and USA. The Report provides a good overall view of the 'state of the art' of the topic, covering both the achievements and the deficiencies requiring future research.

The outstanding problems centre on how the effects of viscosity can be realistically modelled, particularly in three dimensional flow, and what might be done to deal with the effects of compressibility.

However, methods based on vortex dynamics seem particularly suited to problems involving well defined, large scale vortical flows for which they provide a more direct physical insight into the nature of the flow than other methods.

ISBN 92-835-0405-4

presented at the AGARD Fluid Dynamics Panel Round Table Discussion held in Aix-en-Provence, France, in April 1986. The papers cover current and projected developments in France, Germany, Greece, Italy, Netherlands, UK and USA. The Report provides a good overall view of the 'state of the art' of the topic, covering both the achievements and the deficiencies requiring future research.

The outstanding problems centre on how the effects of viscosity can be realistically modelled, particularly in three dimensional flow, and what might be done to deal with the effects of compressibility.

However, methods based on vortex dynamics seem particularly suited to problems involving well defined, large scale vortical flows for which they provide a more direct physical insight into the nature of the flow than other methods.

ISBN 92-835-0405-4

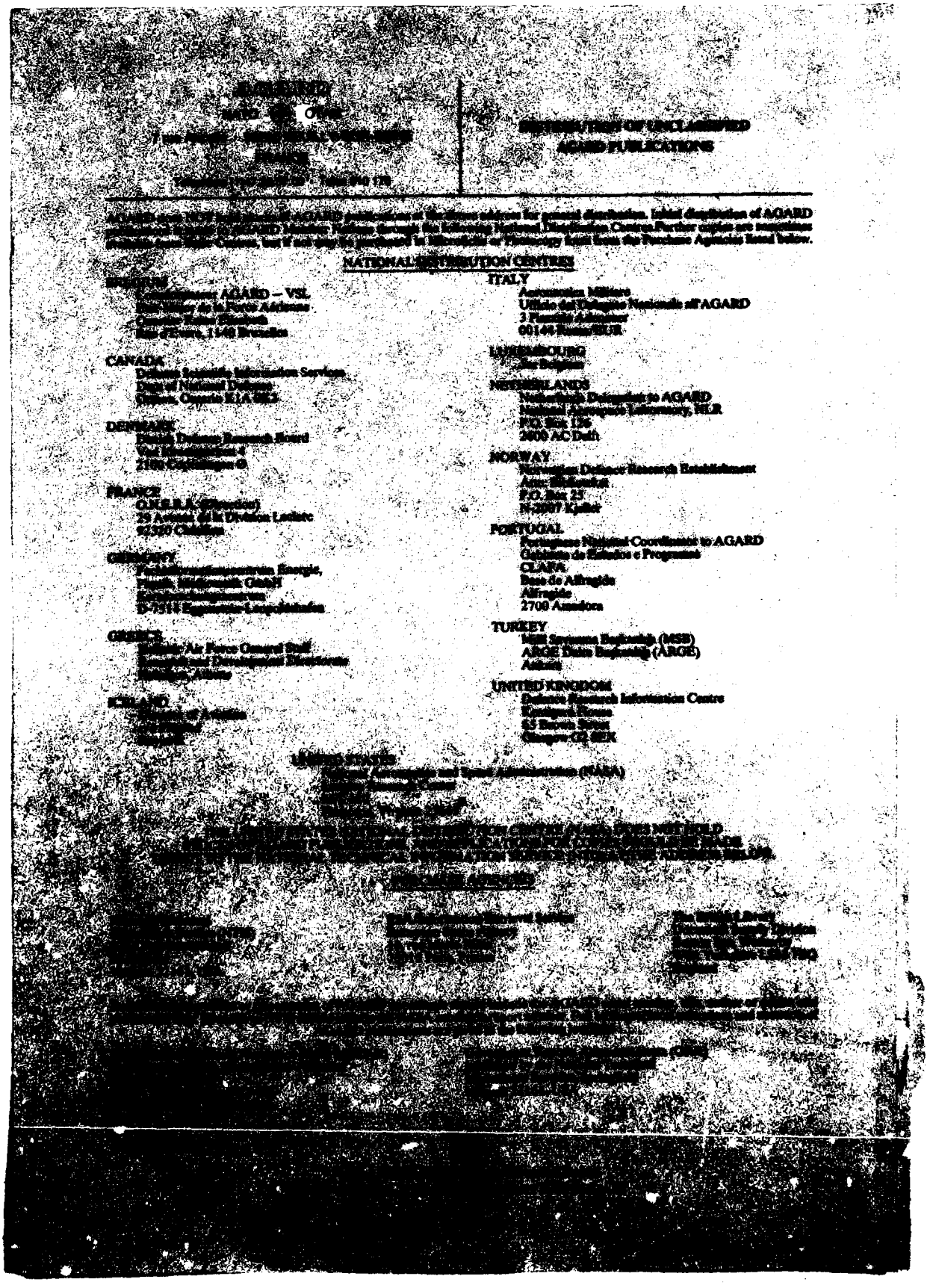

NATIONAL DISTRIBUTION CENTRES

ITALY
Aeronautica Militare
Ufficio del Delegato Nazionale all'AGARD
3 Piazzale Adenauer
00144 Roma/EUR

LUXEMBOURG
See Belgium

NETHERLANDS
Netherlands Delegation to AGARD
National Aerospace Laboratory, NLR
P.O. Box 126
2600 AC Delft

NORWAY
Norwegian Defence Research Establishment
Attn: Biblioteket
P.O. Box 25
N-2007 Kjeller

PORTUGAL
Portuguese National Coordinator to AGARD
Gabinete de Estudos e Programas
CLAFA
Base de Alfragide
Alfragide
2700 Amadora

TURKEY
Milli Savunma Başkanlığı (MSB)
ARGE Daire Başkanlığı (ARGE)
Ankara

UNITED KINGDOM
Defence Research Information Centre
Kentigern House
65 Brown Street
Glasgow G2 8EX

END

DATE
FILMED

5-87